

UNCLASSIFIED

AD NUMBER

ADB088421

LIMITATION CHANGES

TO:

Approved for public release; distribution is unlimited.

FROM:

Distribution authorized to U.S. Gov't. agencies only; Critical Technology; Test and Evaluation; JUN 1982. Other requests shall be referred to Air Force Wright Aeronautical Laboratory, Materials Lab, Wright-Patterson AFB, OH 45433. This document contains export-controlled technical data.

AUTHORITY

afwal/imst ltr 27 feb 1987

THIS PAGE IS UNCLASSIFIED

AD Bo 82 421

AUTHORITY:

AEWAL / East etc.

27 Feb 87

AFWAL-TR-84-4078



R&D ON COMPOSITION AND PROCESSING OF TITANIUM ALUMINIDE ALLOYS FOR TURBINE ENGINES

M.J. Blackburn

J.T. Hill

M.P. Smith

United Technologies Corporation

Pratt & Whitney

Engineering Division

West Palm Beach, Florida 33402

July 1984

Final Technical Report for Period 1 October 1982 to 31 January 1984

SUBJECT TO EXPORT CONTROL LAWS

THIS DOCUMENT CONTAINS INFORMATION FOR MANUFACTURING OR USING MUNITIONS OF WAR. EXPORT OF THE INFORMATION CONTAINED HEREIN, OR RELEASE TO FOREIGN NATIONALS WITHIN THE UNITED STATES, WITHOUT FIRST OBTAINING AN EXPORT LICENSE, IS A VIOLATION OF THE INTERNATIONAL TRAFFIC-IN-ARMS REGULATIONS. SUCH VIOLATION IS SUBJECT TO A PENALTY OF UP TO 2 YEARS IMPRISONMENT AND A FINE OF \$100,000 UNDER 22 USC 2778.

INCLUDE THIS NOTICE WITH ANY REPRODUCED PORTION OF THIS DOCUMENT.

Distribution limited to US Government agencies only; Test and Evaluation; June 1982. Other requests for this document must be referred to AFWAL/MLLM, WPAFB, OHIO 45433.

**MATERIALS LABORATORY
AIR FORCE WRIGHT AERONAUTICAL LABORATORIES
AIR FORCE SYSTEMS COMMAND
WRIGHT-PATTERSON AIR FORCE BASE, OHIO 45433**

**DTIC
ELECTE
DEC 27 1984
A**

84 12 14 040

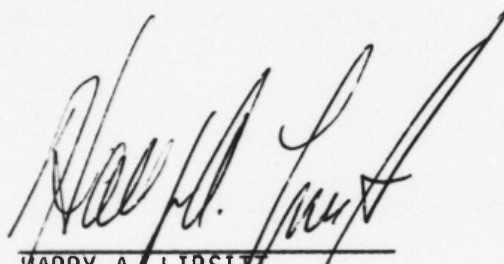
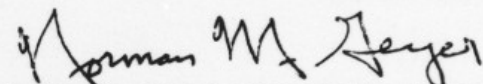
AD-B088 421

DTIC FILE COPY


NOTICE

When Government drawings, specifications, or other data are used for any purpose other than in connection with a definitely related Government procurement operation, the United States Government thereby incurs no responsibility nor any obligation whatsoever; and the fact that the Government may have formulated, furnished, or in any way supplied the said drawings, specifications, or other data, is not to be regarded by implication or otherwise as in any manner licensing the holder or any other person or corporation, or conveying any rights or permission to manufacture, use, or sell any patented invention that may in any way be related thereto.

This technical report has been reviewed and is approved for publication.


HARRY A. LIPSITZ
Project Engineer
NORMAN M. GEYER
Technical Area Manager
Processing & High Temperature
Materials Branch
Metals & Ceramics Division

FOR THE COMMANDER:


HENRY C. GRAHAM, Chief
Processing & High Temperature
Materials Branch
Metals & Ceramics Division

"If your address has changed, if you wish to be removed from our mailing list, or if the addressee is no longer employed by your organization, please notify AFWAL/MLLM, W-P AFB, Ohio 45433 to help maintain a current mailing list".

Copies of this report should not be returned unless return is required by security considerations, contractual obligations, or notice on a specific document.

Unclassified

SECURITY CLASSIFICATION OF THIS PAGE (When Data Entered)

REPORT DOCUMENTATION PAGE		READ INSTRUCTIONS BEFORE COMPLETING FORM
1. REPORT NUMBER AFWAL-TR-84-4078	2. GOVT ACCESSION NO. AD-608842	3. RECIPIENT'S CATALOG NUMBER
4. TITLE (and Subtitle) R&D ON COMPOSITION AND PROCESSING OF TITANIUM ALUMINIDE ALLOYS FOR TURBINE ENGINES		5. TYPE OF REPORT & PERIOD COVERED Final Technical Report October 1982 - January 1984
7. AUTHOR(s) M. J. Blackburn M. P. Smith J. T. Hill		6. PERFORMING ORG. REPORT NUMBER FR-17537
9. PERFORMING ORGANIZATION NAME AND ADDRESS UTC - Pratt & Whitney Government Products Division West Palm Beach, FL 33402		8. CONTRACT OR GRANT NUMBER(s) F33615-80-C-5163
11. CONTROLLING OFFICE NAME AND ADDRESS Materials Laboratory (AFWAL/MLLM) Air Force Wright Aeronautical Laboratories (AFSC) Wright Patterson AFB, Ohio 45433		10. PROGRAM ELEMENT, PROJECT, TASK AREA & WORK UNIT NUMBERS 24200127
14. MONITORING AGENCY NAME & ADDRESS (if different from Controlling Office)		12. REPORT DATE July 1984
		13. NUMBER OF PAGES 110
		15. SECURITY CLASS. (of this report) UNCLASSIFIED
		15a. DECLASSIFICATION/DOWNGRADING SCHEDULE
16. DISTRIBUTION STATEMENT (of this Report) Distribution limited to U.S. Government agencies only; Test and Evaluation; June 1982. Other requests for this document must be referred to AFWAL/MLLM, WPAFB, Ohio 45433		
17. DISTRIBUTION STATEMENT (of the abstract entered in Block 20, if different from Report)		
18. SUPPLEMENTARY NOTES <div style="text-align: center;">Gamma</div>		
19. KEY WORDS (Continue on reverse side if necessary and identify by block number) Titanium Aluminides, Mechanical Properties, Titanium Alloy Microstructures, Titanium Machining, Fracture Toughness, Thermomechanical Fatigue, Crack Propagation Testing		
20. ABSTRACT (Continue on reverse side if necessary and identify by block number) Material based on the intermetallic phase TiAl (γ) exhibits several attractive features that make it a candidate for gas turbine engine applica- tions. Low density, good oxidation resistance and high temperature strength are such characteristics and could result in substitution for the nickel alloys currently used for turbine engine components that operate at inter- mediate temperatures. The Ti-48Al-1V alloy has been identified as the primary		

DD FORM 1 JAN 73 1473

EDITION OF 1 NOV 65 IS OBSOLETE

Unclassified

SECURITY CLASSIFICATION OF THIS PAGE (When Data Entered)

Cont'd

Cont'd

Unclassified

gamma

Composition of interest in the gamma system and an extensive amount of mechanical property data have been generated in a related program. The aim of this effort was to characterize fatigue crack growth behavior and damage tolerance.

The apparent fracture toughness of the 7TiAl alloy did not vary appreciably with test temperature to 705°C (1300°F) and was marginal over the design relevant range of temperature. The room temperature apparent fracture toughness was, however, too high for cold proof testing to be a viable flow detection strategy. The rate of cyclic crack growth increased with increasing test temperature and P-ratio. da/dN data seem to be correlated best by the crack tip opening displacement. Thermomechanical fatigue crack growth data are not markedly different from isothermal test results for the three design relevant cycles studied.

Unclassified

11

FOREWORD

This is the final Technical Report (PWA Report FR-17537) covering work performed under Contract F33615-80-C-5163.

The investigation was conducted by the Pratt and Whitney Engineering Division, Connecticut operations under the technical direction of Dr. H. A. Lipsitt, AFWAL/MLLM, Wright-Patterson Air Force Base, Ohio.

Dr. M. J. Blackburn was the Program Manager, Mr. M. P. Smith, Mr. J. T. Hill and Mr. R. M. Masci were the responsible engineers. Mr. D. P. Haase, Mr. G. E. Dube and Mr. P. D. Retzer were the experimental assistants.



Accession For	
NTIS GRA&I	<input type="checkbox"/>
DTIC TAB	<input checked="" type="checkbox"/>
Unannounced	<input type="checkbox"/>
Justification	
By	
Distribution/	
Availability Codes	
Dist.	Avail and/or Special
B-3	

TABLE OF CONTENTS

SECTION	PAGE
I INTRODUCTION	1
1. Background	1
2. Approach	2
II EXPERIMENTAL DETAILS	4
1. Task III Alloy Selection	4
2. Task IV Baseline Isothermal Fracture Mechanics Testing	7
3. Task V Prestress Effects on Fracture Toughness	10
4. Task VI Subcomponent Testing to Demonstrate Benefits of Prestressing	13
5. Task VII Athermal (TMF) Strain Controlled Crack Growth Testing	14
III EXPERIMENTAL RESULTS	18
1. Task IV Baseline Isothermal Crack Growth Testing	18
2. Task V Prestressing Effects on Fracture Toughness	54
3. Task VI Subcomponent Testing to Demonstrate Benefits of Prestressing	58
4. Task VII Athermal (TMF) Crack Growth Testing	60
IV DISCUSSION	74
1. Introduction	74
2. Baseline Isothermal Fracture Mechanics Testing	74
3. Athermal (TMF) Crack Growth Testing	82
4. Prestressing Effects on Fracture Toughness	88
5. Subcomponent Testing To Demonstrate Warm Prestressing Benefits	93
V ANALYSIS AND CONCLUSIONS	96
REFERENCES	98

LIST OF ILLUSTRATIONS

<u>Number</u>	<u>Title</u>	<u>Page</u>
1	Typical Microstructure of Cast + HIP Ti-48A1-1V Alloy After Solution Heat Treatment of 1287°C (2350°F)/1 Hour/Followed by Air Cooling	5
2	Specimen Configurations Selected for Evaluation of Damage Tolerant Design for Cast/HIP Ti-48A1-1V Alloy	6
3	JT9D Ti-48A1-1V Cast Low Pressure Turbine Blade	8
4	Specimens Used for Determining Crack Growth Behavior of Ti-48A1-1V. (a) Specimen with external ridges for strain controlled test; (b) Smooth specimen for load controlled test; (c) EDM starter notch (arrow).	8
5	Technique Used to Produce a Centered Surface Crack in Ti-48A1-1V Fracture Toughness Specimen	11
6	Test Plan to Determine Prestress Effects on Fracture Toughness of Ti-48A1-1V	12
7	Subcomponent Demonstration Plan for Ti-48A1-1V	14
8	Thermomechanical Response of Three Locations on the Low Pressure Turbine Blade	15
9	Test Cycles for Thermomechanical Crack Growth of Ti-48A1-1V	17
10a	Hysteresis Loop Showing Small Cyclic Plasticity at +0.07% Strain Range, 815°C (1500°F), 6 cpm for Ti-48A1-1V Specimen 10766	19
10b	Hysteresis Loops Showing that No Cyclic Hardening or Softening Occurred at $\pm 0.2\%$ 815°C (1500°F), 6 cpm for Specimen 10766	19
11	Crack Length (2a) Versus Cycles (N) Curve for Ti-48A1-1V Specimen 10766 Tested at 815°C (1500°F), R = -1, $\pm 0.2\%$ at a Rate of 6 Cycles Per Minute	20
12	da/dN Versus Delta K Curves for Ti-48AL-1V Specimen 10766 Tested at 815°C (1500°F) and R = -1. The circles represent a $\Delta\epsilon$ of +0.2% tested at 6 cpm; the diamonds represent the da/dN when the strain was reduced to $\pm 0.125\%$ and a one minute dwell introduced	20

LIST OF ILLUSTRATIONS (Continued)

<u>Number</u>	<u>Title</u>	<u>Page</u>
13	Effect of Constant Strain Holds at 815°C (1500°F) on the Width of the Hysteresis Loops; $R = -1$, $\Delta\epsilon = 0.125\%$.	21
14	Crack Length (2a) Versus Cycles (N) for Ti-48A1-1V Specimen 10766 Tested at 815°C (1500°F), $R = -1$, $\Delta\epsilon = +0.125\%$, With a One Minute Dwell During the Cycle	21
15	Mean Stress Drift and Cyclic Hardening at Three Strain Amplitudes for Ti-48A1-1V Specimen 10768 Tested at 815°C (1500°F), $R = 0$. a) 0.2%; b) 0.25%; c) 0.275%	23
16	Stabilized Hysteresis Loops for Ti-48A1-1V Specimen 10768 Tested at 815°C (1500°F), $R = 0$. a) $\Delta\epsilon = 0.2\%$; b) $\Delta\epsilon = 0.25\%$; c) $\Delta\epsilon = 0.275\%$	24
17	Crack Length (2a) Versus Cycles (N) for Ti-48A1-1V Specimen 10768, Tested at 815°C (1500°F), $R = 0$, $\Delta\epsilon = 0.275\%$	25
18	da/dN Versus Delta K Curve for Ti-48A1-1V Specimen 10768, Tested at 815°C (1500°F), $R = 0$, $\Delta\epsilon = 0-0.275\%$	25
19	Crack Length Versus Cycles for Strain Controlled Specimen 10768 Showing Effect of One Minute Dwell on Crack Growth Rate at 815°C (1500°F) and $R = 0$	26
20	Effect of One Minute Dwell on da/dN Versus Delta K for Strain Controlled Specimen 10768 at 815°C (1500°F) and $R = 0$	26
21	Representative Hysteresis Loops Taken at Various Times During Dwell Testing of Specimen 10768	27
22	Crack Length (2a) Versus Cycles (N) for Ti-48A1-1V Specimen 10767 Tested at 650°C (1200°F), $R = 0$, $\Delta\epsilon = 0.21\%$	27
23	da/dN Versus Delta K Curve for Ti-48A1-1V Specimen 10767, Tested at 650°C (1200°F) at Two Different R Ratios and Strains as Shown	28
24	Crack Length (2a) Versus Cycles (N) for Ti-48A1-1V Specimen 10774, Tested at 650°C (1200°F), $R = -1$, $\Delta\epsilon = 0.18\%$	28

LIST OF ILLUSTRATIONS (Continued)

<u>Number</u>	<u>Title</u>	<u>Page</u>
25	Crack Growth Data for Load Controlled Specimen 10776 Tested at RT and 565°C (1050°F) at R = 0 and R = -1. a) Crack Length (2a) Versus Cycles (N); b) da/dN Versus Delta K	30
26	Crack Growth Data for Load Controlled Specimen 10776 Tested at 565°C (1050°F) and R = -1. a) Crack Length (2a) Versus Cycles (N); b) da/dN Versus Delta K	31
27	Crack Growth Data for Load Controlled Specimen 10778 Tested to Verify R = 0 Results of 10776, Run at 565°C (1050°F). a) Crack Length 2a Versus Cycles (N); b) da/dN Versus Delta K	32
28	Crack Growth Data for Load Controlled Specimen 10778 to Verify R = -1 Results of 10776, Run at 565°C (1050°F). a) Crack Length (2a) Versus Cycles (N); b) da/dN Versus Delta K	33
29	Crack Growth Data for Load Controlled Specimen 10777 Tested at 315°C (600°F) and R = 0. a) Crack Length (2a) Versus Cycles (N); b) da/dN Versus Delta K	34
30	Crack Growth Data for Load Controlled Specimen 10777, Tested at 315°C (600°F) and R = -1. a) Crack Length (2a) Versus Cycles (N); b) da/dN Versus Delta K	36
31	Crack Growth Data for Strain Controlled Specimen 10769 Tested at 730°C (1360°F) and R = -1. a) Crack Length (2a) Versus Cycles (N); b) da/dN Versus Delta K	37
32	Stress Versus Cycles for Specimen 10769 Showing Lack of Softening or Hardening During Test.	38
33	Stress Strain (Hysteresis) Loops Taken at Various Cycles During Testing of Specimen 10769. Note similarity of shape.	38
34	Crack Growth Data for Strain Controlled Specimen 10770 Tested at 736°C (1360°F) and R = -1, to Amplify Results of 10769. a) Crack Length (2a) Versus Cycles (N); b) da/dN Versus Delta K	39
35	Representative Hysteresis Loops for Strain Controlled Specimen 10770 During Dwell Portion of Test	40

LIST OF ILLUSTRATIONS (Continued)

<u>Number</u>	<u>Title</u>	<u>Page</u>
36	Crack Growth Data for Strain Controlled Specimen 10770 Showing Effect of One Minute Dwell Versus Rapid Cycle, a) Crack Length Versus Cycles; b) da/dN Versus stress intensity	41
37	Crack Growth Data for Load Controlled Specimen 10772 Tested at 650°C (1200°F) and R = -1. a) Crack Length (2a) Versus Cycles (N); b) da/dN Versus Delta K	42
38	Crack Growth Data for Load Controlled Specimen 10772 Tested at 650°C (1200°F) During R = 0 Portion of Test. a) Crack Length (2a) Versus Cycles (N); b) da/dN Versus Delta K	43
39	Mean Stress Curves Versus Cycles for Strain Controlled Specimen 10771 Tested at 736°C (1360°F) and R = 0 Showing 30% Decrease, Although No Hardening or Softening Was Observed	44
40	Crack Growth Data for Strain Controlled Specimen 10771 Tested at 736°C (1360°F) and R = 0. a) Crack Length (2a) Versus Cycles (N); b) da/dN Versus Delta K	45
41	Mean Stress Versus Cycles for R = 0 Portion of Test of Specimen 10771 Tested at 736°C (1360°F) With a One Minute Dwell at Maximum Strain. Note decrease in mean stress of about 30%	45
42	Crack Growth Data for Strain Controlled Specimen 10771 Tested at 736°C (1360°F) and R = 0 During One Minute Dwell Portion of Test. a) Crack Length (2a) Versus Cycles (N); b) da/dN Versus Delta K	46
43	Mean Stress Versus Cycles Curves for Strain Controlled Specimen 10773 Tested at 815°C (1500°F) and R = -3 Showing Some Hardening After First Cycle But None Afterwards	47
44	Crack Growth Data for Strain Controlled Specimen 10773 Tested at 815°C (1500°F) and R = -3. a) Crack Length (2a) Versus Cycles (N); b) da/dN Versus Delta K	48
45	Stress Versus Cycle Curves for Strain Controlled Specimen 10773 During One Minute Dwell Portion Test at 815°C (1500°F) and R = -3	49

LIST OF ILLUSTRATIONS (Continued)

<u>Number</u>	<u>Title</u>	<u>Page</u>
46	Crack Growth data for Strain Controlled Specimen 10773 Tested at 815°C (1500°F), R = -3 With a One Minute Dwell Imposed. a) Crack Length (2a) Versus Cycles (N); b) da/dN Versus Delta K	50
47	Crack Growth Data for Strain Controlled Specimen 10775, Tested at 736°C (1360°F) R = -3 Conditions, Rapid Cycle Results. a) Crack Length (2a) Versus Cycles (N); b) da/dN Versus Delta K	51
48	Crack Growth Data for Strain Controlled Specimen 10775, Tested at 736°C (1360°F), R = -3 Conditions With a One Minute Hold in Compression. a) Crack Length (2a) Versus Cycles (N); b) da/dN Versus Delta K	52
49	Crack Growth Data for Load Controlled Specimen 10774 Tested at 650°C (1200°F) With A One Minute Dwell at Max Tension, R = 0. a) Crack Length (2a) Versus Cycles (N); b) da/dN Versus Delta K	53
50	Thermocycle Selected for Initial Evaluation of TMF Specimen 11291	61
51	Crack Length (2a) Versus Cycles (N) for TMF Specimen 11291 Cycled as Shown	61
52	da/dN Versus Delta K for TMF Specimen Tested at Two Strain Ranges Over the Range 315-815°C (600-1500°F)	62
53	Crack Length (2a) Versus Cycles (N) for TMF Specimen 11291, Cycled as Shown	62
54	Strain Versus Temperature Curve for TMF Specimen 11292 Run in a Type II Cycle Between 315-736°C (600-1360°F) at R = 0	63
55	Crack Growth Data for TMF Specimen 11292 (Type II Cycle). a) Crack Length (2a) Versus Cycles (N); b) da/dN Versus Delta K	64
56	Stress Versus Temperature Curves for TMF Specimen 11293 Run in a Type III Cycle From 315-650°C (600-1200°F) in a Clockwise Manner	66

LIST OF ILLUSTRATIONS (Continued)

<u>Number</u>	<u>Title</u>	<u>Page</u>
57	Crack Growth Data for TMF Specimen 11297 (Type III Clockwise Cycle). a) Crack Length (2a) Versus Cycles (N); b) da/dN Versus Delta K	67
58	Crack Growth Data for TMF Specimen 11294 (Type III Counterclockwise Cycle). a) Crack Length Versus Cycles; b) da/dN Versus Delta K	68
59a	Crack Growth Data for TMF Specimen 11295 (Type I Cycle Counterclockwise). a) Crack Length (2a) Versus Cycles (N); b) da/dN Versus Delta K	69
60a	Crack Length (2a) Versus Cycles (N) for TMF Specimen 11296 Cycled In Type II TMF With a One Minute Hold at Maximum Strain	70
60b	Crack Length (2a) Versus Cycles (N) for TMF Specimen 11296 Cycled In Type II TMF With a One Minute Hold at Maximum Strain Following Reinitiation of Crack	70
60c	da/dN Delta Kmax for Specimen 11296, Type II TMF Cycling With a One Minute Hold at Maximum Strain	70
61a	Crack Growth Data for TMF Specimen 11297 Counterclockwise Cycling With a One Minute Hold at Maximum Temperature. Crack Length (2a) Versus Cycles (N); b) da/dN Versus Delta K	72
62	Composite Plot, Rapid Cycle da/dN Versus Kmax R = 0	76
63	Composite Plot, Rapid Cycle da/dN Versus Kmax R = -1	76
64	Composite Plot, Rapid Cycle da/dN Versus Kmax R = -3	77
65a	Dynamic Modulus of Ti-48Al-1V Versus Temperature	77
65b	0.2% Yield Strength of Ti-48Al-1V Versus Temperature	78
65c	Opening Crack Tip Stretch Versus Temperature	78
66	da/dN Versus Crack Tip Opening, Rapid Cycle Load Controlled Test Results	80

LIST OF ILLUSTRATIONS (Concluded)

<u>Number</u>	<u>Title</u>	<u>Page</u>
67	da/dN Versus Crack Tip Opening, Rapid Cycle Strain Controlled Test Results	80
68	Strain Controlled da/dN Versus Crack Tip Opening, Dwell Data	81
69	Load Controlled da/dN Versus Crack Tip Opening, Dwell Data	81
70	Dwell Fatigue Test data at 815°C (1500°F), Oxide Wedging Model Improves Correlation	83
71	Dwell Fatigue Test Data at 736°C (1360°F), Oxide Wedging Model Improves Correlation	84
72	Dwell Fatigue Tests at 650° (1200°F)	85
73	da/dN Versus Cracking Tip Opening, TMF Cycle I	85
74	da/dN Versus Crack Tip Opening, TMF Cycle II	86
75	da/dN Versus Crack Tip Opening, TMF Cycle III	87
76	Fracture Surface of da/dN Specimen 10766 after Misc. 815°C (1500°F) dwell test. Note heavy oxide in (b) and cleavage fracture in (c) and (d).	89
77	Cross Section of Isothermal da/dN Specimens Tested at Various Temperatures. a) 815°C (1500°F) at Starter Slot b) 815°C (1500°F) away from Starter Slot c) 736°C (1360°F) at Starter Slot d) 650°C (1200°F) at Starter Slot	90
78	Cold Proof Test, Results and Analysis	91
79	The Effect of Test Temperature and Sequence on the Apparent Fracture Toughness	92

LIST OF TABLES

Number	Title	Page
1	Chemical Composition in Weight % of Titanium Aluminide Test Bar Samples Compared to Initial Ingot Analysis	4
2	Specimens Allocated for Baseline Fracture Mechanics Testing	7
3	Specimens Allocated for Baseline Fracture Mechanics Testing of Ti-48Al-1V	9
4	Specimens Allocated for Baseline Fracture Mechanics Testing of Ti-48Al-1V	10
5	Subcomponent Precrack Information	13
6	Cold Proof Test Results of Three Point Bend Specimens	55
7	Tensile Warm Prestress Results	56
8	Compressive Warm Prestress Results	57
9	Subcomponent Test Results	59

SECTION I

INTRODUCTION

1. BACKGROUND

In the past, major advances in gas turbine engine technology had been associated with the development of improved nickel and cobalt base superalloys and the conventional alpha-beta titanium alloys. The high temperature properties of current alpha-beta titanium alloys have improved to the point where the majority of compressors in advanced engines utilize these lightweight materials. Further extension of the use of lightweight materials to higher temperature structures in the turbine or afterburner sections of the engine is highly desirable; however conventional titanium alloys offer only limited scope for improvement, and thus, few new applications can be anticipated in these areas.

Titanium rich alloys, based on the intermetallic compounds $TiAl$ and Ti_3Al , have been identified which offer considerable advantage over conventional alloys in high temperature environments as a result of their excellent creep rupture behavior and very light weight. Design analyses and payoff studies conducted on these materials have indicated significant weight savings can be achieved in a wide range of engine applications. Turbine rotor weight savings from 30 to 40 percent (three to five percent of engine weight) would be achieved with widespread application of the titanium aluminides in rotating hardware; weight savings of up to 16 percent could be achieved in engine static structure applications such as vanes, cases and bearing supports. Beyond the immediate and obvious savings in engine weight, it is possible to translate these benefits into significant fuel savings with attendant effects on operation cost.

During the past eight years, Pratt & Whitney has participated in Air Force Materials Laboratory sponsored programs directed toward the understanding and exploitation of alloys based on both the Ti_3Al and $TiAl$ phases. Contract F33615-C-75-1167 performed alloy and process development on Ti_3Al alloys; Contracts F33615-C-74-1140 and F33615-C-75-1166 have conducted similar development efforts on $TiAl$ alloys. The goals in all programs were to identify processes and characterize alloys from the base systems that exhibited useful properties. Results from the first parts of these studies have been presented in previous reports (References 1-7).

Alloys based on the intermetallic phases in the titanium aluminum systems (Ti_3Al and $TiAl$) are now available with sufficient tensile ductility at room temperature to indicate that components can be fabricated for and function in a gas turbine environment. This should allow the benefit of lower density and higher temperature capability of the alloys to be realized. However, a potential limit to the usefulness of titanium aluminides is the low toughness and rapid crack growth rates observed at ambient temperatures.

The program described here had two major objectives: to scale up the alloys and to then determine the potential effect of engine cycles on the performance of one alloy. During the Task I portion of the current program, compositions from the Ti₃Al and TiAl alloy systems showing the best balance of properties were selected. Large ingots were cast in both compositions and processed using a variety of techniques to demonstrate the feasibility of producing several product forms such as near net shape castings, forgings and sheet. The effect of metal removal and finishing methods on the surface condition of gamma alloys was studied. Task II consisted of comprehensive physical and mechanical property measurements on the selected alloys. Included was an evaluation of the influence of simulated service exposure on surface stability and properties. The results of Task I and II are discussed in the earlier report on this program (Reference 8).

2. APPROACH

The objectives of the remainder of the current program were to gather additional base line fracture mechanics data for an alloy based upon the TiAl system and explore methods to increase the apparent fracture toughness of the alloy at temperatures below where full tensile ductility is exhibited. Data obtained in this phase of the program will permit the sensitivity of the TiAl material to pre-existent or service operation induced defects to be assessed; specifically to determine if extraordinary inspection methods are required to assure damage tolerance in components designed to fully utilize the design tensile, creep or fatigue properties of the alloy or conversely, to determine if operating stress levels are to be limited to satisfy damage tolerance criteria. The specimens and tests were designed to model the behavior of a specific turbine engine component, a low pressure turbine blade. Thus, the results of this program are directly applicable to the component development activity under Contract F33615-79-C-2091 in which JT9D 5th stage low pressure turbine blades are being cast. The blade is described in more detail below. This portion of the program was divided into five technical tasks.

In Task III an alloy of the gamma TiAl family was selected, bar and plate stock were cast and hot isostatically pressed (HIP'ed) for subsequent machining into fracture toughness and crack growth specimens.

In Task IV, tubular crack growth specimens were utilized to obtain isothermal crack growth data spanning the temperature range from 21°C to 815°C (70°F to 1500°F.)

In Task V, precracked slow bend specimens were stressed to the yield point at ambient conditions to evaluate the efficacy of cold proof testing as a flaw detection technique. Additional precracked slow bend specimens were prestressed at a temperature above the ductile-brittle transition temperature. The purpose of this task was to assess the beneficial effect of warm prestressing above the ductile-brittle transition temperature on the room temperature fracture toughness of the titanium aluminide. Two unload/cool down cycles from the prestress conditions were considered.

The purpose of Task VI was to verify that the cold proof test and warm prestressing effects studied in Task V were applicable to notched specimens (which can serve as simulated subcomponents). A number of center-cracked plate specimens were cycled to obtain fatigue cracks of about 6mm (0.25 inch) in length. A hole was then drilled in each specimen, removing all but the tip of the crack. One-half of the specimens were tested for single cycle fracture toughness and for fatigue resistance at room temperature. The remaining specimens were warm prestressed prior to testing at room temperature for single cycle fracture toughness and/or fatigue resistance.

The purpose of Task VII was to determine the crack propagation resistance of gamma titanium aluminide for design-relevant thermomechanical fatigue cycles. Based on potential applications for the gamma alloys, component details subject to fatigue damage were identified and for each, estimates of the cyclic temperature/load history throughout a typical engine were determined. A test matrix of design-relevant thermomechanical crack growth tests was established and test data accumulated. The resultant data were reviewed relative to the isothermal crack growth data produced in Task IV.

SECTION II

EXPERIMENTAL DETAILS

1. TASK III - ALLOY SELECTION

a. Material Procurement and Processing

Based upon the results of contracts F33615-79-C-2091 and F33615-80-C-5163, a cast gamma TiAl alloy with composition of Ti-48%Al-1%V (Ti-34 w/o Al-1.3 w/o V) appeared to offer the best balance of properties and was selected as the study material for this contract. Related studies indicated that a 1232°C/172 MPa/4 hour (2250°F/25 ksi/4 hour) hot isostatic press (HIP) operation effectively sealed internal porosity without incurring an increase in grain size, while the preferred heat treatment consisted of a single step solution heat treatment at 1287°C (2350°F) in argon followed by fan air cooling. Twenty-four cast bars 25mm diameter x 300mm long (1 inch diameter x 12 inch long) and eight cast plates 100mm wide x 200mm long x 3.2mm thick (4 inch x 8 inch x 0.125 inch) were procured from Howmet, Ti-Cast Division, Whitehall MI. The cast material was HIP'ed and heat treated as described above. Chemical composition of the material was acceptable and analysis is given in Table 1. Typical microstructure of the heat treated alloy is shown in Figure 1.

TABLE 1

CHEMICAL COMPOSITION IN WEIGHT % OF TITANIUM
ALUMINIDE TEST BAR SAMPLES COMPARED
TO INITIAL INGOT ANALYSIS

Specimen Location	Al	V	Fe	C	Si	O ₂	N ₂	H ₂
Ingot Top	33.3	1.36	0.10	-	0.04	0.10	0.015	-
Ingot Bottom	33.3	1.37	0.10	-	0.04	0.11	0.015	-
Cast Bar	33.6	1.3	0.09	0.027	-	0.119	0.013	0.0014
Aim Weight %	34.0+ 1.0	1.3+ 0.3	<0.10	<0.05	<0.2	0.1	-	-
Atomic %	48.0	1.0	-	0.08	-	-	-	-

b. Specimen Machining

Test specimens selected for the program are shown in Figure 2. A combination of electro discharge machining (EDM) and conventional grinding using previously developed parameters was employed to produce the specimens. Little trouble was encountered in spite of the complex configurations involved.



100X



100X



500X

Figure 1

Typical Microstructure of Cast + HIP Ti-48Al-1V Alloy After
Solution Heat Treatment of 1287°C (2350°F)/1 Hour/Followed by
Air Cooling

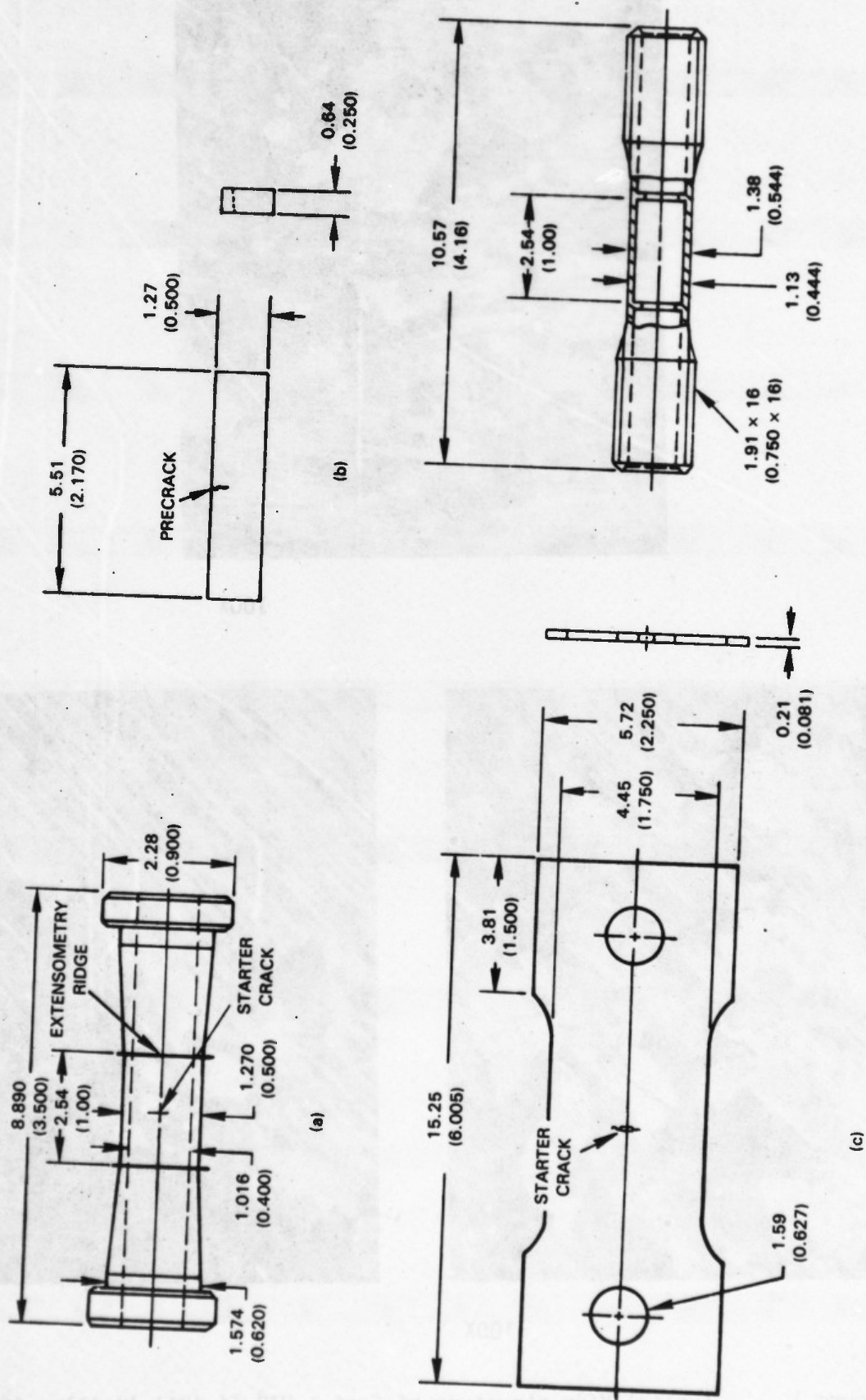


Figure 2 Specimen Configurations Selected for Evaluation of Damage Tolerant Design for Cast/HIP Ti-48Al-1V Alloy

2. TASK IV BASELINE ISOTHERMAL FRACTURE MECHANICS TESTING

a. Load and Displacement Controlled Isothermal Crack Growth Testing

The purpose of this testing was to establish the crack growth rate behavior of the TiAl alloy at component relevant temperatures and R-ratios (minimum to maximum stress ratio). To establish a matrix of test conditions, the operating environment of a gamma TiAl low pressure turbine blade was considered (Figure 3).

The airfoil is subjected to a thermomechanical load cycle. At the fatigue critical leading and trailing edge locations outboard of the quarter span section, local strains are primarily the result of chordal temperature gradients. Peak operating temperatures may approach 815°C (1500°F) and the local mechanical strain history is typically compressive in nature. To simulate crack growth at this location, the externally ridged tubular crack growth specimen configuration illustrated in Figure 4a was utilized. Isothermal strain controlled testing was conducted at 738°C (1360°F) and 815°C (1500°F). The matrix of simple cycle strain controlled tests and allocation of the test specimens is presented in Table 2.

TABLE 2
SPECIMENS ALLOCATED FOR BASELINE FRACTURE MECHANICS TESTING
OF Ti-48Al-1V

Simple Cycle Strain Controlled Test Conditions (6 cpm)

Strain Ratio	Test Temperature °C (°F)	
	740 (1360)	815 (1500)
0	10771	10768
-1	10769/70	10766
-3	10775	10773

Prolonged exposure at high temperature can significantly influence the rate of cyclic crack growth. The test plan also provided for accumulation of limited dwell-fatigue crack growth data under strain controlled conditions. Following the acquisition of the simple cycle (6 cycles per minute) crack growth data, the specimen test conditions were altered to include a one minute constant strain hold at either the tensile or compressive strain limit. The test plan for this portion of the effort is presented in Table 3.

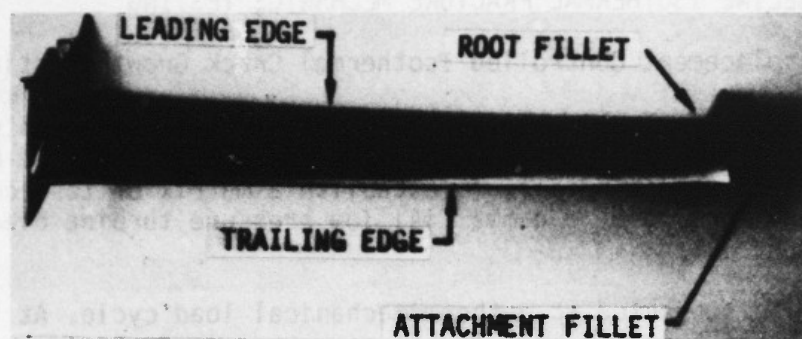
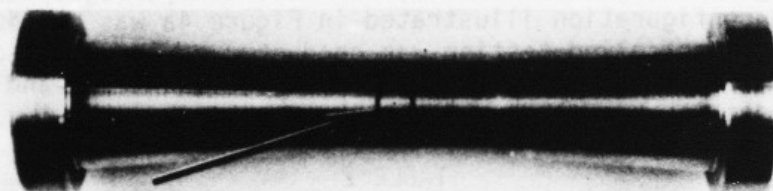


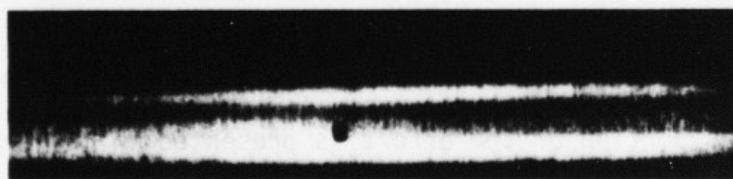
Figure 3 JT9D Ti-48A1-1V Cast Low Pressure Turbine Blade



(a)



(b)



(c)

Figure 4 Specimens Used for Determining Crack Growth Behavior of Ti-48A1-1V. (a) Specimen with external ridges for strain controlled test; (b) Smooth specimen for load controlled test; (c) EDM starter notch (arrow).

TABLE 3
SPECIMENS ALLOCATED FOR BASELINE FRACTURE MECHANICS TESTING
OF Ti-48A1-1V

Dwell Fatigue Test Conditions

Strain Ratio	Cycle Type	Test Temperature °C (°F)	
		740 (1360)	815 (1500)
0	1 min. dwell at tensile strain limit	10771	10768
-1	1 min dwell at tensile and compressive strain limit	10770	10766
-3	1 min. dwell at compressive strain limit	10775	10773

The turbine blade attachment (Figure 3) is subjected to centrifugal and gas pressure loading but no appreciable thermal stress. Peak operating temperatures may approach 650°C (1200°F) and the local mechanical strain history is typically tensile in nature. The attachment net section creep strain rate and cyclic inelastic strains are negligible. Load controlled testing of smooth ridgeless tubular crack growth specimens, illustrated in Figure 4b, was performed to study crack growth at the lower temperature. The matrix of simple cycle load controlled tests is presented in Table 4. Load controlled testing was performed on an Instron servo controlled test machine with 9100Kg (20,000 pound) load capability. Feedback was provided by a calibrated strain load cell and was capable of controlling the accuracy of the load relative to the function generator input signal to within one percent of the load range. Strain controlled tests were conducted in a load frame of similar load capacity; a linear variable differential transformer (LVDT) was used to measure the specimen elongation between the ridges located on the outer diameter (OD) of the specimen gage section. The output signal was compared to the programmed input signal and a differential signal generated for adjusting the strain amplitude. Strain was controlled to within 1% of the strain amplitude. Strain controlled specimens were heated by a low frequency (10 HZ) induction generator. A precalibrated radiation pyrometer (Ircon Model 7000) was used to control specimen temperature to within $\pm 2.8^{\circ}\text{C}$ ($\pm 5^{\circ}\text{F}$) at elevated temperature. Load controlled specimens were furnace heated with temperature control provided by a thermocouple mounted directly on the specimen. A 0.25mm (0.010 inch) starter notch was machined by EDM in each specimen (Figure 4c). Following initiation, crack length was monitored using a 50X travelling telescope equipped with a calibrated micrometer graduated to 0.013mm (0.0005 inch). Crack length (2a) versus cycle number (N) data was plotted, smoothed and curve fit using the moving seven point polynomial method to obtain da/dN versus k data.

TABLE 4
SPECIMENS ALLOCATED FOR BASELINE FRACTURE MECHANICS TESTING
OF T1-48A1-1V

Simple Cycle Load Controlled Test Conditions (6 cpm)

Stress Ratio	Test Temperature °C (°F)			
	RT	316 (600)	565 (1050)	650 (1200)
0	10765	10777	10776, 10778	10774, 10772, 10767
-1		10777	10776, 10778	10774, 10772, 10767

The stress intensity solution for the hollow tubular crack growth specimen is given as:

$$K \langle \sigma \text{ or } \epsilon \rangle = \langle \sigma \text{ or } \epsilon \rangle \sqrt{\pi a} f(a^2/Rt)g(a/R)$$

where:

$\langle \sigma \text{ or } \epsilon \rangle$ is the nominal strain or stress range

$f(a^2/Rt)$ is the curvature correction factor for a circumferential crack in a cylinder of radius, R, and thickness, t, obtained from references (Reference 9, 10))

$g(a/R)$ is the geometric correction factor to convert projected length to arc length.

Crack growth data obtained immediately after a load change were considered suspect due to transient overload effects. Data were considered valid and reported when the crack length had extended an additional twenty percent beyond the point of load or cycle change. In general, both $R = 0$ and $R = -1$ crack growth data were obtained from the same specimen by altering the loading condition when adequate $R = 0$ data had been obtained.

3. TASK V PRESTRESSING EFFECTS ON FRACTURE TOUGHNESS

Twenty unnotched slow bend specimens (Figure 2b) were allocated for this task. Various techniques for starting small surface flaws were evaluated since the program required that eight specimens be prepared containing centered flaws no larger than 0.5mm (0.020 inch) while the twelve remaining specimens be precracked so that all contained centered surface flaws of the same length between 0.8 and 1.3mm (0.032 and 0.050 inch). It was necessary to develop a nonstandard precracking technique to achieve this requirement. It consisted of placing two slots in the center of the bend specimen by EDM techniques leaving a small ligament as a crack starter (Figure 5). The specimen was fatigue

tested in compression and the crack growth monitored. When the crack reached the base of the ligament, fatigue testing was stopped. The starter slot was then removed by grinding, leaving a shallow surface flaw centered on the specimen. Three specimens either failed or were found to be uncracked following starter notch removal; however, the remaining seventeen specimens were deemed to be adequate for subsequent testing. Of the seventeen specimens, two were through flawed, five had shallow cracks 0.25mm (0.010 inch) deep, and the balance had surface cracks of intermediate length. All specimens were furnace heat treated for one hour at 537°C (1000°F) to mark the crack front.

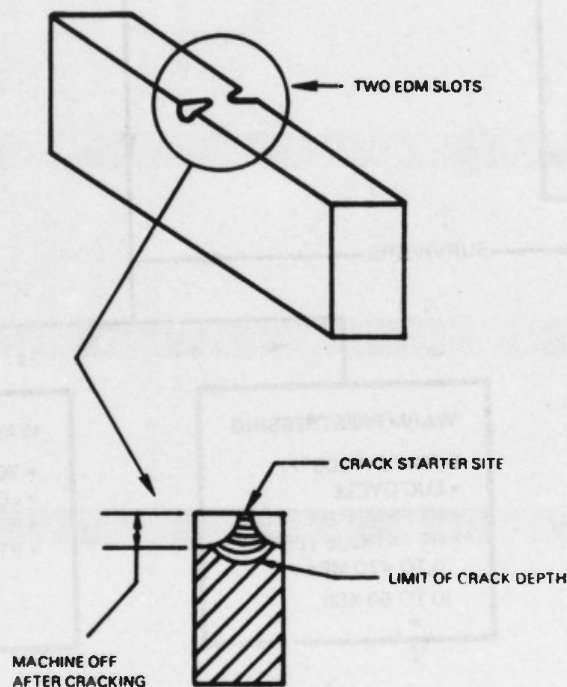
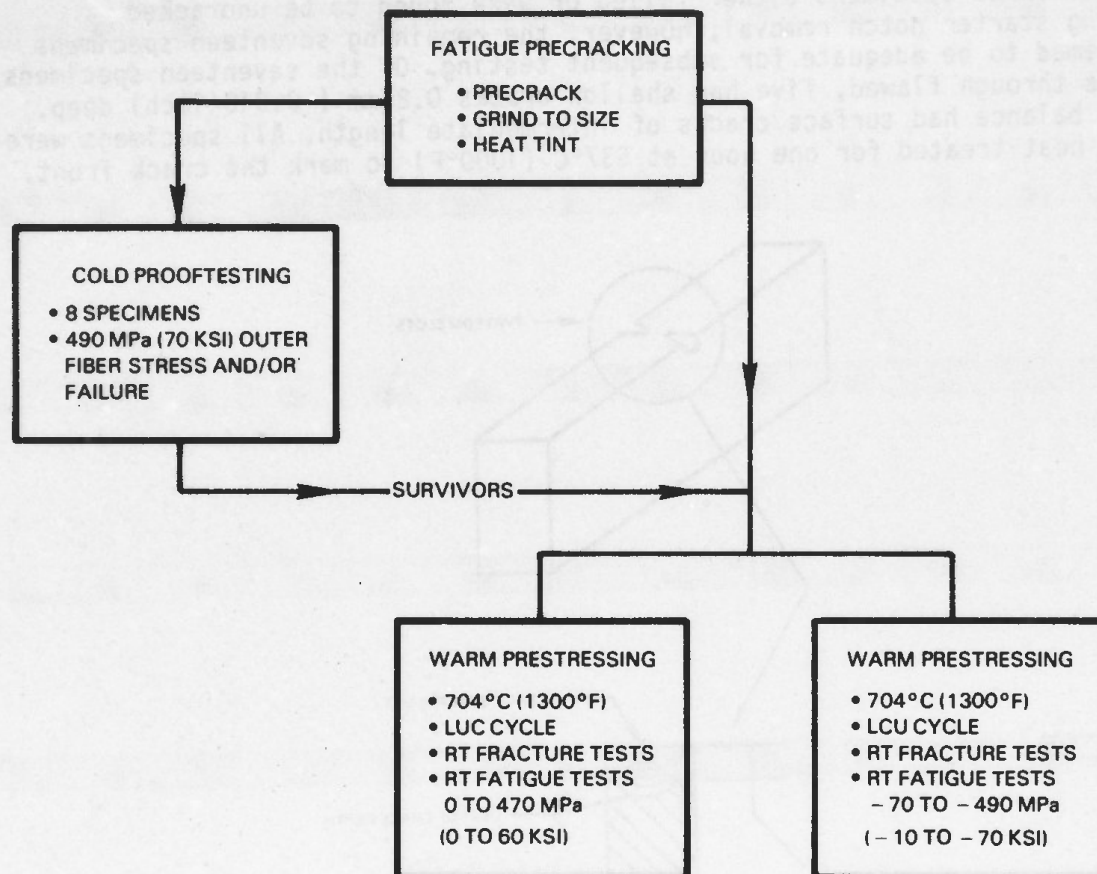


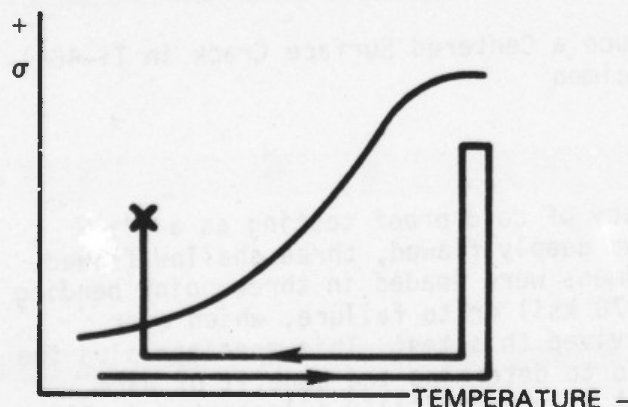
Figure 5 Technique Used to Produce a Centered Surface Crack in Ti-48Al-1V Fracture Toughness Specimen

Using these specimens, the efficacy of cold proof testing as a flaw detection method was investigated. Two deeply flawed, three shallow flawed, and three intermediately flawed specimens were loaded in three point bending to an outer fiber stress of 490 MPa (70 ksi) or to failure, whichever occurred first. Only one specimen survived this test. This specimen plus the nine virgin specimens were then tested to determine the benefit of warm prestressing. The plan for this effort is schematically illustrated in Figure 6. Five of the virgin specimens were subjected to the 704°C (1300°F) load-unload-cooldown (LUC) warm prestress cycle simulating a mechanical prestress operation, Figure 6b. Three of the specimens failed during this warm prestress operation. One of the surviving specimens was monotonically loaded to failure at room temperature and the other was room temperature fatigue tested to failure at 0-420 MPa (0-60 ksi) outer fiber stress. The one shallow

a) TEST PLAN



b) LOAD-UNLOAD-COOLDOWN CYCLE (LUC)



c) LOAD-COOLDOWN-UNLOAD CYCLE (LCU)

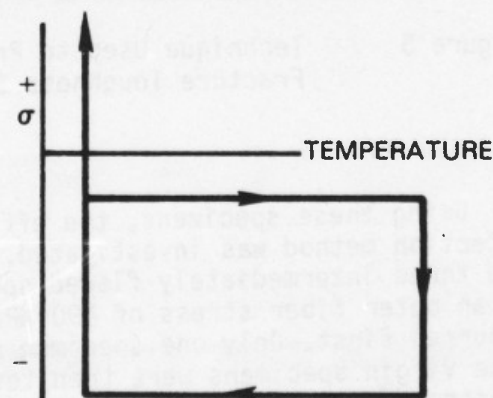


Figure 6 Test Plan to Determine Prestress Effects on Fracture Toughness of Ti-48Al-1V

cracked specimen that survived the cold proof test and four virgin specimens were subjected to the 704°C (1300°F) load-cooldown-unload (LCU) warm compression prestress cycle simulating a selective warm surface prestrain, Figure 6c. Three specimens were fatigue tested at -70 to -490 MPa (-10 to -70 ksi) and the remaining two were tensile tested to failure. P-8 records were recorded for all prestress or monotonic failure testing. Post-failure investigation included detailed characterization of the initial flaw size.

4. TASK VI SUBCOMPONENT TESTING TO DEMONSTRATE THE BENEFITS OF WARM PRESTRESSING.

A limited effort was conducted to demonstrate the advantages (or lack thereof) of cold and warm proof testing of intermetallic components. Eight EDM preflawed flat plate specimens (Figure 2c) were prepared for the purpose. Each center crack panel specimen was room temperature cycled at a maximum nominal stress of 120-140 MPa (17-20 ksi) until a fatigue precrack of approximately 6.4mm (0.25 inch) in length was obtained. Two specimens failed during precracking. Table 5 presents pertinent information for the surviving specimens. A 6.4mm (0.25 inch) hole was then electro discharge machined in each plate to remove all but 0.12mm to 0.56mm (0.005 inch to 0.022 inch) of the crack tip. All specimens were heat tinted at 537°C (1000°F) for one hour to mark the crack front prior to subsequent testing. Replicas were also taken under load to determine the length of the cracks subsequent to placement of the hole. The test plan is presented in Figure 7. Three specimens were prestressed at 704°C (1300°F) to 270 MPa (38.5 ksi). The load was maintained for one half hour at this condition. Reinforcing tabs were placed in the grip ends of the six test specimens to prevent grip failures during subsequent room temperature tensile and fatigue testing. One warm prestressed and one virgin specimen were proof tested to failure at room temperature. The four remaining specimens were fatigue tested to failure at room temperature.

TABLE 5
SUBCOMPONENT PRECRACK INFORMATION

SPECIMEN SERIAL NUMBER	PRECRACK		PRECRACK	
	STRESS		LENGTH	
	LEVEL			
	MPa	(ksi)	mm	(in)
3f	120	(17)	7.1	(0.279)
4f	140	(20)	6.6	(0.260)
5f	140	(20)	6.5	(0.255)
6f	140	(20)	6.6	(0.259)
7f	140	(20)	7.4	(0.290)
8f	140	(20)	6.5	(0.255)

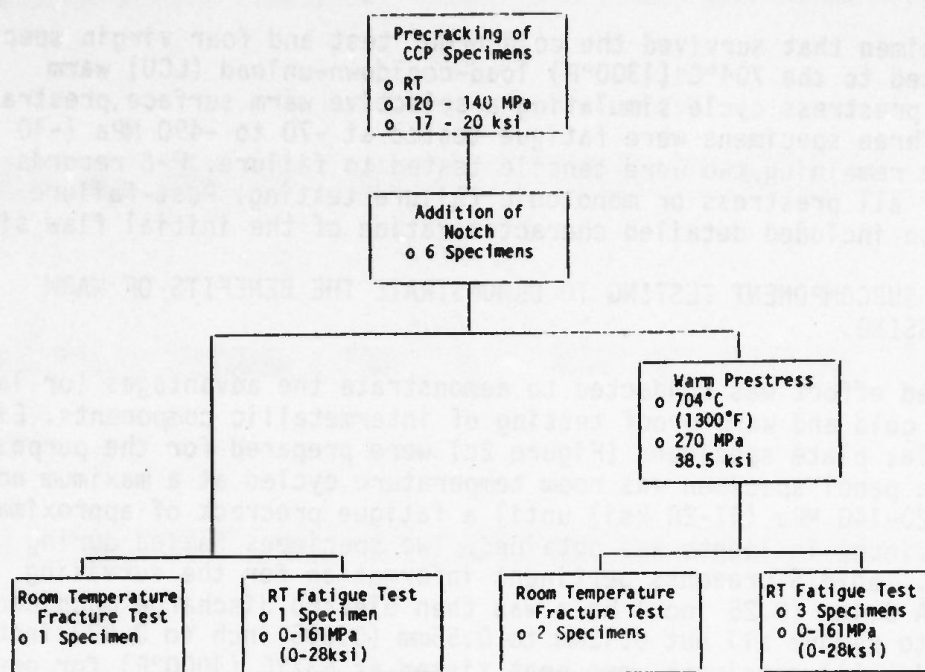


Figure 7 Subcomponent Demonstration Plan for Ti-48Al-1V

5. TASK VII ATHERMAL (TMF) STRAIN CONTROLLED CRACK GROWTH TESTING

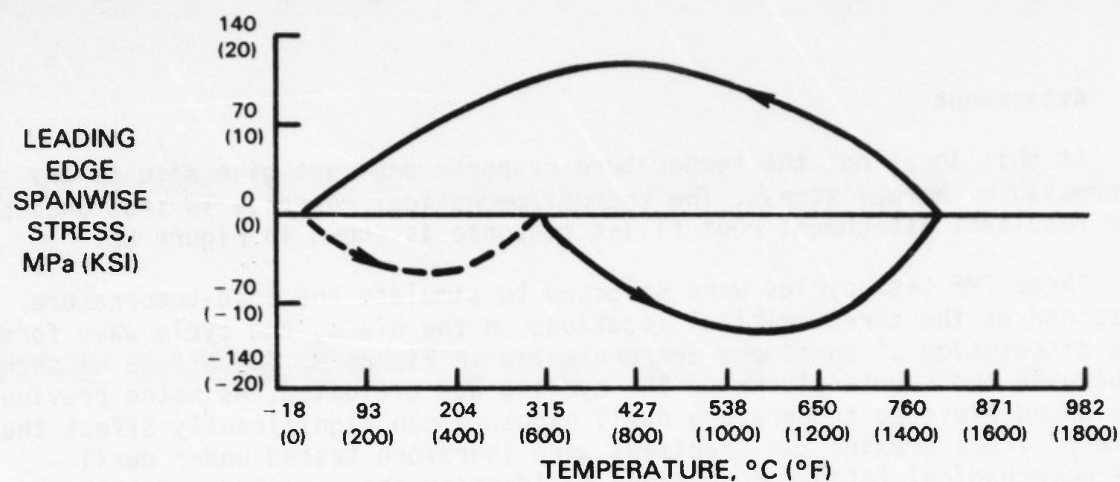
Crack growth in engine parts does not occur under isothermal conditions. The utility of isothermal fracture mechanics data for residual life calculations is, therefore, open to question, particularly if properties are noted to change dramatically with temperature. To determine if simultaneous cycling of the temperature and load influences the growth of a crack, three test cycles were proposed. Test cycles were selected to simulate the conditions at three critical locations on the turbine blade, as described below.

a. Midspan Airfoil Leading or Trailing Edge

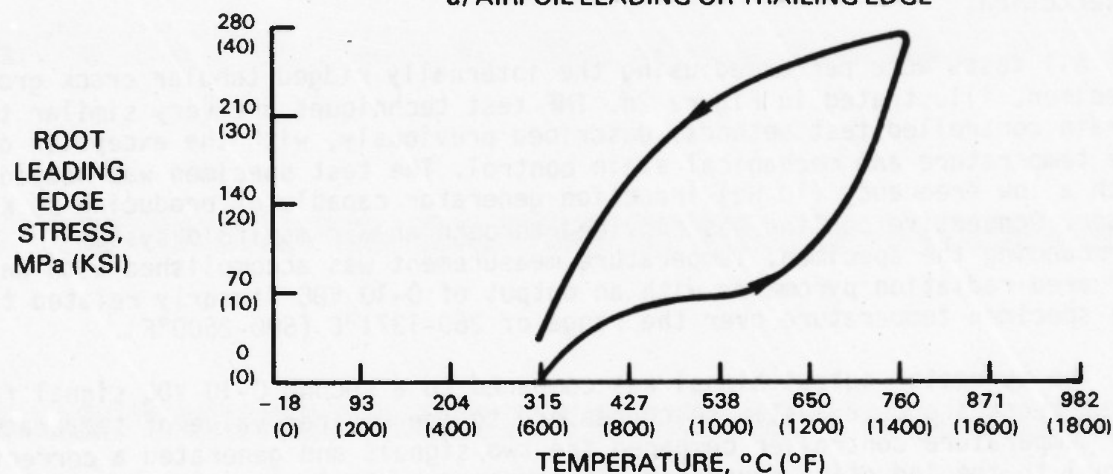
This location is subject to foreign object damage. Mechanical loadings at this position on the blade are low and stresses are induced by the gradient in temperature between the airfoil leading edge and midchord during transient operating conditions. A thermal-stress analysis of a prototype low pressure turbine blade was conducted, the resultant leading edge response is shown in Figure 8a.

b. Airfoil Root/Platform Fillet

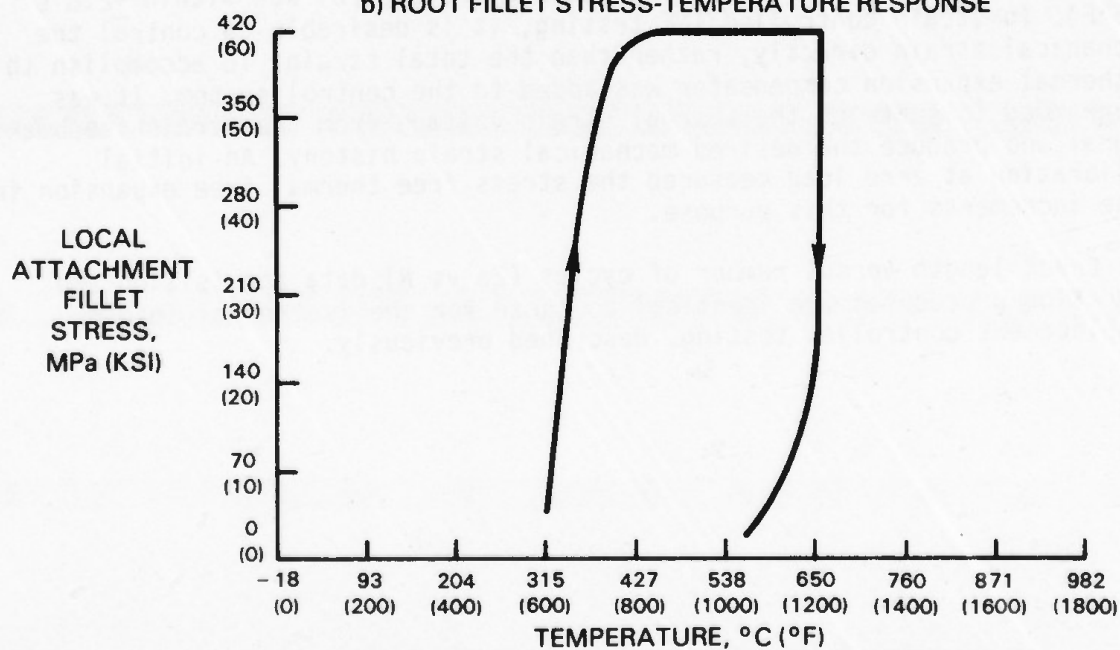
At this location, mechanical loading is not inconsequential. During the transient acceleration to high output power, the thermal stresses are compressive and the combined thermal-mechanical stresses are near zero. At steady-state conditions, the loading on the fillet is predominantly mechanical. During the transient deceleration to idle, the thermal stresses are tensile which add to the mechanical loading. The resultant airfoil root leading edge fillet response is shown in Figure 8b.



a) AIRFOIL LEADING OR TRAILING EDGE



b) ROOT FILLET STRESS-TEMPERATURE RESPONSE



c) ATTACHMENT FILLET STRESS-TEMPERATURE RESPONSE

Figure 8 Thermomechanical Response of Three Locations on the Low Pressure Turbine Blade

c. Attachment

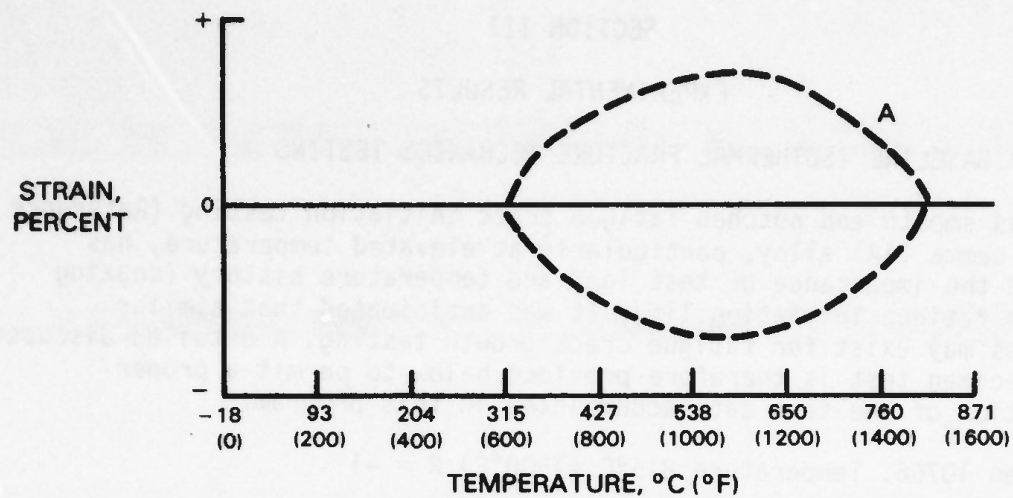
At this location, the temperature response does not give rise to any appreciable thermal stress. The thermal/mechanical response is thus uncoupled. The resultant attachment root fillet response is shown in Figure 8c.

Three TMF test cycles were selected to simulate the load-temperature response at the three critical locations on the blade, the cycle wave forms and disposition of specimens are presented in Figure 9. The effect of both clockwise and counterclockwise TMF cycling was evaluated. As noted previously, prolonged elevated temperature dwell exposure can significantly affect the rate of crack growth; two specimens were therefore tested under dwell - thermomechanical fatigue conditions to identify the magnitude of this interaction.

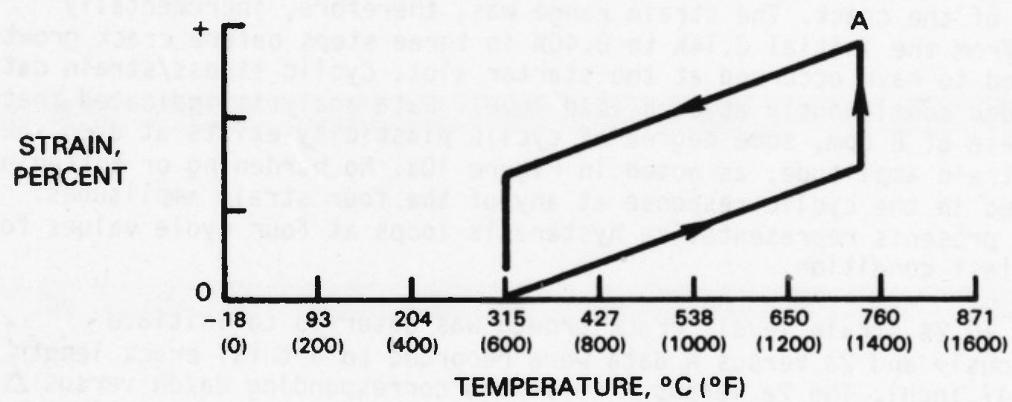
All tests were performed using the internally ridged tubular crack growth specimen, illustrated in Figure 2d. TMF test techniques are very similar to strain controlled test methods, described previously, with the exception of the temperature and mechanical strain control. The test specimen was heated with a low frequency (10 Hz) induction generator capable of producing 20 KW power. Convective cooling was provided through an air manifold system surrounding the specimen. Temperature measurement was accomplished with an infrared radiation pyrometer with an output of 0-10 VDC linearly related to the specimen temperature over the range of 260-1371°C (500-2500°F).

The pyrometer output signal was compared to a second 0-10 VDC signal from a reference source adjusted to correspond to the desired value of temperature. The temperature controller compared the two signals and generated a corrective signal to the induction generator. Temperature control was within $\pm 2.8^{\circ}\text{C}$ ($\pm 5^{\circ}\text{F}$). In strain controlled TMF testing, it is desirable to control the mechanical strain directly, rather than the total strain. To accomplish this, a thermal expansion compensator was added to the control system. It was programmed to subtract the thermal strain voltage from the strain feedback signal and produce the desired mechanical strain history. An initial calibration at zero load measured the stress free thermal free expansion in fine increments for this purpose.

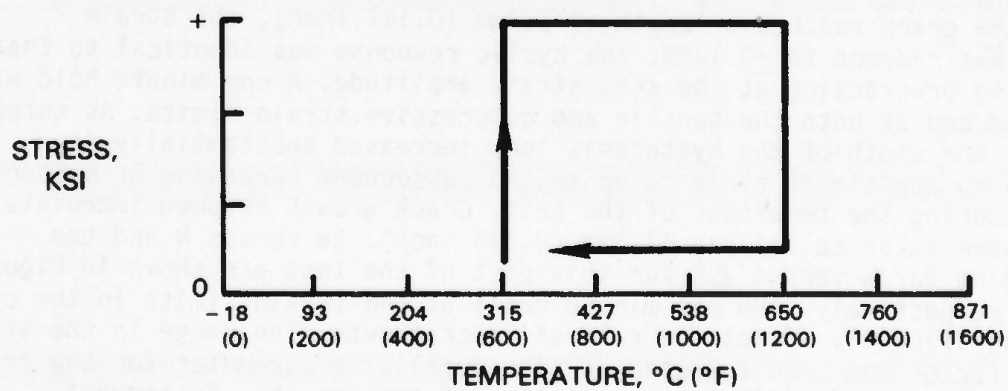
Crack length versus number of cycles (2a vs N) data acquisition and reduction procedures are identical to those for the isothermal load or displacement controlled testing, described previously.



a) CYCLE TYPE I — AIRFOIL LEADING EDGE
AND TRAILING EDGE CYCLE



b) CYCLE TYPE II — AIRFOIL ROOT LEADING EDGE



c) CYCLE TYPE III — ATTACHMENT FILLET

Figure 9 Test Cycles for Thermomechanical Crack Growth of Ti-48Al-1V

SECTION III

EXPERIMENTAL RESULTS

1. TASK IV BASELINE ISOTHERMAL FRACTURE MECHANICS TESTING

Previous smooth and notched fatigue crack initiation testing (Reference 11) of the gamma TiAl alloy, particularly at elevated temperature, has highlighted the importance of test load and temperature history (coaxing effects) on fatigue initiation life. It was anticipated that similar interactions may exist for fatigue crack growth testing. A detailed discussion of each specimen test is therefore provided below to permit a proper interpretation of the test data accumulated in this program.

a. Specimen 10766, Temperature 815°C (1500°F) R = -1

Precracking of the specimen was difficult due to the higher level of ductility at elevated temperature and surface oxidation which reduced the visibility of the crack. The strain range was, therefore, incrementally increased from the initial 0.14% to 0.40% in three steps before crack growth was observed to have occurred at the starter slot. Cyclic stress/strain data were recorded continuously at each load level. Data analysis indicated that at a cyclic rate of 6 cpm, some degree of cyclic plasticity exists at even the smallest strain amplitude, as noted in Figure 10a. No hardening or softening was observed in the cyclic response at any of the four strain amplitudes. Figure 10b presents representative hysteresis loops at four cycle values for the $\pm 0.2\%$ test condition.

At the $\pm 0.2\%$ strain level, crack growth was observed to initiate instantaneously and 2a versus N data were recorded to a total crack length of 3.7mm (0.147 inch). The 2a versus N curve and corresponding da/dN versus ΔK relationship for this portion of the testing are shown in Figures 11 and 12, respectively.

When the crack reached a length of 3.7mm (0.147 inch), the strain amplitude was reduced to $\pm 0.125\%$. The cyclic response was identical to that noted during precracking at the same strain amplitude. A one minute hold was then introduced at both the tensile and compressive strain limits. As noted in Figure 13, the width of the hysteresis loop increased substantially in comparison to the simple cycle response. No subsequent hardening or softening was noted during the remainder of the test. Crack growth resumed immediately and data were taken to failure 11.3mm (0.446 inch). 2a versus N and the corresponding da/dN versus ΔK for this part of the test are shown in Figures 14 and 12 respectively. The one minute dwell at the strain limits in the cycle did not significantly affect the rate of crack growth. The range in the stress intensity factor has been selected as the normalizing parameter for the crack growth rate data to facilitate presentation of the results. Subsequent discussion will consider alternate normalizing parameters for crack growth modeling.

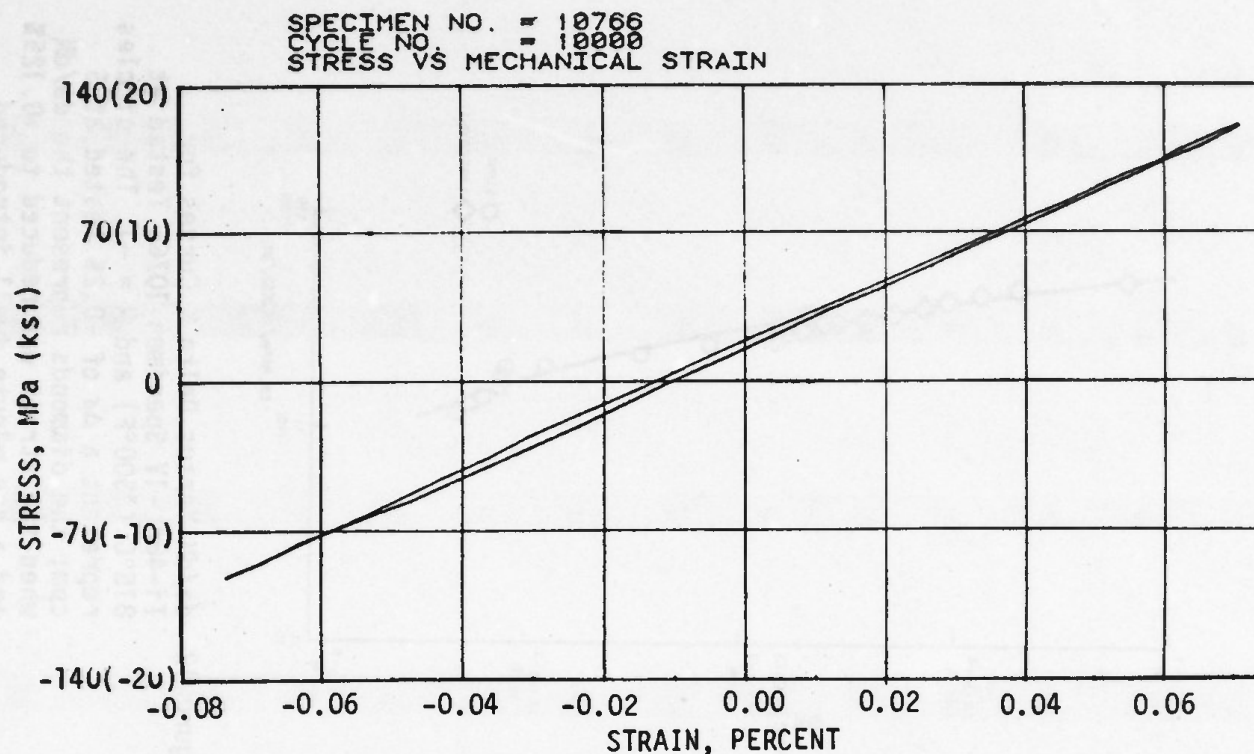


Figure 10a Hysteresis Loop Showing Small Cyclic Plasticity at $\pm 0.07\%$ Strain Range, 815°C (1500°F), 6 cpm for Ti-48Al-1V Specimen 10766

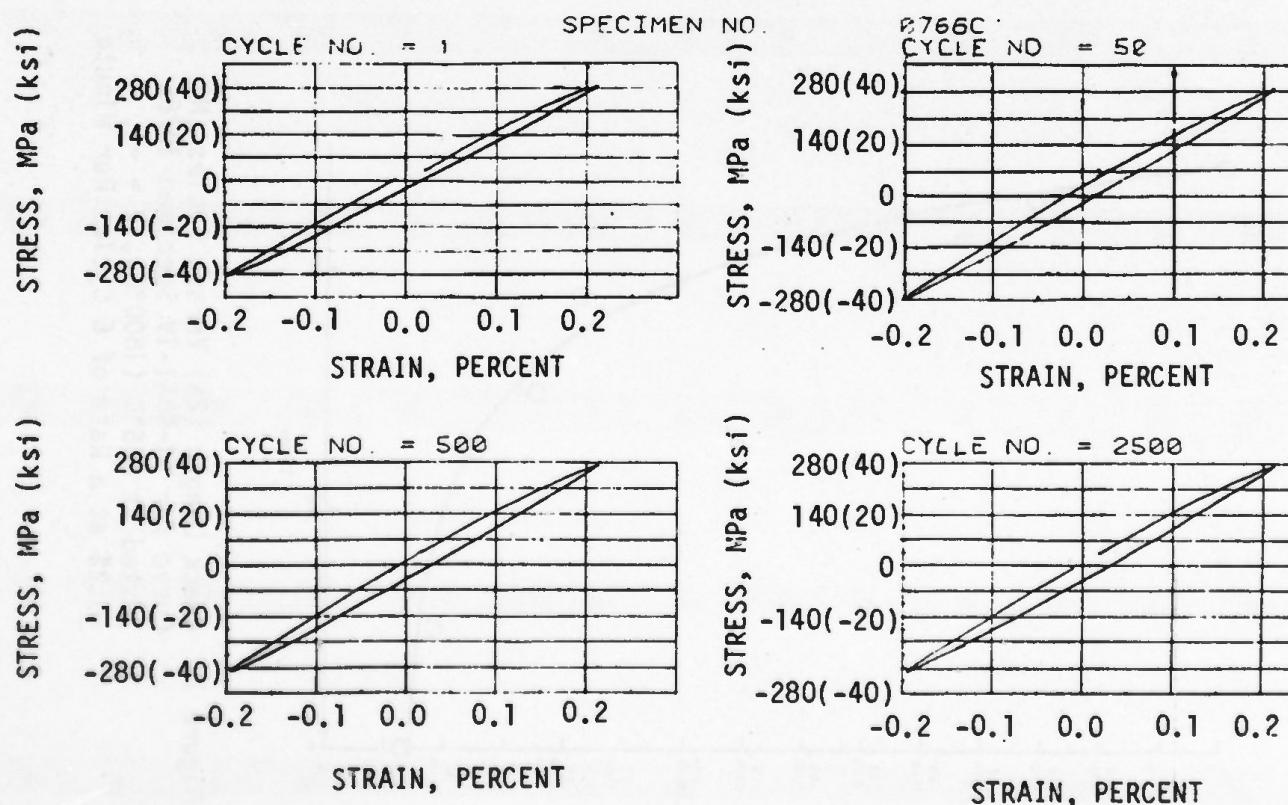


Figure 10b Hysteresis Loops Showing that No Cyclic Hardening or Softening Occurred at $\pm 0.2\%$ 815°C (1500°F), 6 cpm for Specimen 10766

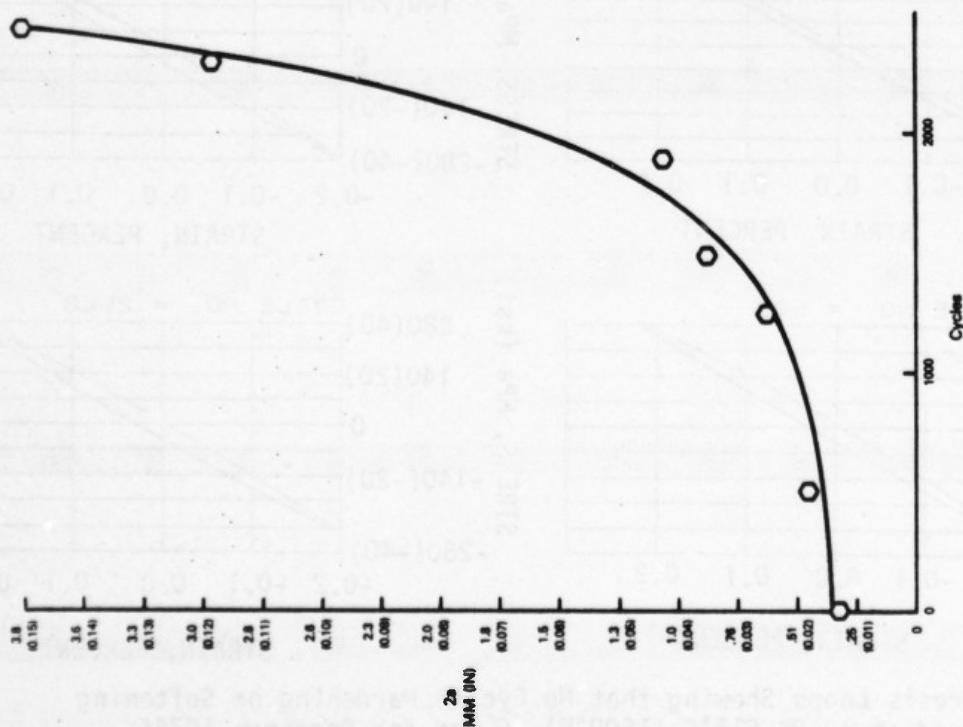


Figure 11 Crack Length (2a) Versus Cycles (N)
Curve for Ti-48Al-1V Specimen 10766
Tested at 815°C (1500°F), R = -1,
+0.2% at a Rate of 6 Cycles Per Minute

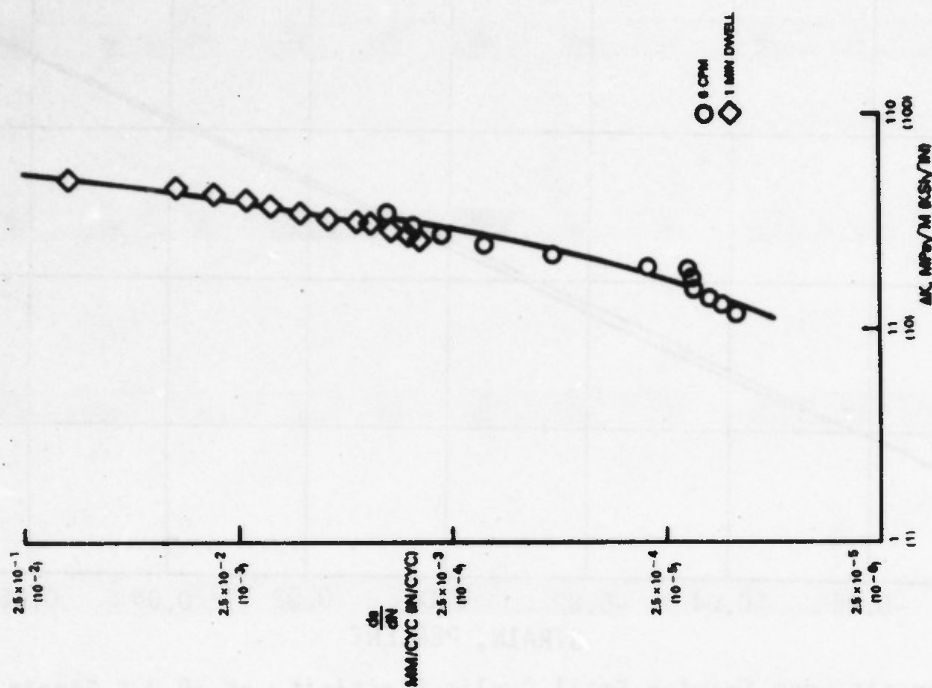


Figure 12 da/dN Versus Delta K Curves for
Ti-48Al-1V Specimen 10766 Tested at
815°C (1500°F) and R = -1. The circles
represent a $\Delta\epsilon$ of +0.2% tested at 6
cpm; the diamonds represent the da/dN
when the strain was reduced to +0.125%
and a one minute dwell introduced

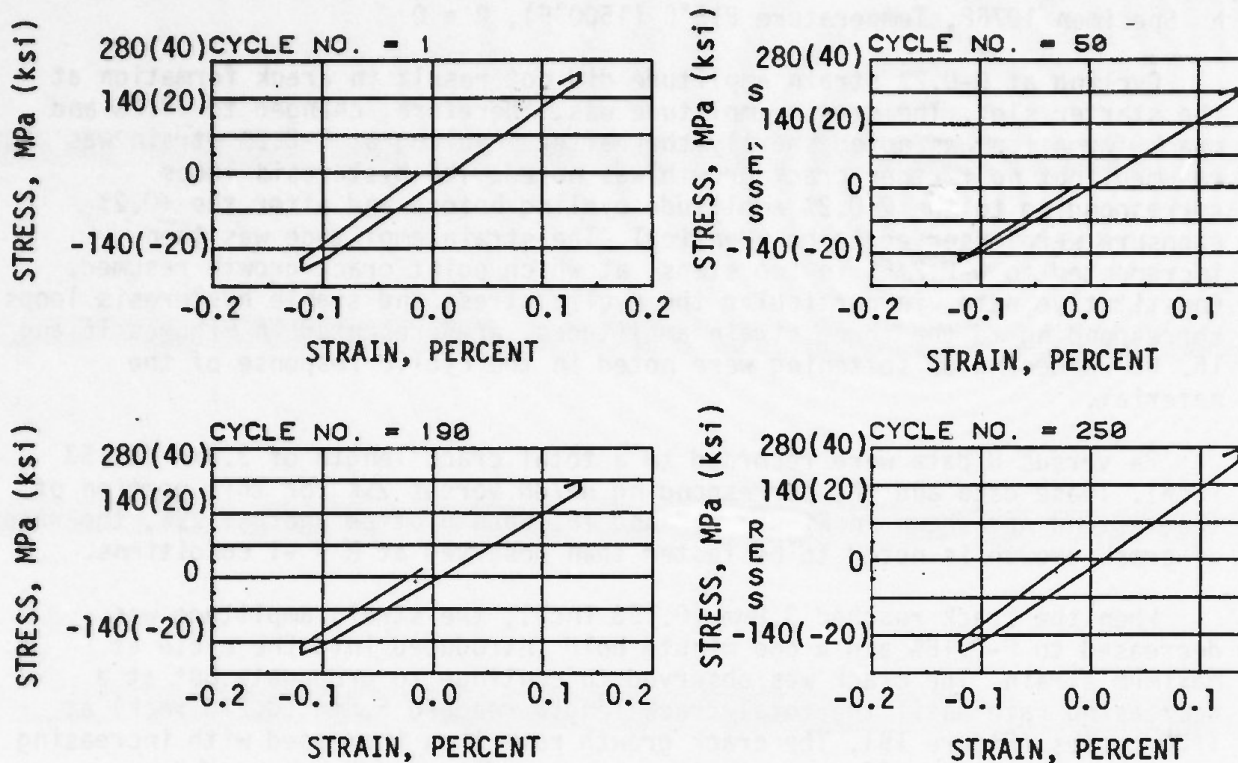


Figure 13 Effect of Constant Strain Holds at 815°C (1500°F) on the Width of the Hysteresis Loops; $R = -1$, $\Delta\epsilon = 0.125\%$.

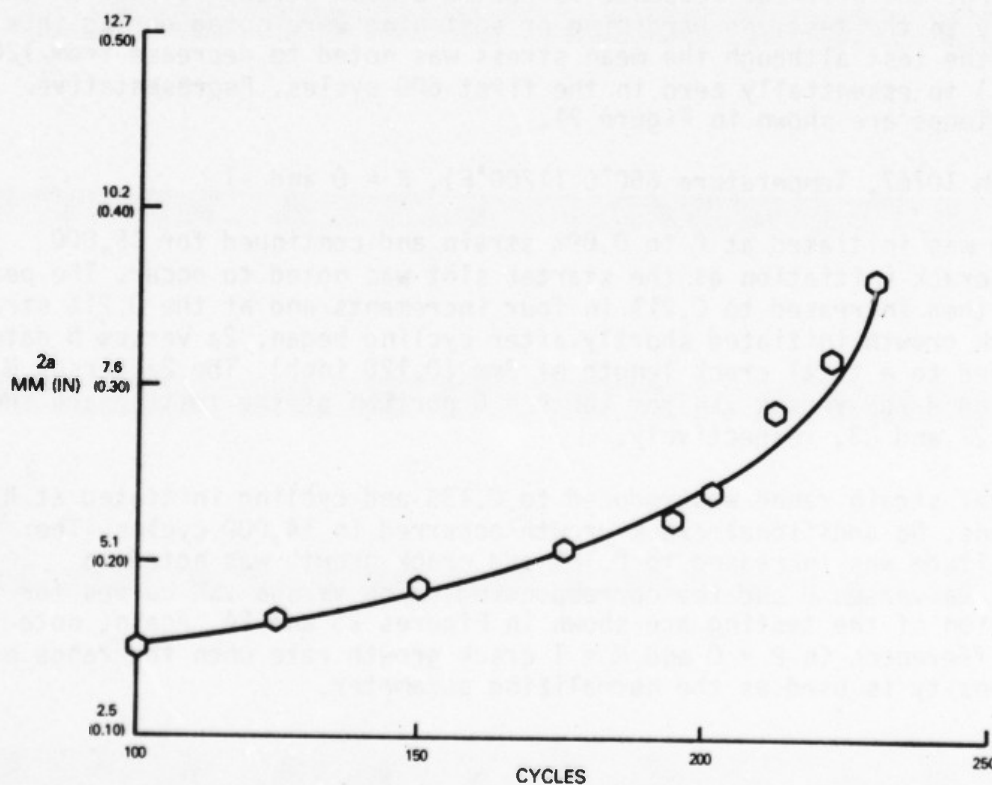


Figure 14 Crack Length ($2a$) Versus Cycles (N) for Ti-48Al-1V Specimen 10766 Tested at 815°C (1500°F), $R = -1$, $\Delta\epsilon = \pm 0.125\%$, With a One Minute Dwell During the Cycle

b Specimen 10768, Temperature 815°C (1500°F), $R = 0$

Cycling at 0-0.2% strain amplitude did not result in crack formation at the starter slot. The strain amplitude was, therefore, changed to +0.2% and crack formation was noted shortly thereafter. Cycling at 0-0.2% strain was resumed, but no further crack growth was noted. The hysteresis loops corresponding to the 0-0.2% amplitude cycling before and after the +0.2% exposure were observed to be identical. The strain amplitude was then incremented to 0-0.275% in two steps, at which point crack growth resumed. Constitutive data, in particular the cyclic stress and stable hysteresis loops corresponding to the three strain amplitudes, are presented in Figures 15 and 16. No hardening or softening were noted in the cyclic response of the material.

2a versus N data were recorded to a total crack length of 3.8mm (0.153 inch). These data and the corresponding da/dN versus ΔK for this portion of the testing are shown in Figures 17 and 18. When plotted against ΔK , the rate of crack growth is noted to be faster than observed at $R = -1$ conditions.

When the crack reached 3.8mm (0.153 inch), the strain amplitude was decreased to 0-0.18% and a one minute hold introduced into the cycle at maximum strain. The crack was observed to continue to propagate but at a decreasing rate until the total crack length reached 5.6mm (0.220 inch) at 1200 cycles (Figure 19). The crack growth rate then increased with increasing crack length. Figure 20 presents the corresponding da/dN versus ΔK curve. Note the bilinear shape to the curve and the apparent beneficial effect of the one minute dwell exposure at maximum strain. Subsequent analysis (Section V) indicates that the bilinear response is due to a mean stress relaxation that occurs early in the test. No hardening or softening were noted during this portion of the test although the mean stress was noted to decrease from 120 MPa (17 ksi) to essentially zero in the first 600 cycles. Representative hysteresis loops are shown in Figure 21.

c. Specimen 10767, Temperature 650°C (1200°F), $R = 0$ and -1

Cycling was initiated at 0 to 0.09% strain and continued for 15,000 cycles. No crack initiation at the starter slot was noted to occur. The peak strain was then increased to 0.21% in four increments and at the 0.21% strain level, crack growth initiated shortly after cycling began. 2a versus N data were recorded to a total crack length of 3mm (0.120 inch). The 2a versus N and corresponding da/dN versus ΔK for the $R = 0$ portion of the testing are shown in Figures 22 and 23, respectively.

The total strain range was reduced to 0.13% and cycling initiated at $R = -1$ conditions. No additional crack growth occurred in 14,000 cycles. The strain amplitude was increased to 0.18% and crack growth was noted to reinitiate. 2a versus N and the corresponding da/dN versus ΔK curves for the $R = -1$ portion of the testing are shown in Figures 23 and 24. Again, note the apparent differences in $R = 0$ and $R = 1$ crack growth rate when the range of stress intensity is used as the normalizing parameter.

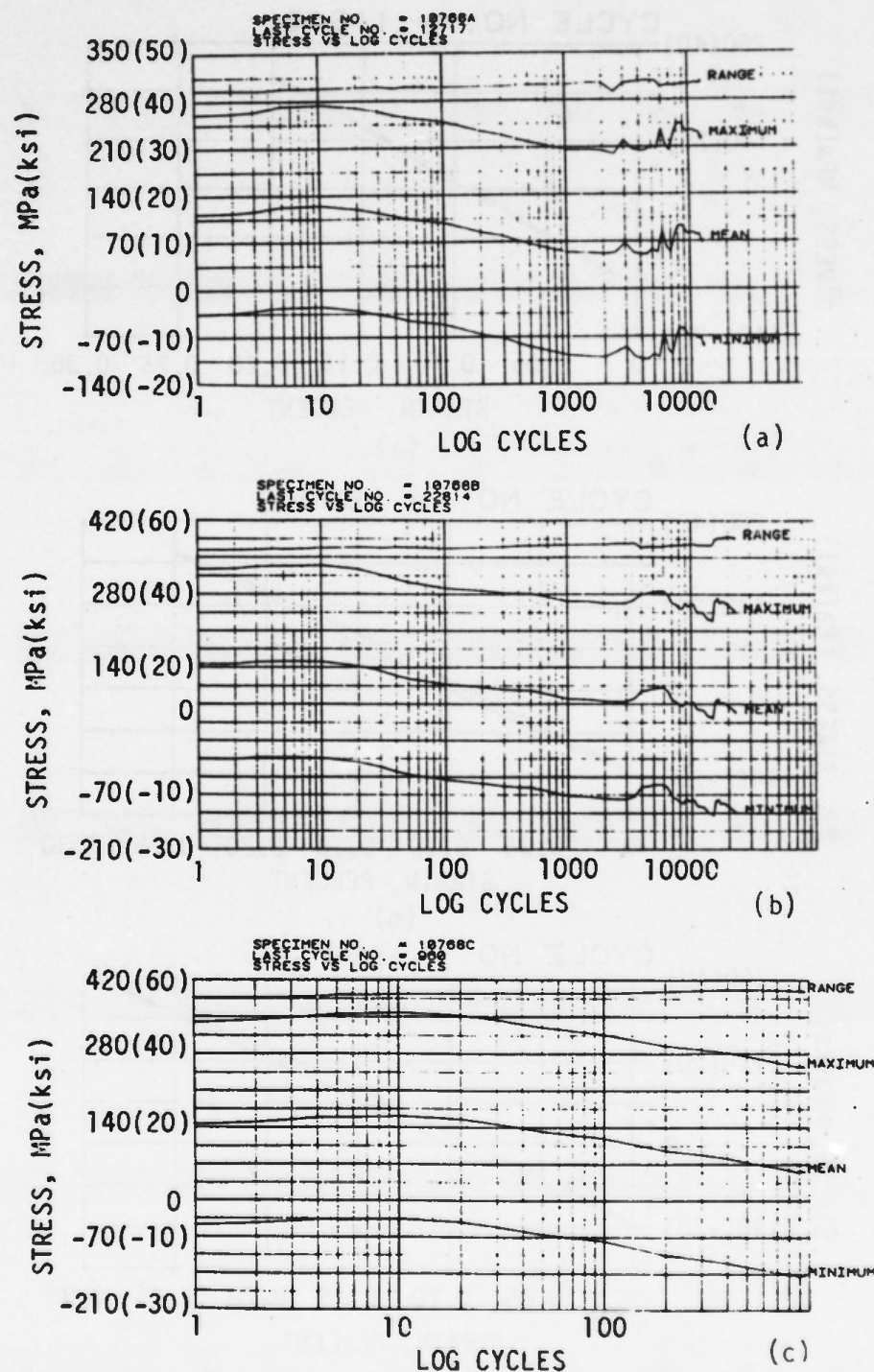
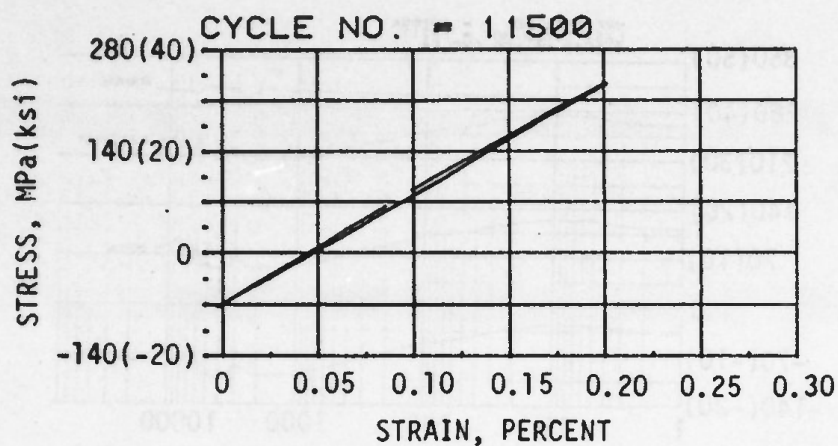
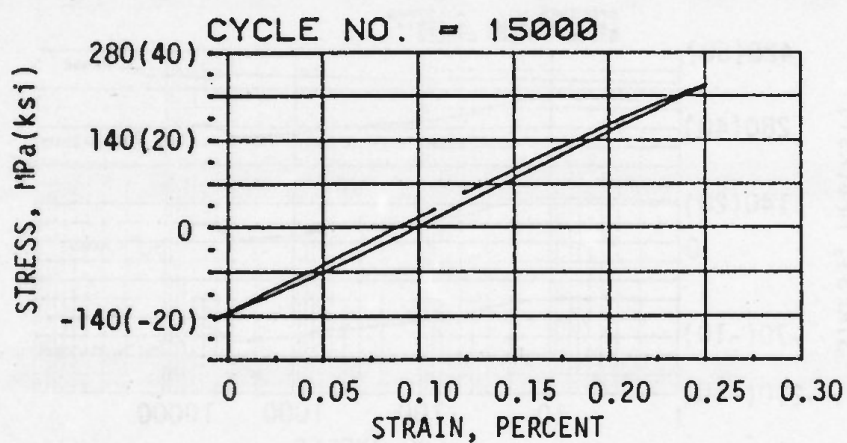


Figure 15

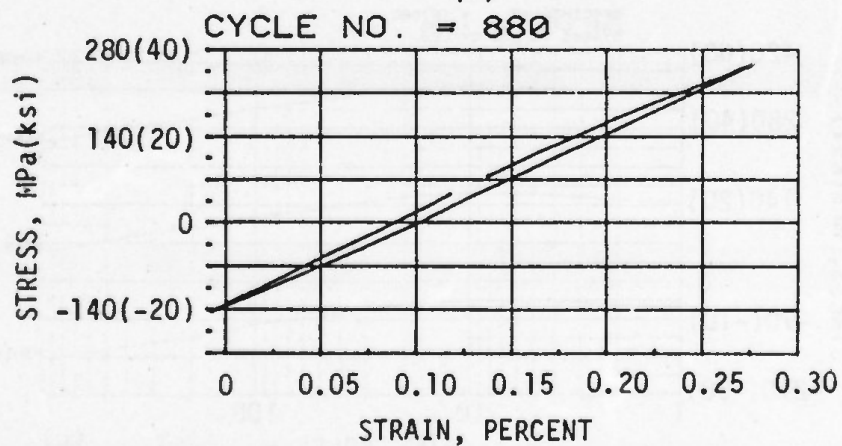
Mean Stress Drift and Cyclic Hardening at Three Strain Amplitudes for Ti-48Al-1V Specimen 10768 Tested at 815°C (1500°F), $R = 0$. a) 0.2%; b) 0.25%; c) 0.275%



(a)



(b)



(c)

Figure 16 Stabilized Hysteresis Loops for Ti-48Al-1V Specimen 10768 Tested at 815°C (1500°F), $R = 0$. a) $\Delta\epsilon = 0.2\%$; b) $\Delta\epsilon = 0.25\%$; c) $\Delta\epsilon = 0.275\%$

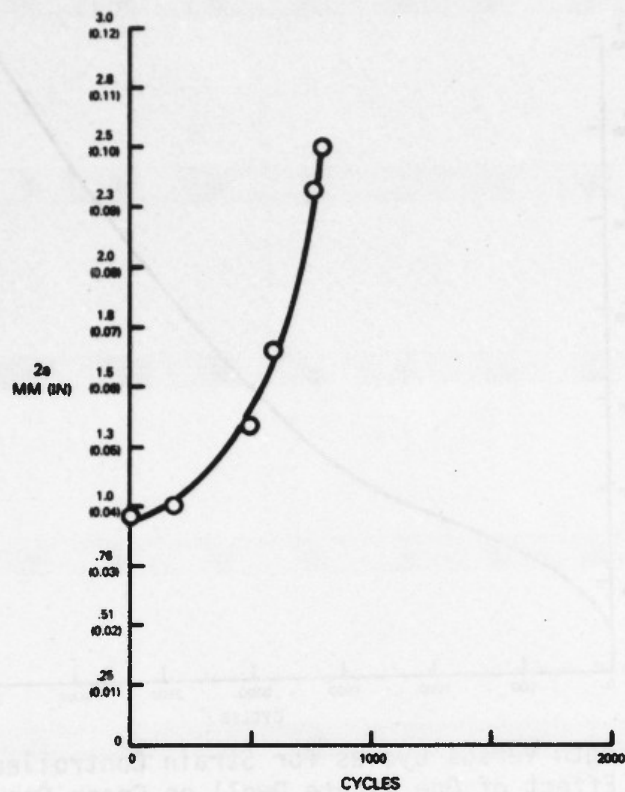


Figure 17 Crack Length (2a) Versus Cycles (N) for Ti-48Al-1V Specimen 10768, Tested at 815°C (1500°F), $R = 0$, $\Delta\epsilon = 0.275\%$

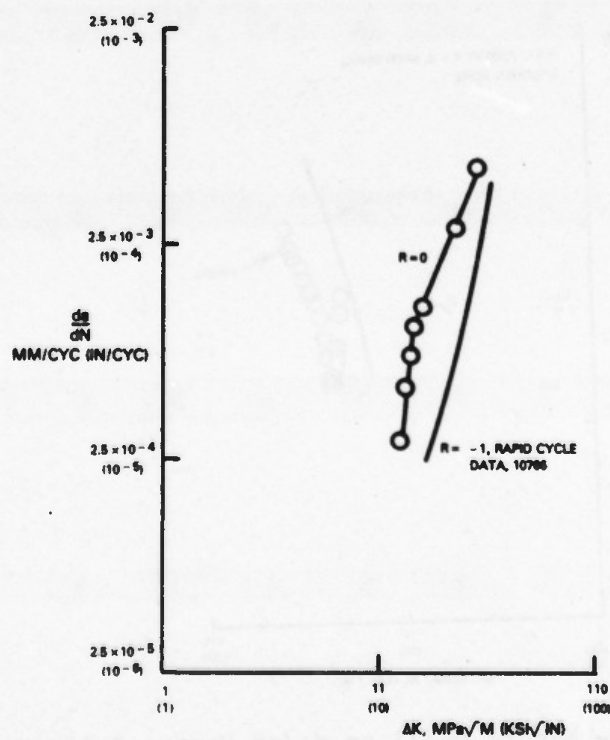


Figure 18 da/dN Versus Delta K Curve for Ti-48Al-1V Specimen 10768, Tested at 815°C (1500°F), $R = 0$, $\Delta\epsilon = 0.275\%$

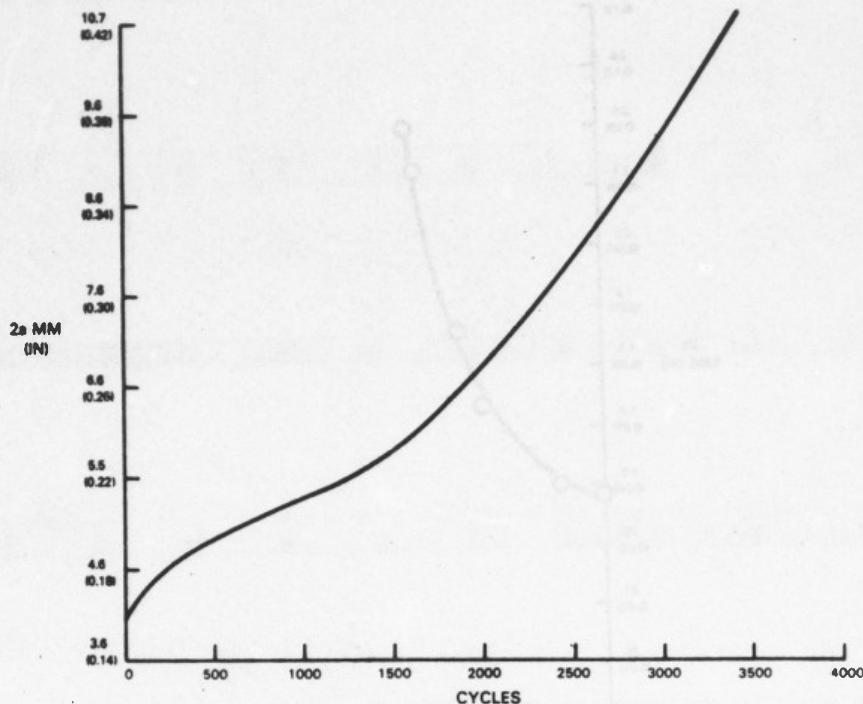


Figure 19 Crack Length Versus Cycles for Strain Controlled Specimen 10768 Showing Effect of One Minute Dwell on Crack Growth Rate at 815°C (1500°F) and $R = 0$

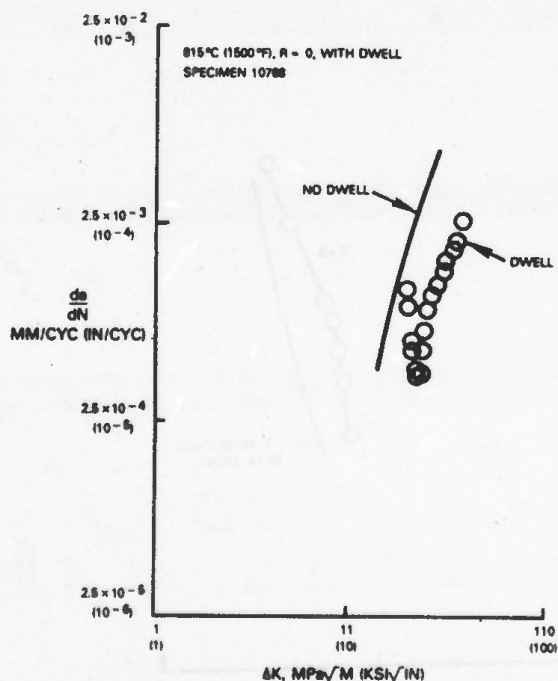


Figure 20 Effect of One Minute Dwell on da/dN Versus Delta K for Strain Controlled Specimen 10768 at 815°C (1500°F) and $R = 0$

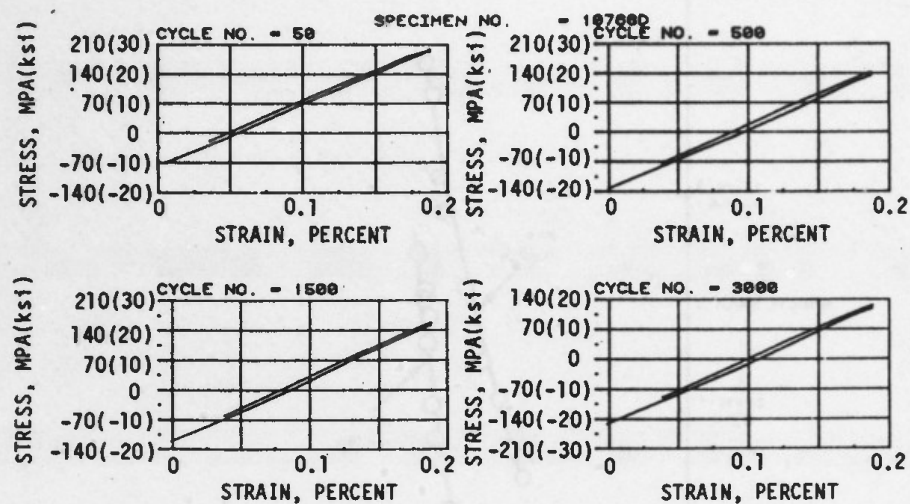


Figure 21 Representative Hysteresis Loops Taken at Various Times During Dwell Testing of Specimen 10768

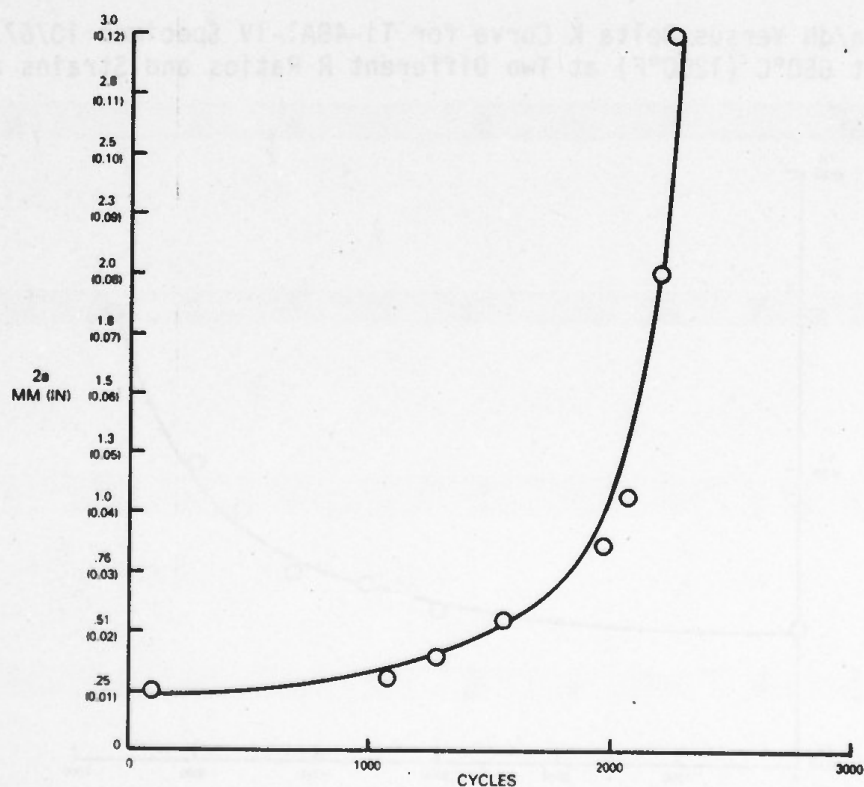


Figure 22 Crack Length ($2a$) Versus Cycles (N) for Ti-48Al-1V Specimen 10767 Tested at 650°C (1200°F), $R = 0$, $\Delta\epsilon = 0.21\%$

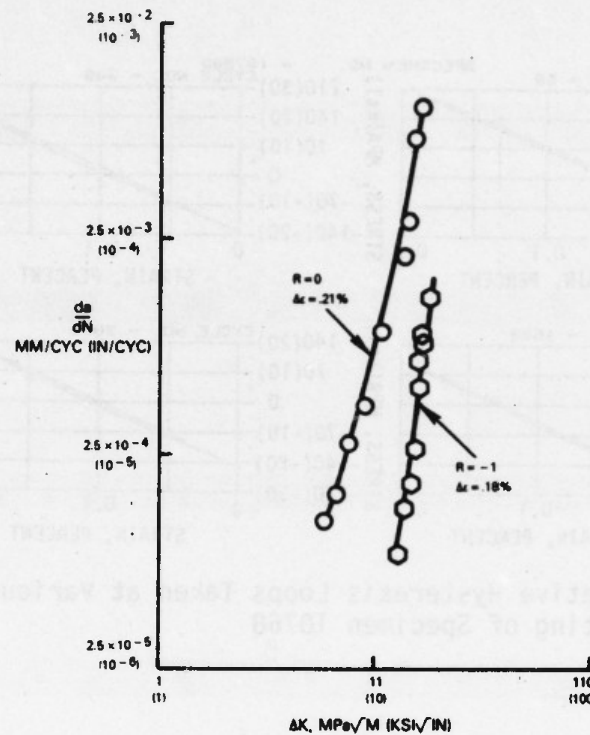


Figure 23 da/dN Versus Delta K Curve for Ti-48Al-1V Specimen 10767, Tested at 650°C (1200°F) at Two Different R Ratios and Strains as Shown

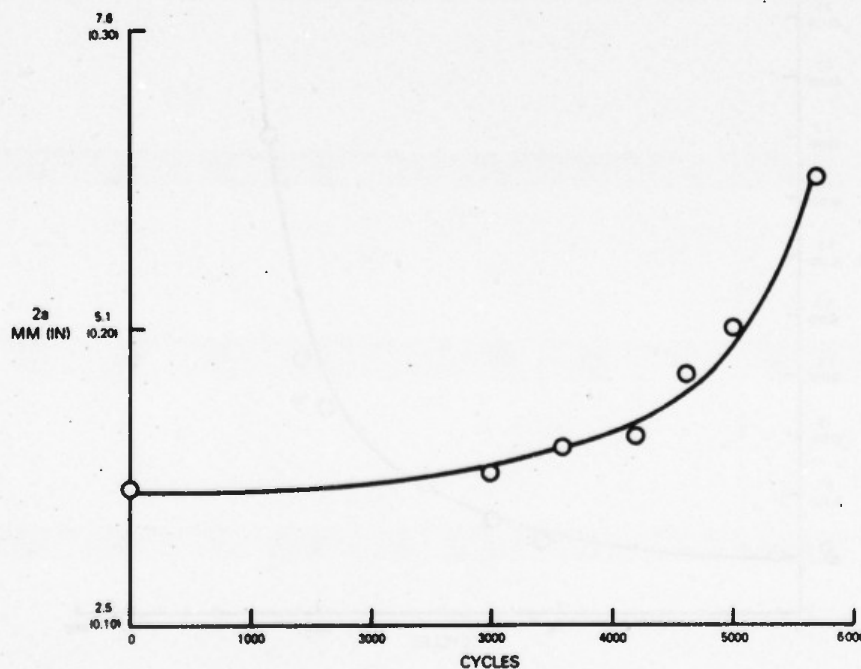


Figure 24 Crack Length ($2a$) Versus Cycles (N) for Ti-48Al-1V Specimen 10774, Tested at 650°C (1200°F), $R = -1$, $\Delta\epsilon=0.18\%$

d. Specimen 10765 At Room Temperature

Load controlled cycling at 0-0.157% strain resulted in initiation of a crack at the starter notch after 12,000 cycles. 2a versus N data were recorded to a total crack length of 3.02mm (0.119 inch). No further data were taken prior to failure. These data and the corresponding da/dN versus ΔK curve are shown in Figure 25.

e. Specimen 10776, 565°C (1050°F), R = 0 and R = -1

Load controlled cycling at 0-0.1675% resulted in initiation of the starter crack in a short period. 2a versus N data were recorded to a length of 3.6mm (0.140 inch), at which point load conditions were changed to +0.05%. The 2a versus N and corresponding da/dN versus ΔK curve for the R = 0 portion of the test are also shown in Figure 25.

The crack did not reinitiate at +0.05% load level in 20,000 cycles and the specimen was subsequently uploaded to +0.06% and +0.075% before crack growth was noted to resume, although not instantaneously. The 2a versus N and corresponding da/dN versus ΔK curve for this R = -1 portion of the testing are shown in Figure 26.

A comparison of the R = 0 and R = 1 data at the different test temperatures suggested an increase in crack growth rate results from an increase in test temperature. An additional 565°C (1050°F) test was, therefore, initiated to determine if the observed trend was real or an artifact of the scatter in crack growth.

f. Specimen 10778, 565°C (1050°F), R = 0 and R = -1

Load controlled cycling at 0-0.1675% resulted in initiation at the starter crack in 6000 cycles. 2a versus N data were recorded to a total length of 4mm (0.157 inch). These data and the corresponding da/dN - ΔK curve for the R = 0 portion of the test are shown in Figure 27. Data falls very close to the previous results for Specimen 10776.

The load condition was changed to +0.06% and subsequently +0.072% before crack growth was observed to reinitiate. The crack continued to grow until the test was suspended at a length of 8mm (0.325 inch). The 2a versus N and corresponding da/dN versus ΔK curves for R = -1 are presented in Figure 28. These data also agree very closely with previous results for Specimen 10776.

g. Specimen 10777, 315°C (600°F), R = 0 and R = -1

Load controlled cycling at 0-0.158% strain resulted in initiation of a crack after 9000 cycles. Crack progression data were recorded for a total length of 3.9mm (0.155 inch). The 2a versus N and corresponding da/dN versus ΔK are shown in Figure 29. The data fell between the R = 0 room temperature and 565°C (1050°F) curves.

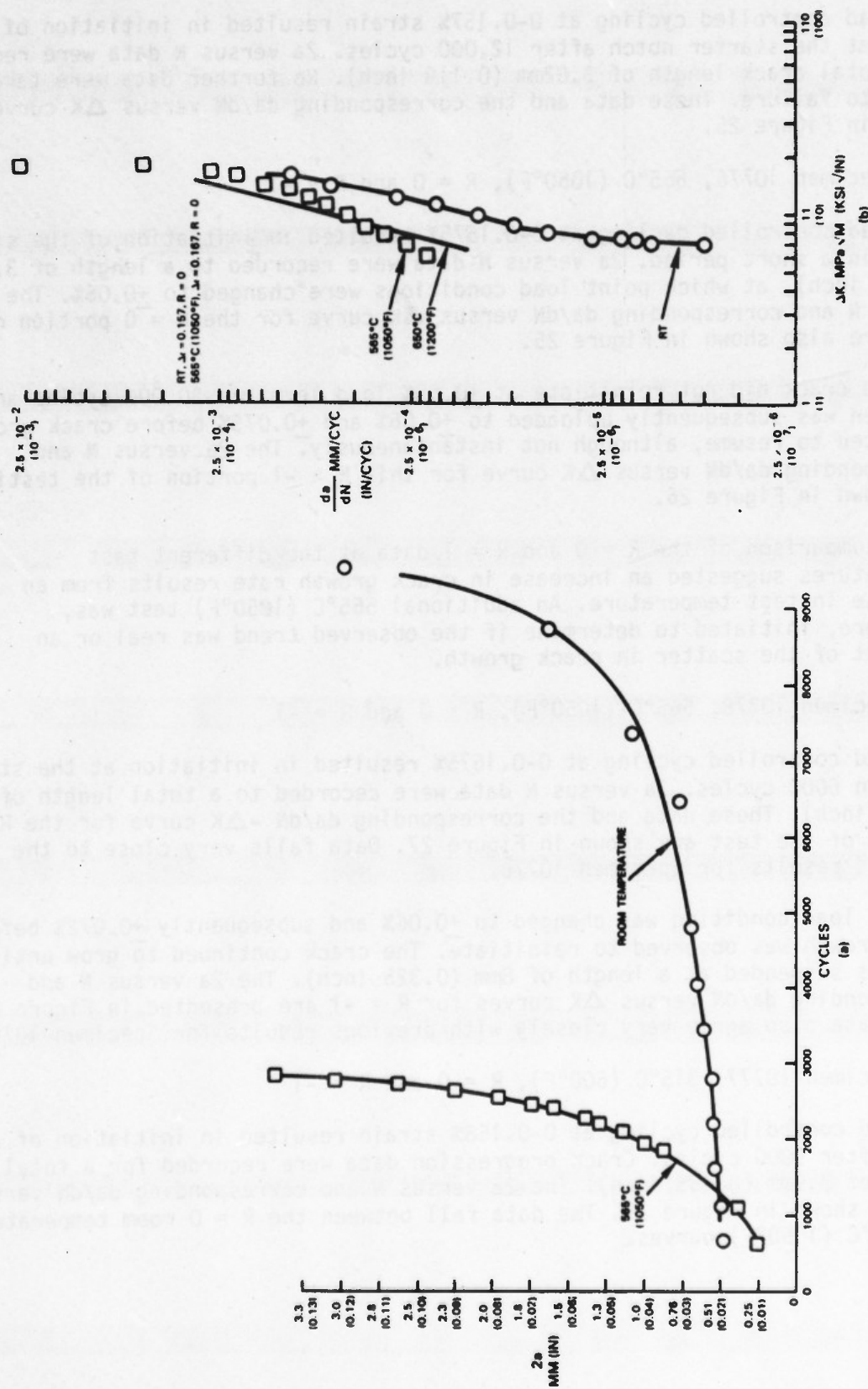


Figure 25 Crack Growth Data for Load Controlled Specimen 10776 Tested at RT and 565°C (1050°F) at R = -1. a) Crack Length (2a) Versus Cycles (N); b) da/dN Versus Delta K

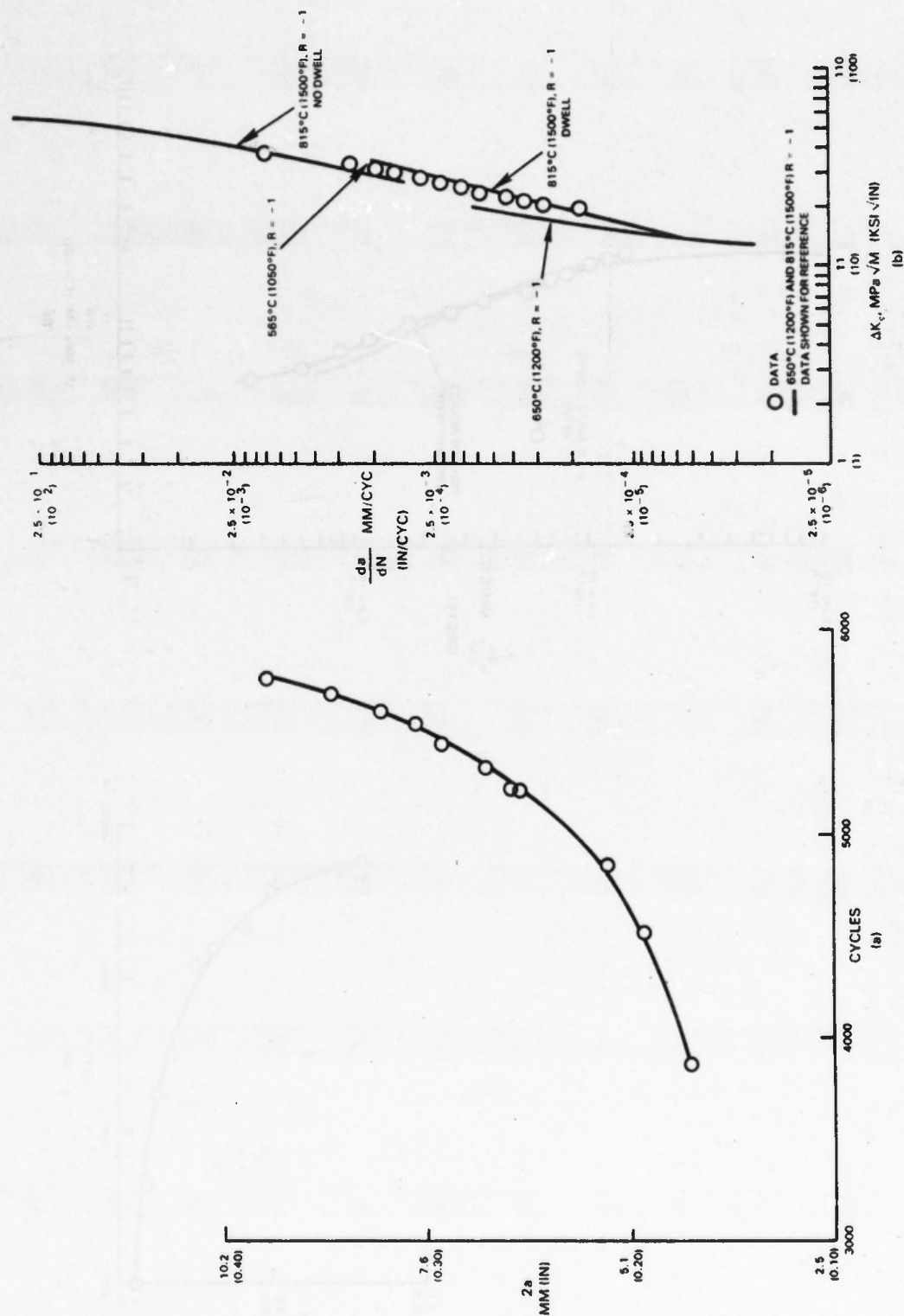


Figure 26 Crack Growth Data for Load Controlled Specimen 10776 Tested at 565°C (1050°F) and R = -1. a) Crack Length (2a) Versus Cycles (N); b) da/dN Versus Delta K

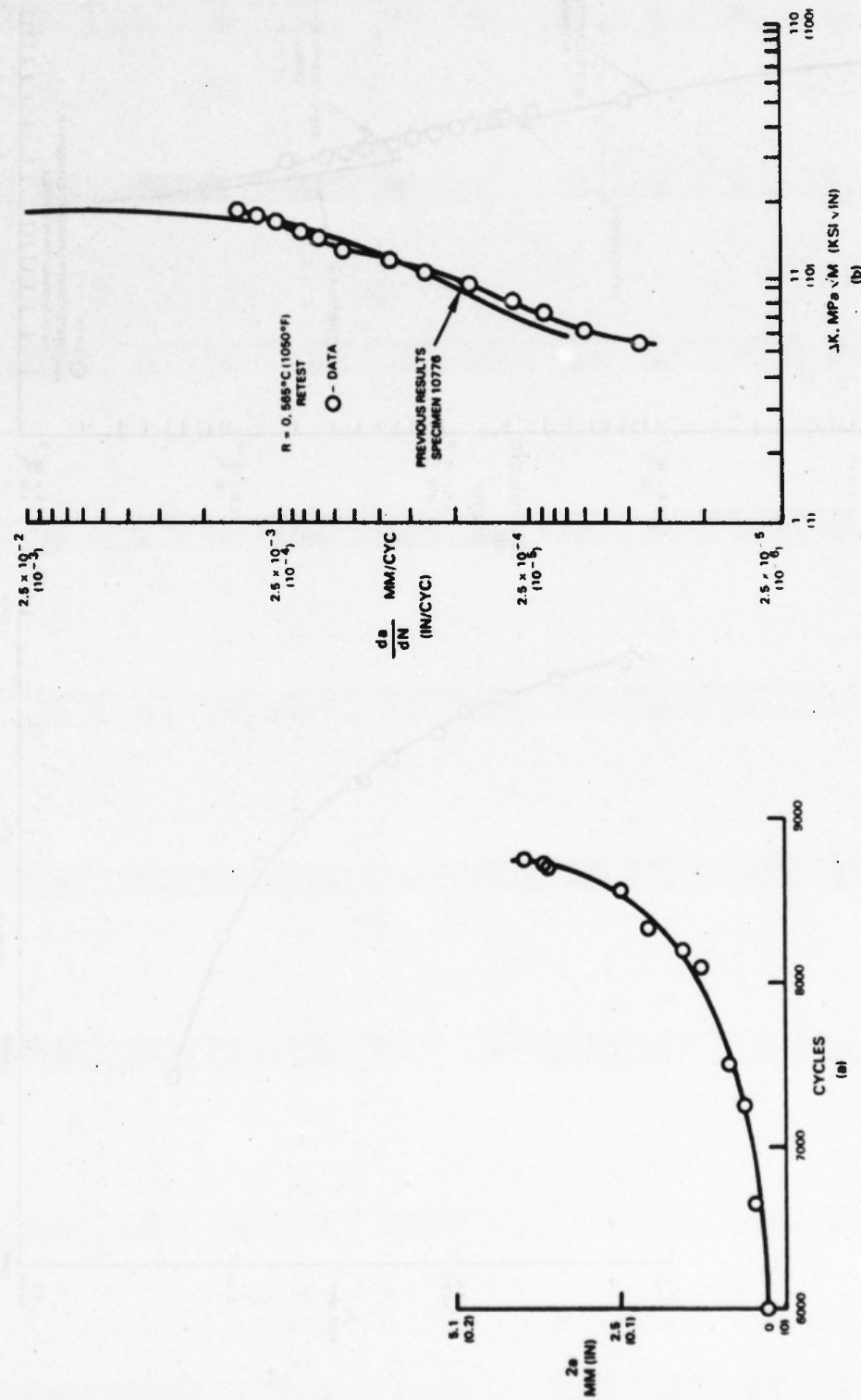


Figure 27 Crack Growth Data for Load Controlled Specimen 10778 Tested to Verify $R = 0$ Results of 10776, Run at $565^\circ C$ ($1050^\circ F$). a) Crack Length $2a$ Versus Cycles (N); b) da/dN Versus Delta K

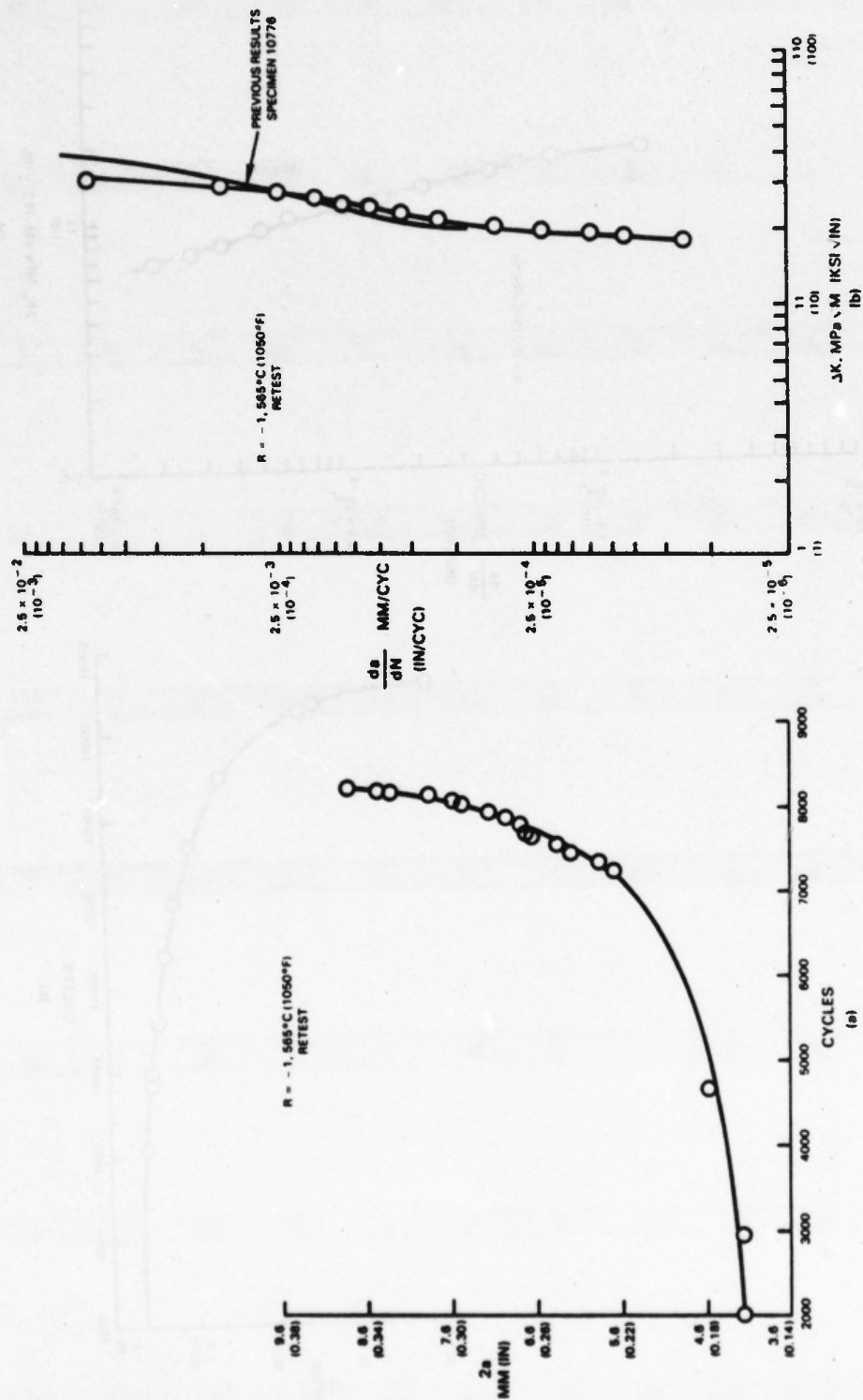


Figure 28 Crack Growth Data for Load Controlled Specimen 10778 to Verify R = -1 Results of 10776, Run at 565°C (1050°F). a) Crack Length (2a) Versus Cycles (N); b) da/dN Versus Delta K

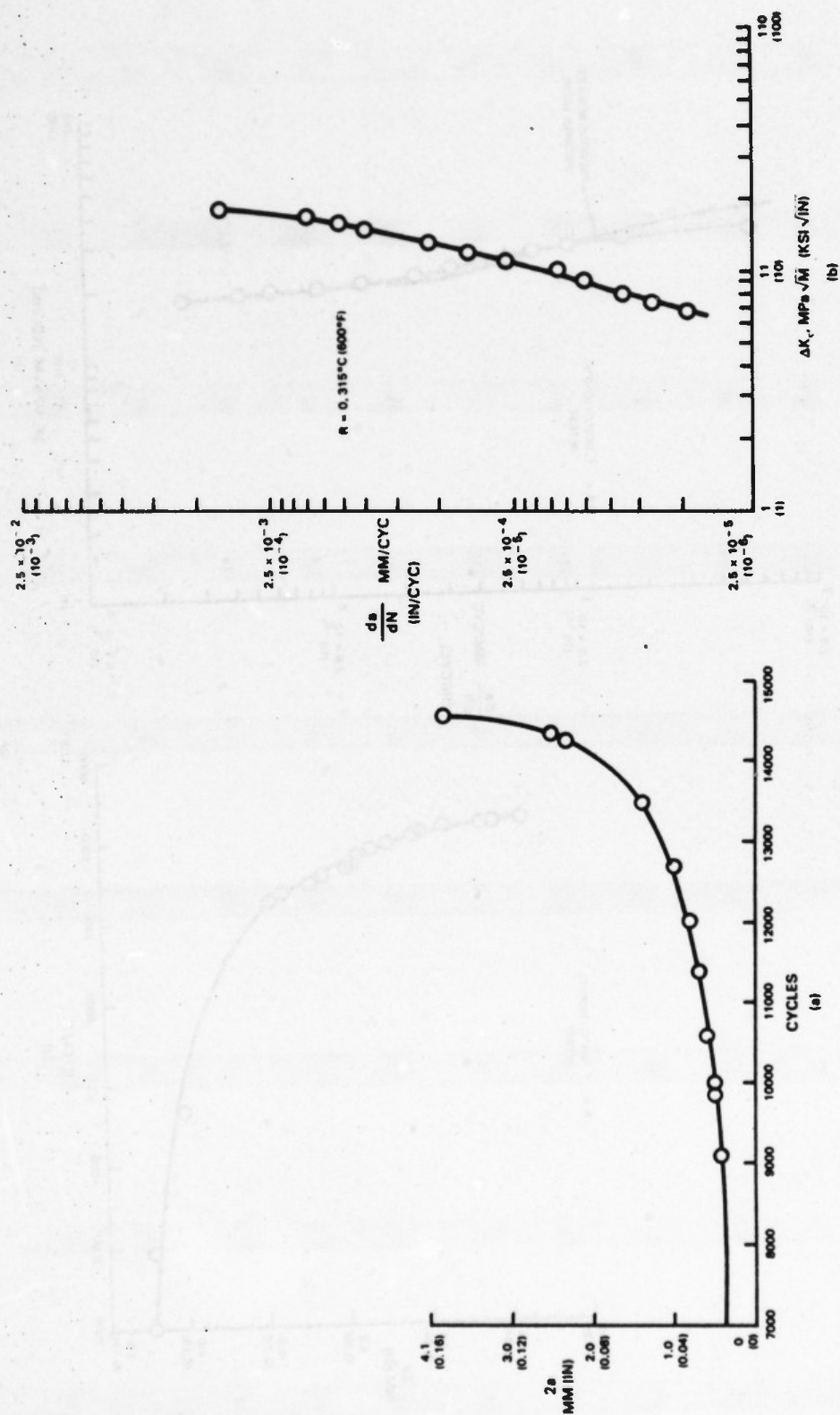


Figure 29 Crack Growth Data for Load Controlled Specimen 10777 Tested at 315°C (600°F) and R = 0. a) Crack Length (2a) Versus Cycles (N); b) da/dN Versus Delta K

Loading was changed to $R = -1$ conditions and cycling resumed at $+0.057\%$. No growth was noted and the strain amplitude was increased to $+0.079\%$ in two steps. $2a$ versus N data obtained at this condition and the corresponding da/dN versus ΔK curve are shown in Figure 30.

h. Specimen 10769, 736°C (1360°F), $R = -1$, Without Dwell

Strain controlled cycling was initiated at $+0.15\%$ and continued for 25,000 cycles with no growth noted from the starter slot. The strain amplitude was increased to $+0.175\%$ and the crack was noted to initiate at 2814 cycles. Only five data points were taken before the specimen failed at a length of 3.4mm (0.135 inch). The $2a$ versus N and corresponding da/dN versus ΔK data are shown in Figure 31. No hardening or softening of the material were noted during the test (Figure 32). Representative hysteresis loops are shown in Figure 33. The sparsity of data and the fracture of the specimen prior to initiation of the dwell testing resulted in testing of an additional specimen, 10770, at identical conditions.

i. Specimen 10770, 736°C (1360°F), $R = -1$, With And Without Dwell

Due to the failure of Specimen 10769, an additional specimen, 10770, was tested under strain control at the 736°C (1360°F), $R = -1$ condition. Cycling was initiated at $+0.17\%$ and continued for 15,300 cycles with no initiation at the starter slot noted. The strain amplitude was increased to $+0.185\%$ at which point flaw growth was observed to begin. Data were taken until a total crack length of 4.1mm (0.163 inch) was reached. Figure 34 presents the $2a$ versus N and resultant da/dN versus ΔK curves for this condition. The crack growth rate is slightly slower than that noted in the testing of Specimen 10669.

The specimen was down loaded to $+0.11\%$ and a one minute constant strain hold was introduced at the tensile and compressive strain limits. Representative hysteresis loops are shown in Figure 35. Minimal growth was noted to occur in 4000 cycles and the strain amplitude was increased to $+0.125\%$. Crack growth resumed after 500 cycles. The $2a$ versus N and resultant da/dN versus ΔK curves are noted in Figure 36. The addition of a one minute hold at the tensile and compressive strain limits alters the shape of the da/dN versus ΔK curve substantially. As noted, a bilinear characteristic is now present. At high ΔK values, the crack growth data from the dwell test is similar to the rapid cycle results. At lower ΔK values, the dwell acts to retard the rate of crack growth. These results are similar to those reported for the 815°C (1500°F) test at $R = 0$ condition, Figure 20.

j. Specimen 10772, 650°C (1200°F), $R = -1$ and $R = 0$

A review of the previous data 650°C (1200°F), indicates that the slope of the $R = -1$ da/dN versus ΔK data obtained from the load controlled test at 650°C (1200°F) and below is slightly greater than that for $R = 0$ data obtained at the corresponding test temperature. This result is somewhat unexpected and was not noted in the 736°C (1360°F) and 815°C (1500°F) strain controlled testing at the three R -ratios. One notable difference between the load controlled and strain controlled test methodology is that the fully reversed

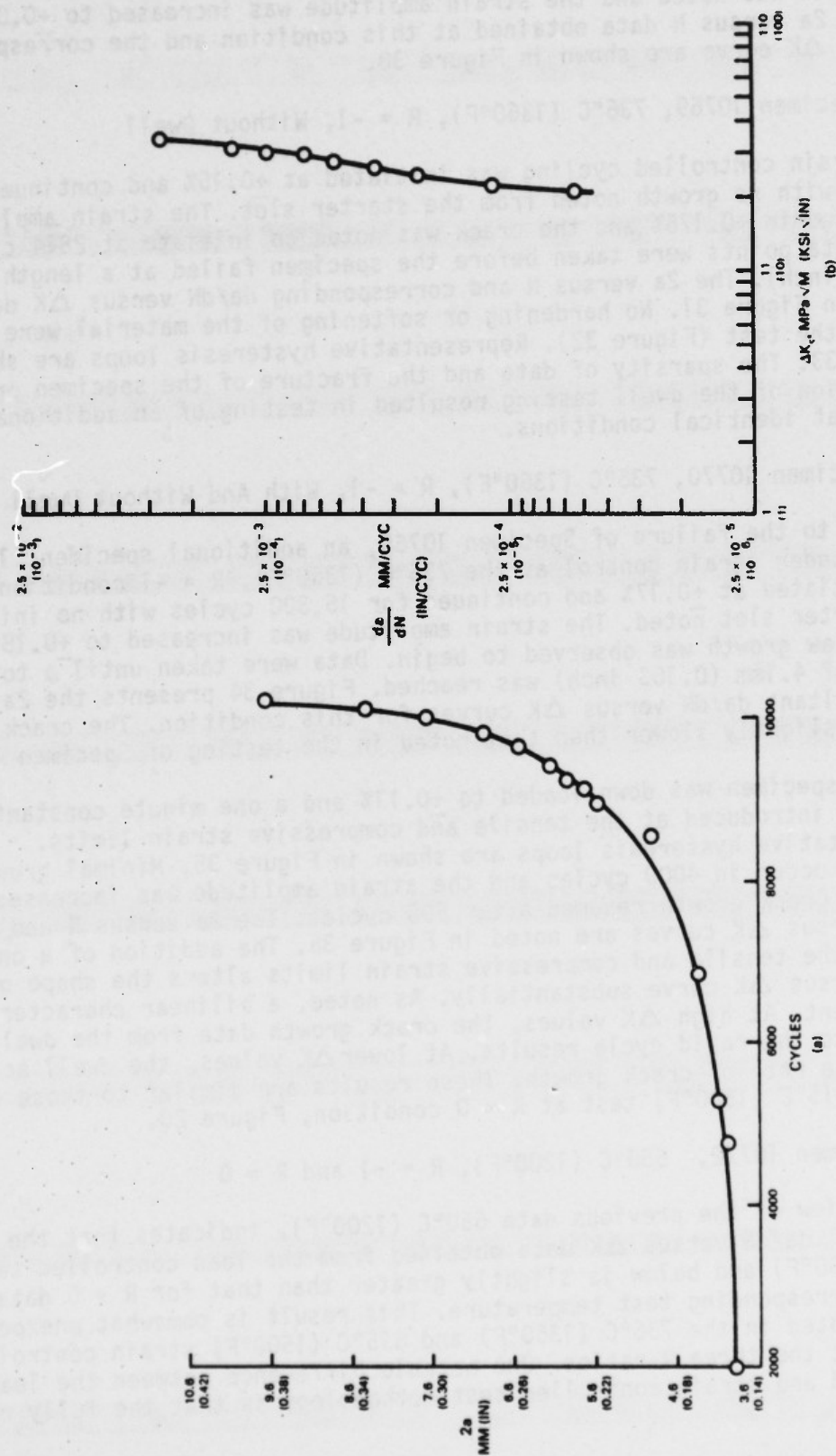


Figure 30 Crack Growth Data for Load Controlled Specimen 10777, Tested at 315°C (600°F) and R = -1. a) Crack Length (2a) Versus Cycles (N); b) da/dN Versus Delta K

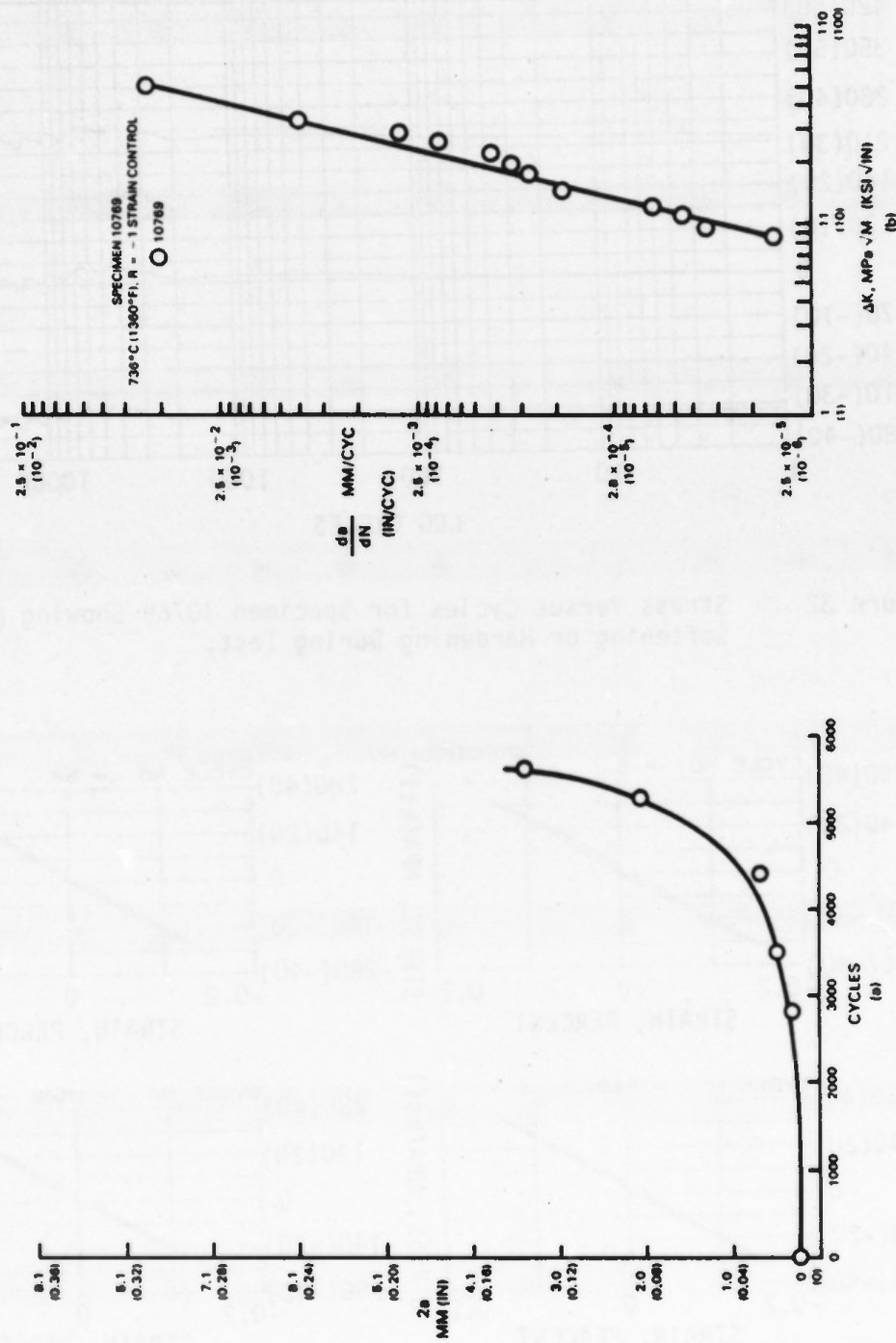


Figure 31 Crack Growth Data for Strain Controlled Specimen 10769 Tested at 730°C (1360°F) and R = -1. a) Crack Length (2a) Versus Cycles (N); b) da/dN Versus Delta K

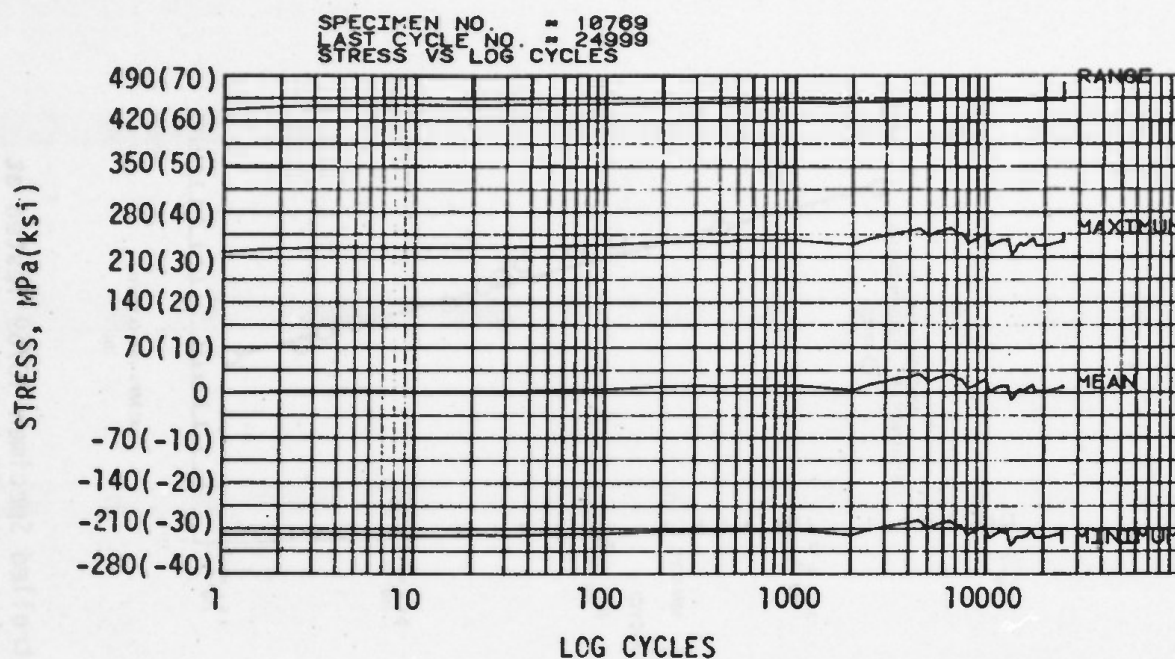


Figure 32 Stress Versus Cycles for Specimen 10769 Showing Lack of Softening or Hardening During Test.

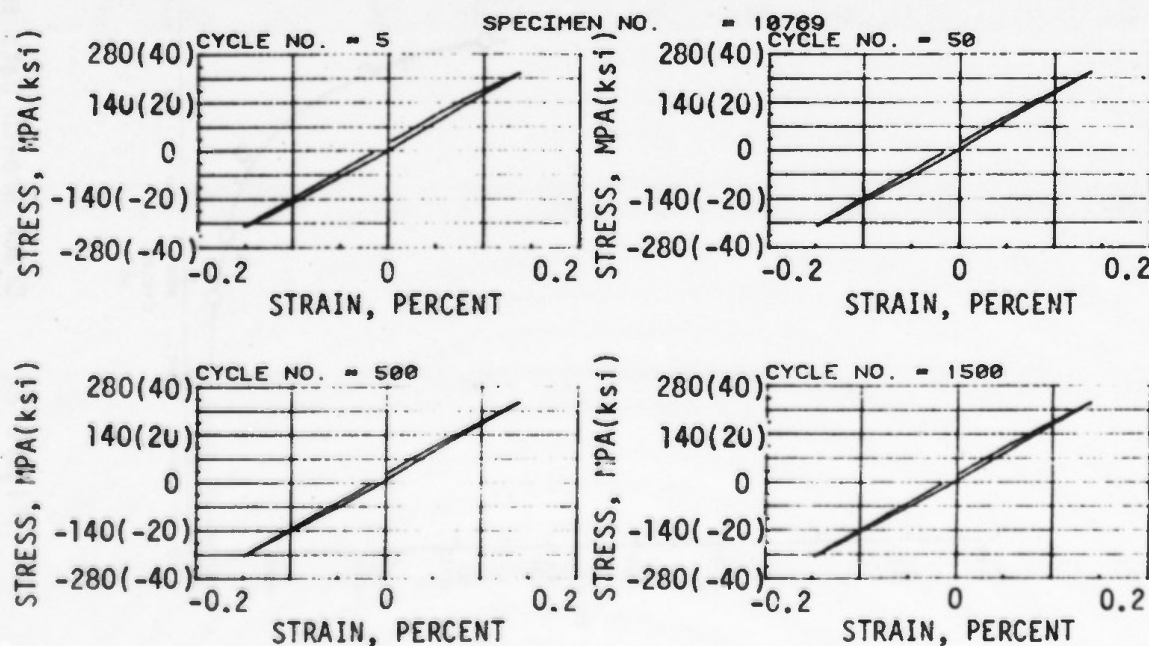


Figure 33 Stress Strain (Hysteresis) Loops Taken at Various Cycles During Testing of Specimen 10769. Note similarity of shape.

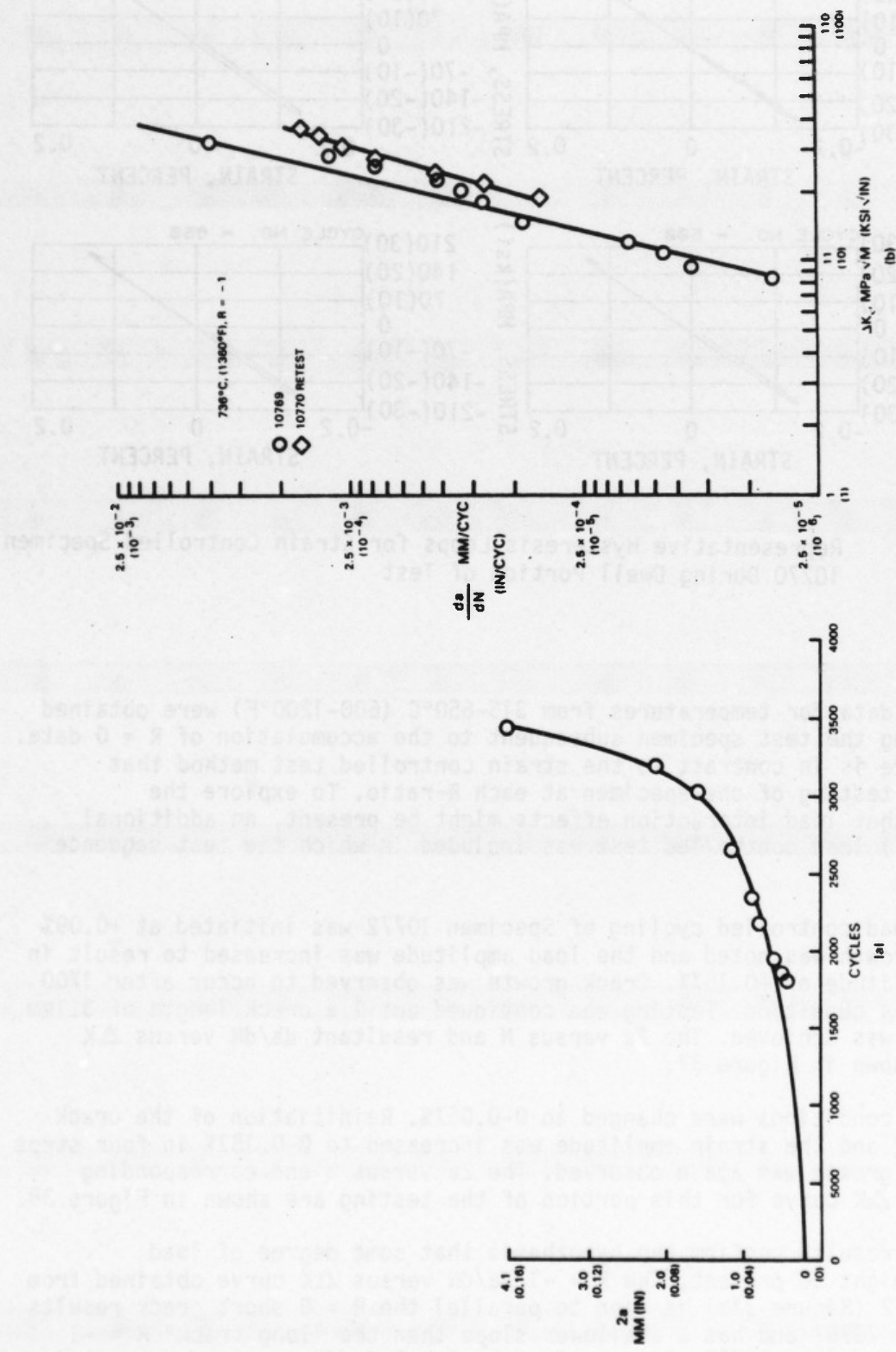


Figure 34 Crack Growth Data for Strain Controlled Specimen 10770 Tested at 736°C (1360°F) and R = -1, to Amplify Results of 10769. a) Crack Length (2a) Versus Cycles (N); b) da/dN Versus Delta K

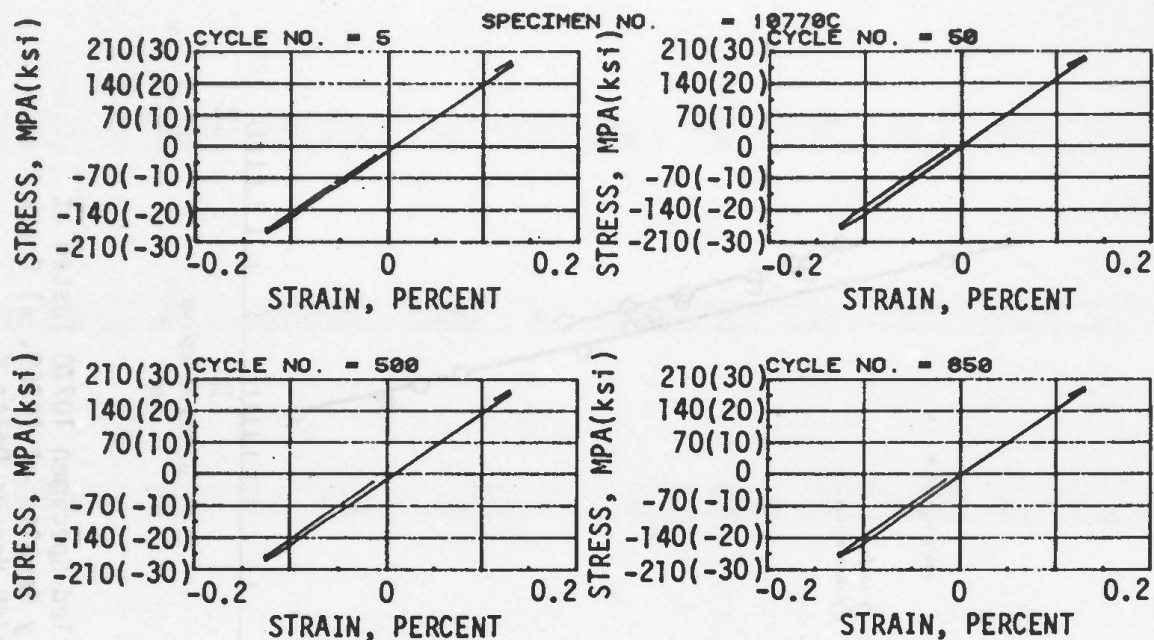


Figure 35 Representative Hysteresis Loops for Strain Controlled Specimen 10770 During Dwell Portion of Test

crack growth data for temperatures from 315-650°C (600-1200°F) were obtained by downloading the test specimen subsequent to the accumulation of $R = 0$ data. This procedure is in contrast to the strain controlled test method that required the testing of one specimen at each R -ratio. To explore the possibility that load interaction effects might be present, an additional 650°C (1200°F) load controlled test was included in which the test sequence was reversed.

$R = -1$ load controlled cycling of Specimen 10772 was initiated at $\pm 0.09\%$ strain. No growth was noted and the load amplitude was increased to result in a strain amplitude of $\pm 0.157\%$. Crack growth was observed to occur after 1700 cycles at this condition. Testing was continued until a crack length of 3.1mm (0.121 inch) was achieved. The $2a$ versus N and resultant da/dN versus ΔK curves are shown in Figure 37.

The load conditions were changed to 0-0.067%. Reinitiation of the crack was not noted and the strain amplitude was increased to 0-0.157% in four steps before crack growth was again observed. The $2a$ versus N and corresponding da/dN versus ΔK curve for this portion of the testing are shown in Figure 38.

The test results confirm the hypothesis that some degree of load interaction might be present. The $R = -1$ da/dN versus ΔK curve obtained from Specimen 10772 (Figure 37b) is seen to parallel the $R = 0$ short crack results from Specimen 10767 and has a shallower slope than the "long crack" $R = -1$ results from Specimen 10767. Conversely, the $R = 0$ da/dN versus ΔK curve from Specimen 10772 (Figure 38b) is steeper than the short crack $R = 0$ results from Specimen 10767.

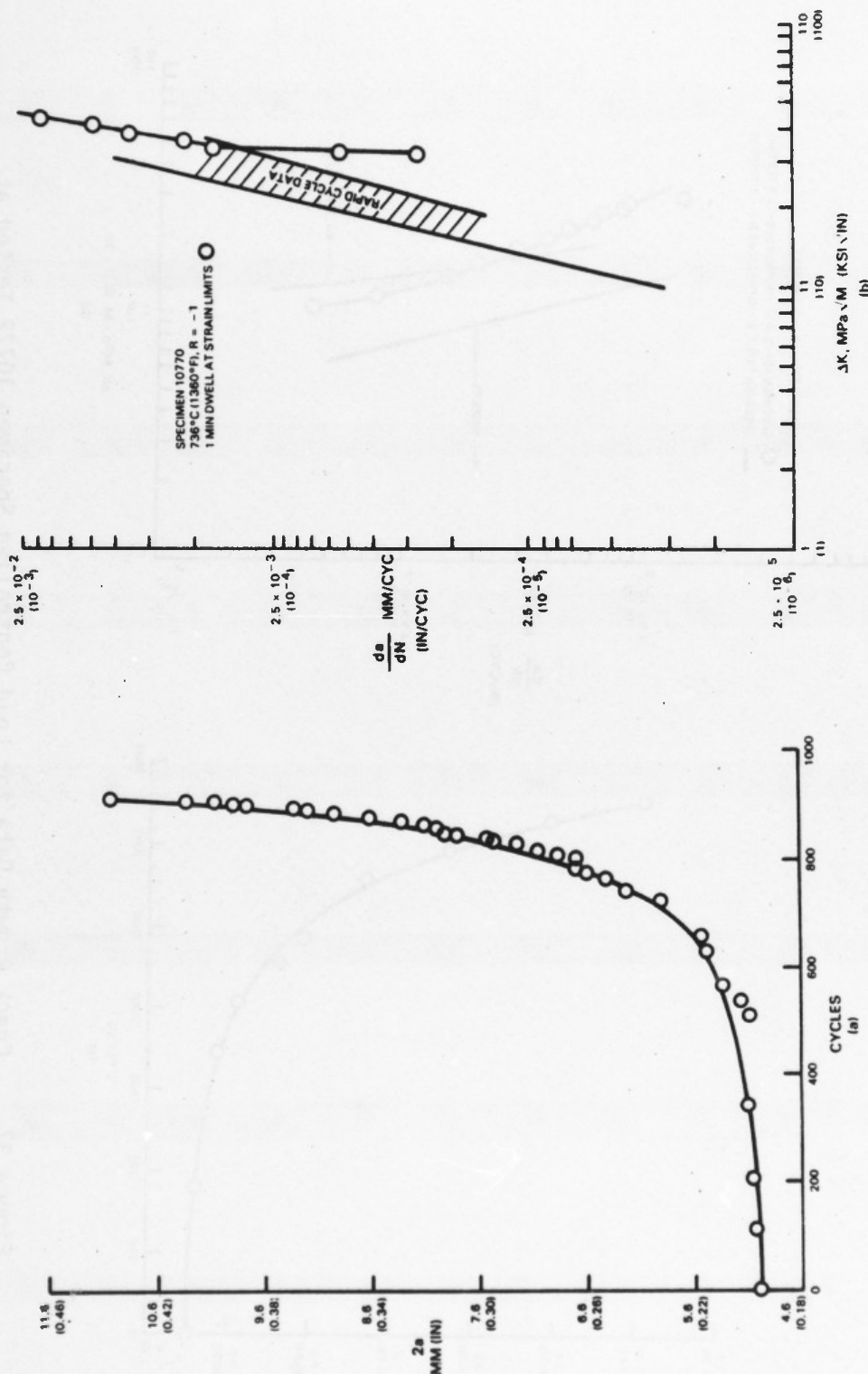


Figure 36 Crack Growth Data for Strain Controlled Specimen 10770 Showing Effect of One Minute Dwell Versus Rapid Cycle, a) Crack Length Versus Cycles; b) da/dN Versus stress intensity

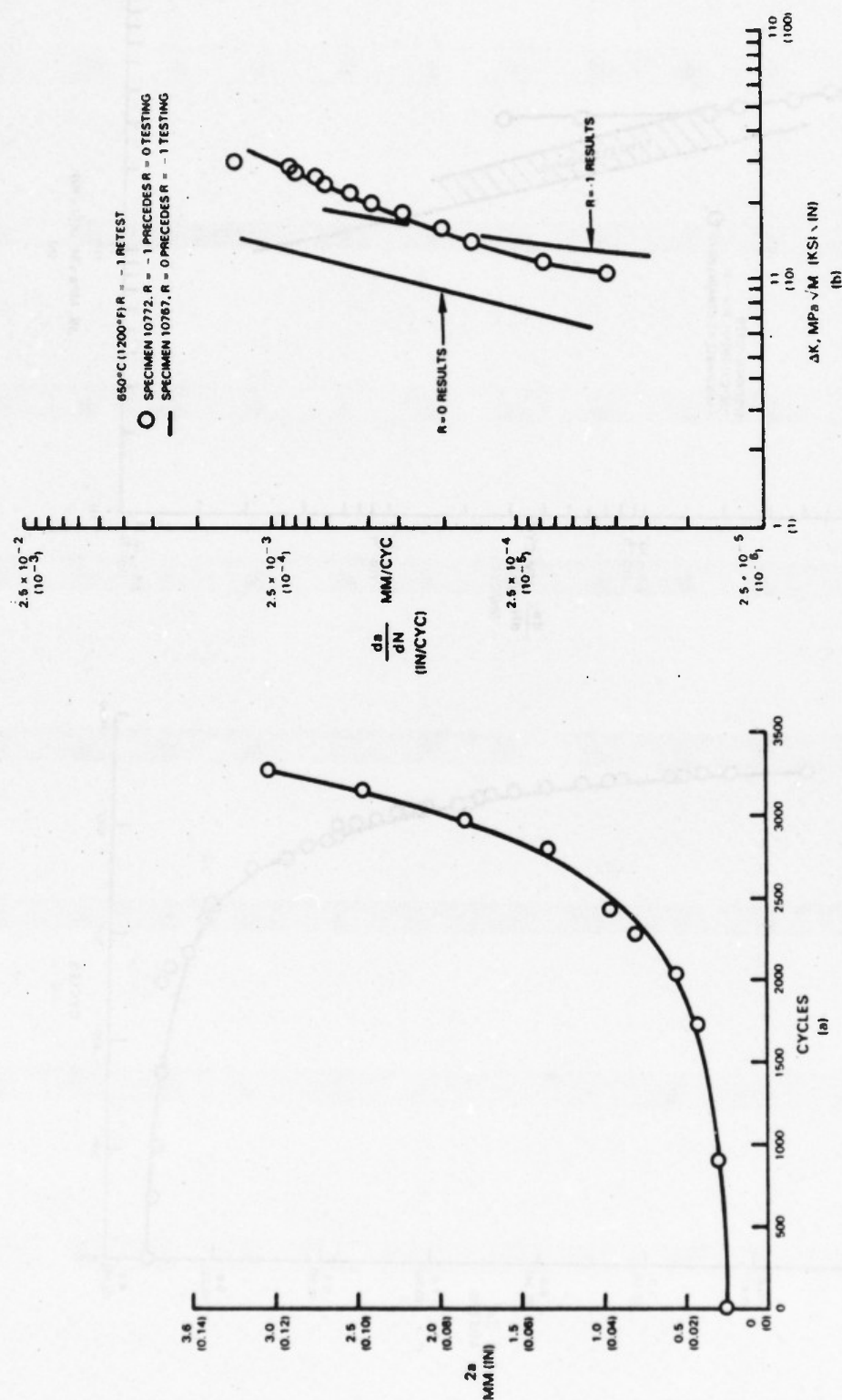


Figure 37 Crack Growth Data for Load Controlled Specimen 10772 Tested at 650°C (1200°F) and R = -1. a) Crack Length (2a) Versus Cycles (N); b) da/dN Versus Delta K

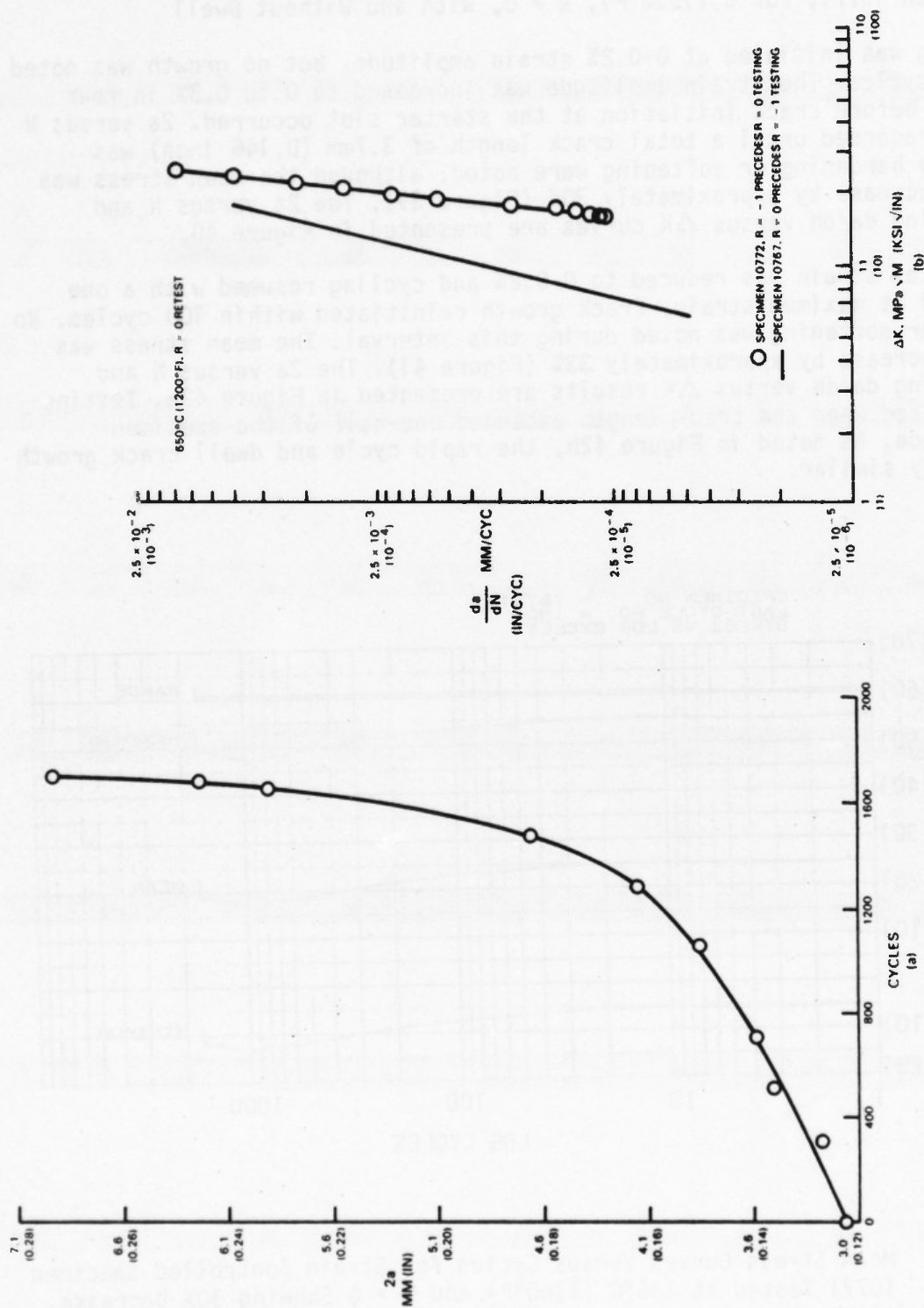


Figure 38 Crack Growth Data for Load Controlled Specimen 10772 Tested at 650°C (1200°F) During R = 0 Portion of Test. a) Crack Length (2a) Versus Cycles (N); b) da/dN Versus Delta K

k. Specimen 10771, 732°C (1360°F), R = 0, With and Without Dwell

Cycling was initiated at 0-0.2% strain amplitude, but no growth was noted in 20,000 cycles. The strain amplitude was increased to 0 to 0.3% in four increments before crack initiation at the starter slot occurred. 2a versus N data were recorded until a total crack length of 3.7mm (0.146 inch) was reached. No hardening or softening were noted, although the mean stress was noted to decrease by approximately 30% (Figure 39). The 2a versus N and corresponding da/dN versus ΔK curves are presented in Figure 40.

The total strain was reduced to 0-0.2% and cycling resumed with a one minute hold at maximum strain. Crack growth reinitiated within 100 cycles. No hardening or softening was noted during this interval. The mean stress was noted to decrease by approximately 33% (Figure 41). The 2a versus N and corresponding da/dN versus ΔK results are presented in Figure 42a. Testing was terminated when the crack length exceeded one-half of the specimen circumference. As noted in Figure 42b, the rapid cycle and dwell crack growth rate is very similar.

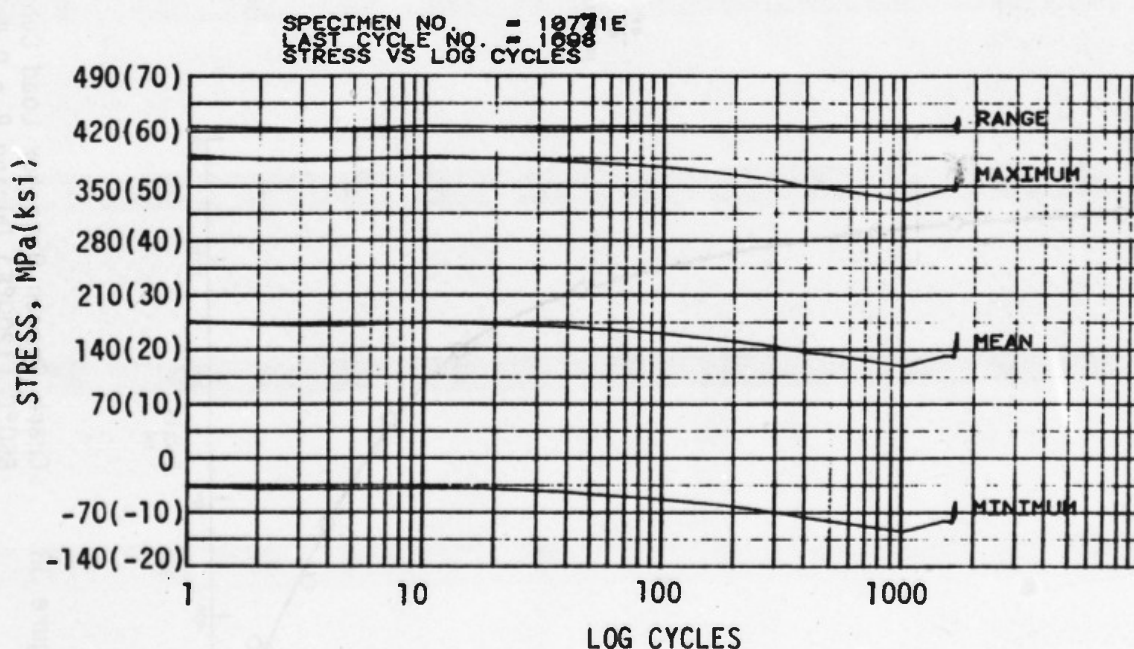


Figure 39 Mean Stress Curves Versus Cycles for Strain Controlled Specimen 10771 Tested at 736°C (1360°F) and R = 0 Showing 30% Decrease, Although No Hardening or Softening Was Observed

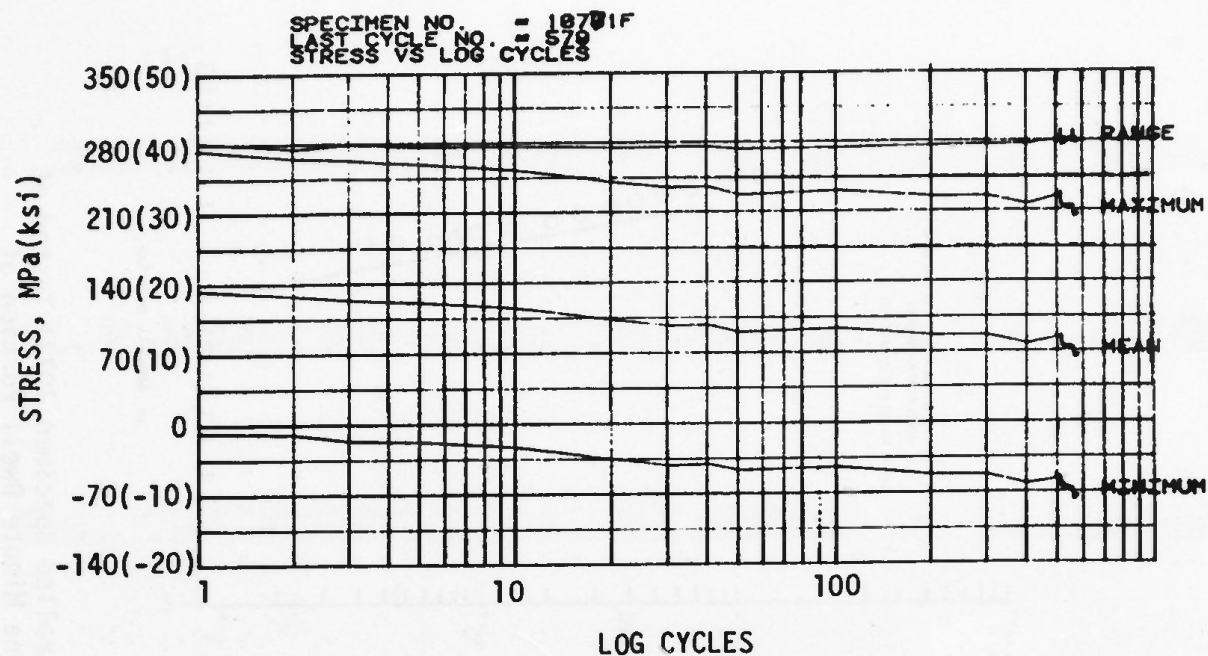


Figure 40 Crack Growth Data for Strain Controlled Specimen 10771 Tested at 736°C (1360°F) and $R = 0$. a) Crack Length (2a) Versus Cycles (N); b) da/dN Versus ΔK

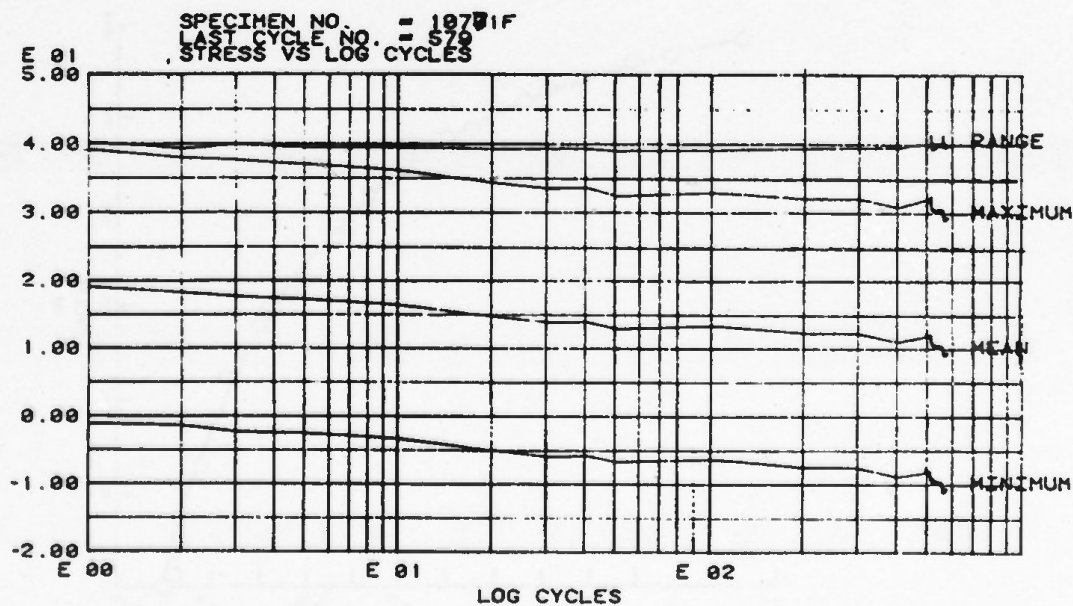


Figure 41 Mean Stress Versus Cycles for $R = 0$ Portion of Test of Specimen 10771 Tested at 736°C (1360°F) With a One Minute Dwell at Maximum Strain. Note decrease in mean stress of about 30%

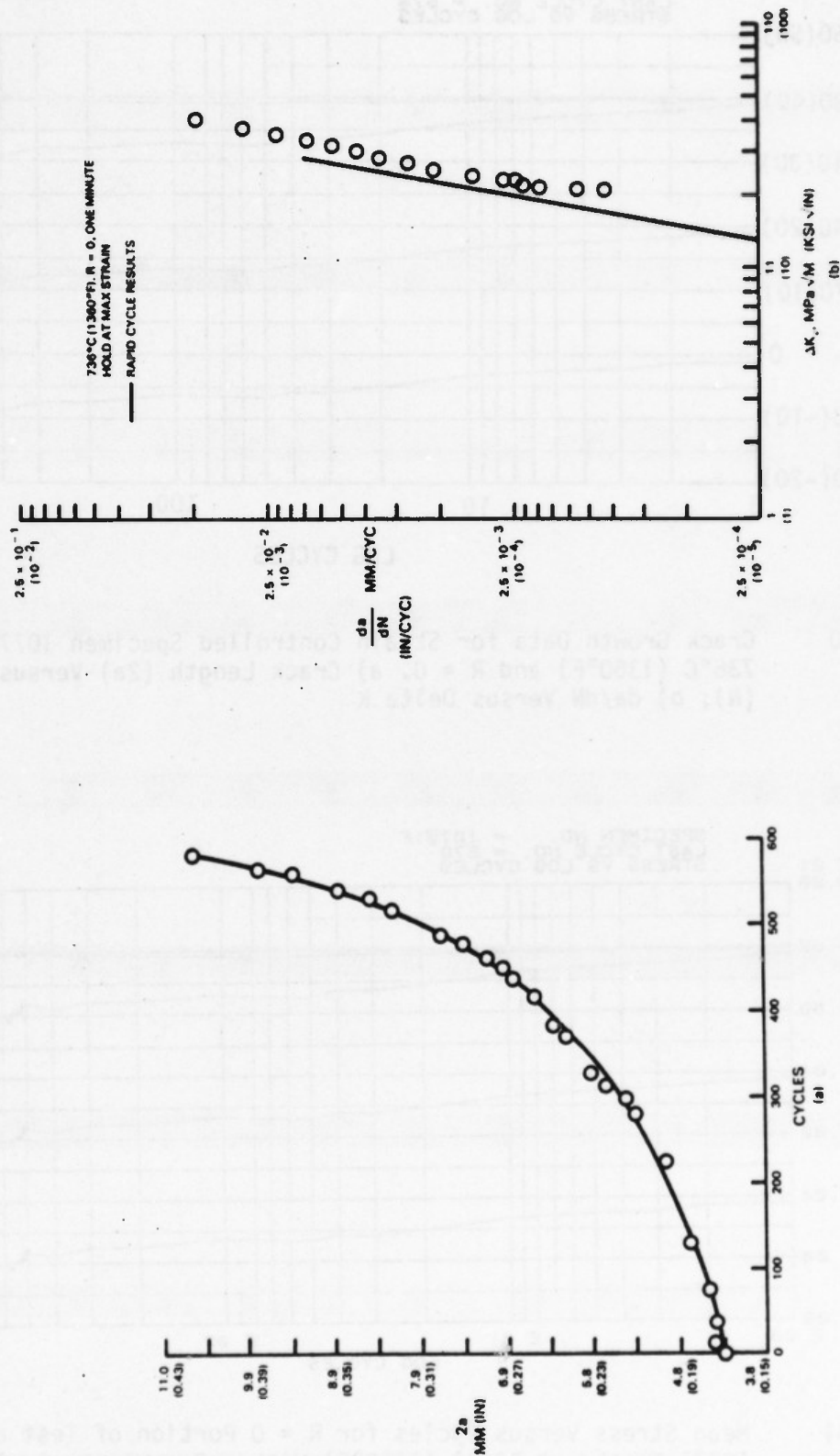


Figure 42 Crack Growth Data for Strain Controlled Specimen 10771 Tested at 736°C (1360°F) and R = 0 During One Minute Dwell Portion of Test. a) Crack Length (2a) Versus Cycles (N); b) da/dN Versus Delta K

1. Specimen 10773, 815°C (1500°F), $R = -3$, With And Without Dwell

Rapid cycle strain controlled testing was initiated at -0.33 to 0.11% amplitude. Crack growth was monitored until a crack length of 3.98mm (0.157 inch) was reached. During this interval, the mean cyclic stress increased from -126 to -52 MPa (-18 to -7.5 ksi) (Figure 43) but no hardening or softening were noted beyond the first cycle. The $2a$ versus N and corresponding da/dN versus ΔK data are presented in Figure 44. $R = 0$ (Specimen 10768) and $R = -1$ (Specimen 10766) rapid cycle crack growth data is presented for reference. Note that the $R = -3$ and $R = -1$ results are very similar.

Strain conditions were reduced to $-0.18 + 0.06$ and cycling resumed with a one minute hold in compression. Crack growth reinitiated and data were recorded until the crack became immeasurably long ($2a = 11.4\text{mm}$ or 0.451 inch). During this interval, the mean stress again decayed from -41 to $+35$ MPa (-13 to $+5$ ksi) (Figure 45). The $2a$ versus N and corresponding da/dN versus ΔK data are presented in Figure 46. The $R = 0$ and $R = -1$ dwell results are presented for reference.

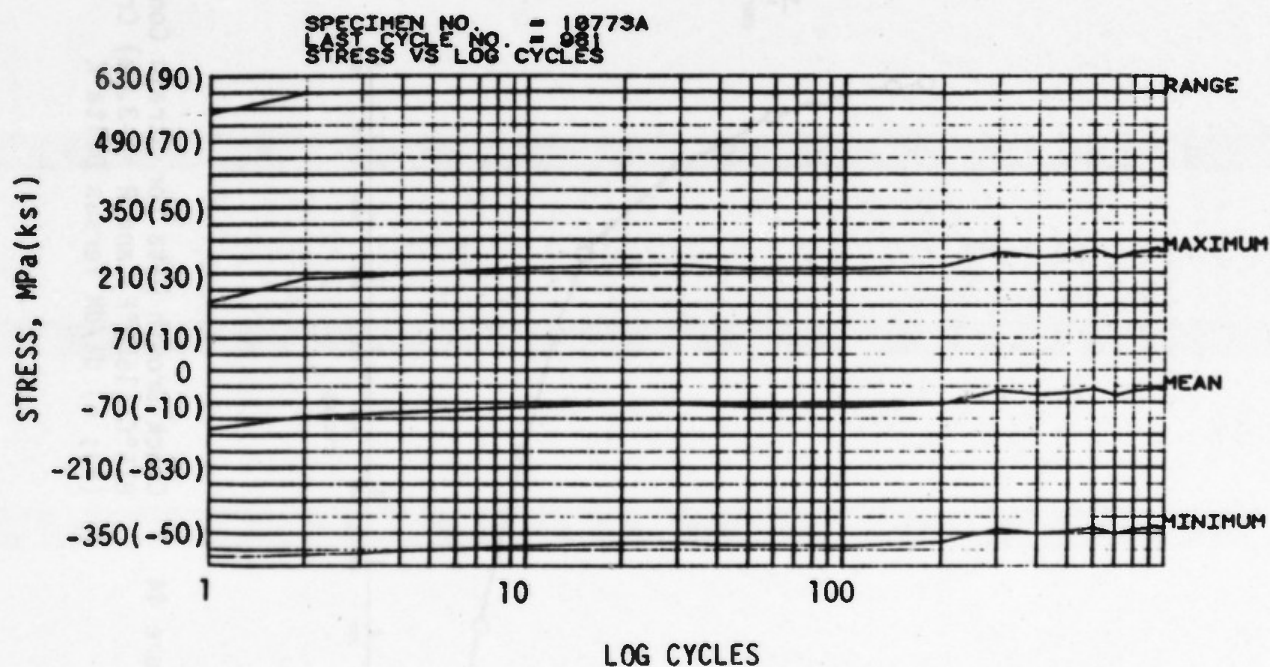


Figure 43 Mean Stress Versus Cycles Curves for Strain Controlled Specimen 10773 Tested at 815°C (1500°F) and $R = -3$ Showing Some Hardening After First Cycle But None Afterwards

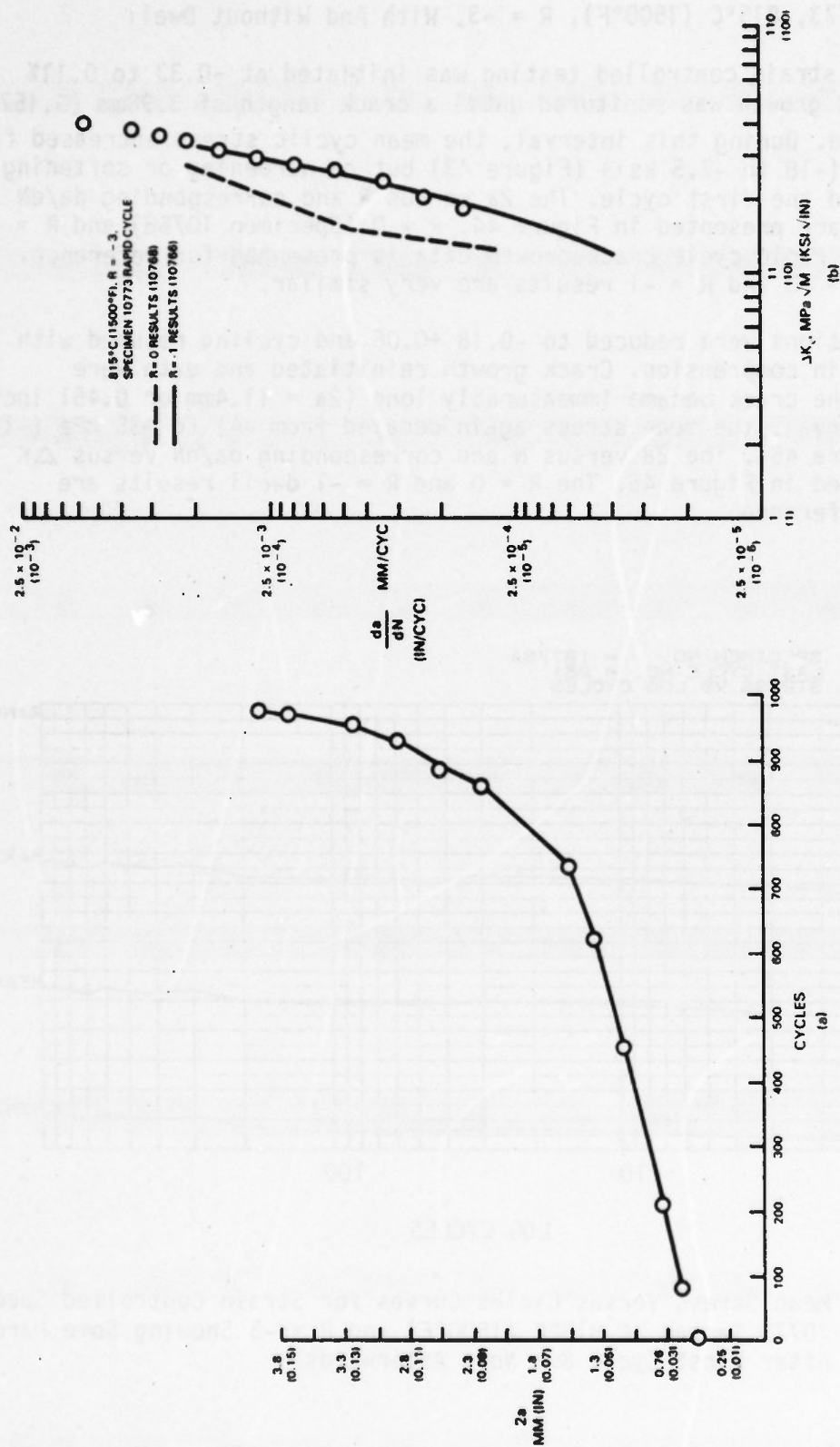


Figure 44 Crack Growth Data for Strain Controlled Specimen 10773 Tested at 815°C (1500°F) and R = -3. a) Crack Length (2a) Versus Cycles (N); b) da/dN Versus Delta K

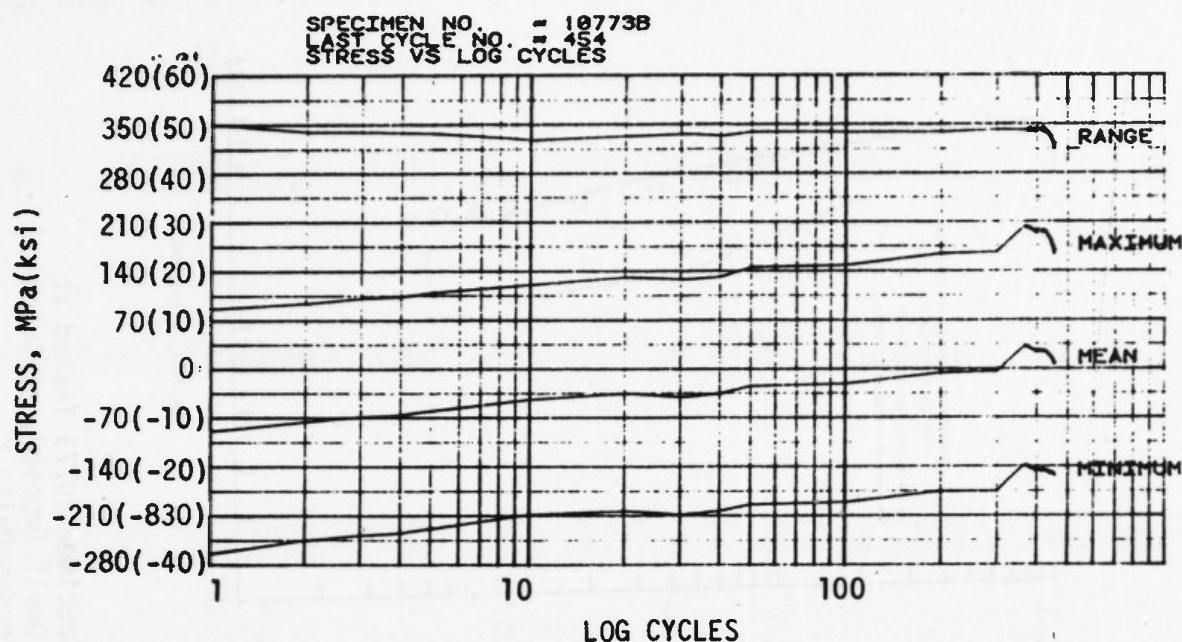


Figure 45 Stress Versus Cycle Curves for Strain Controlled Specimen 10773 During One Minute Dwell Portion Test at 815°C (1500°F) and $R = -3$

m. Specimen 10775, 736°C (1360°F) $R = -3$, With and Without Dwell

Strain controlled cycling was initiated at +0.09 to -0.27% and continued for 3900 cycles before crack growth from the starter slot was observed to initiate. Crack progression was recorded to a total length of 3.7mm (0.144 inch). The 2a versus N and da/dN data are shown in Figure 47. During the course of the test, the peak tensile stress increased from 136 MPa (19 ksi) to 231 MPa (33 ksi). $R = -3$ and $R = -1$ rapid cycle results at 736°C (1360°F) are very similar.

Strain conditions were changed to +0.045 to -0.135% with a one minute hold added at the compressive strain limit. No growth was noted in 10000 cycles and the strain amplitude was increased to +0.05% to -0.15%. Growth resumed after 1140 cycles. 2a versus N data were recorded until the total observed crack length reached 9.8mm (0.387 inch). 2a versus N and the corresponding da/dN data are presented in Figure 48. The peak tensile stress increased from 89.6 to 158.5 MPa (13 to 23 ksi) during the duration of the test. Cyclic inelasticity was negligible during the complete test.

n. Specimen 10774, 650°C (1200°F), $R = 0$, With Dwell

Dwell-fatigue crack growth tests at 743 and 815°C (1370 and 1500°F) suggested a reduction in the rate of crack growth associated with a one minute hold at a tensile strain. A dwell-fatigue test at 650°C (1200°F) was, thus, included in the program to determine if the effect was present at a lower temperature. Dwell-fatigue testing (one minute dwell at the tensile load limit) was initiated at a 0.152% strain level. No growth was noted and the peak strain was increased to 0.208% strain in eight steps. At this level crack growth initiated immediately and 2a versus N data were recorded until a total crack length of 4.3mm (0.170 inch) was reached. 2a versus N and the corresponding da/dN data are presented in Figure 49.

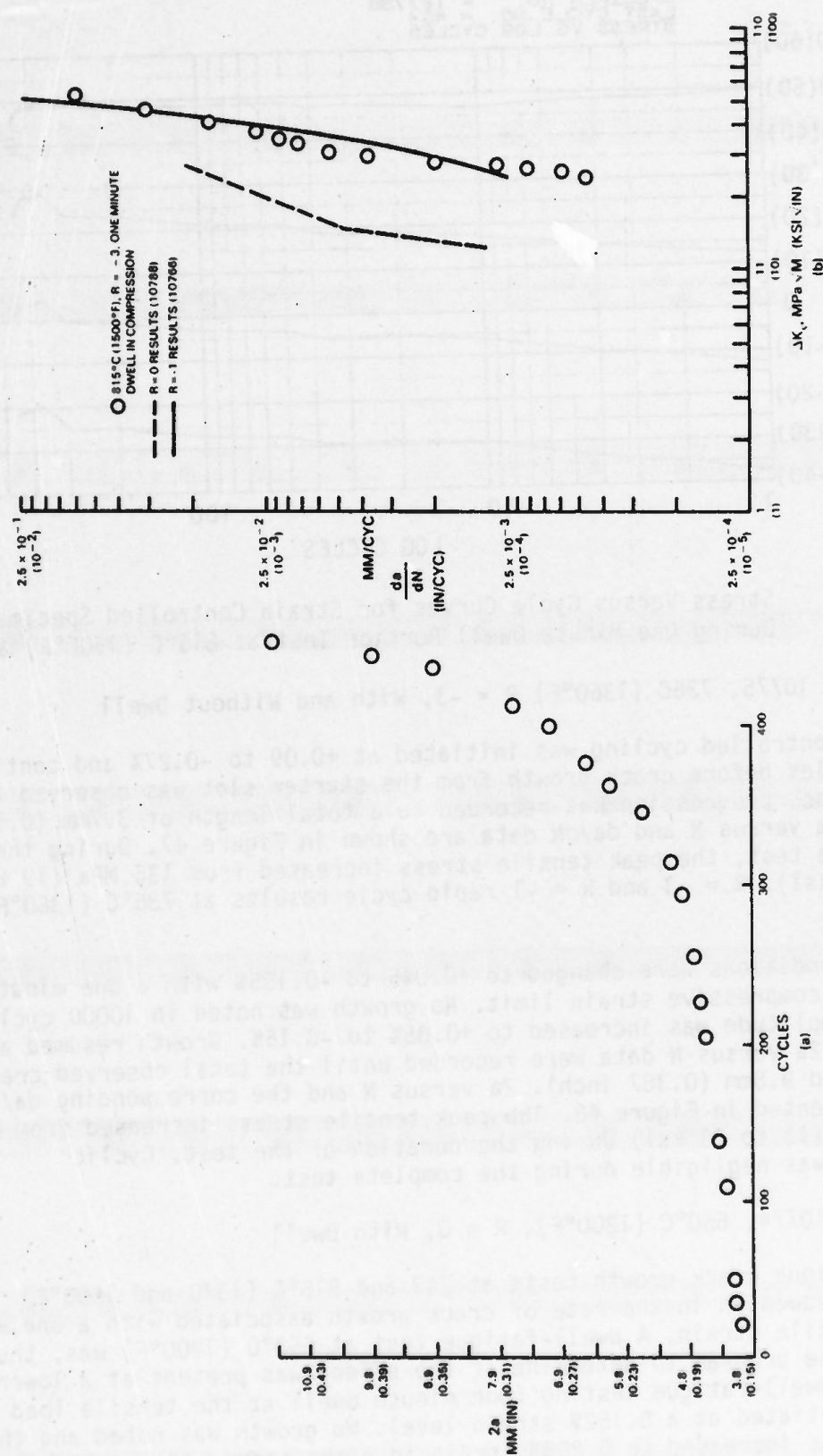


Figure 46 Crack Growth data for Strain Controlled Specimen 10773 Tested at 815°C (1500°F), R = -3 With a One Minute Dwell Imposed. a) Crack Length (2a) Versus Cycles (N); b) da/dN Versus Delta K

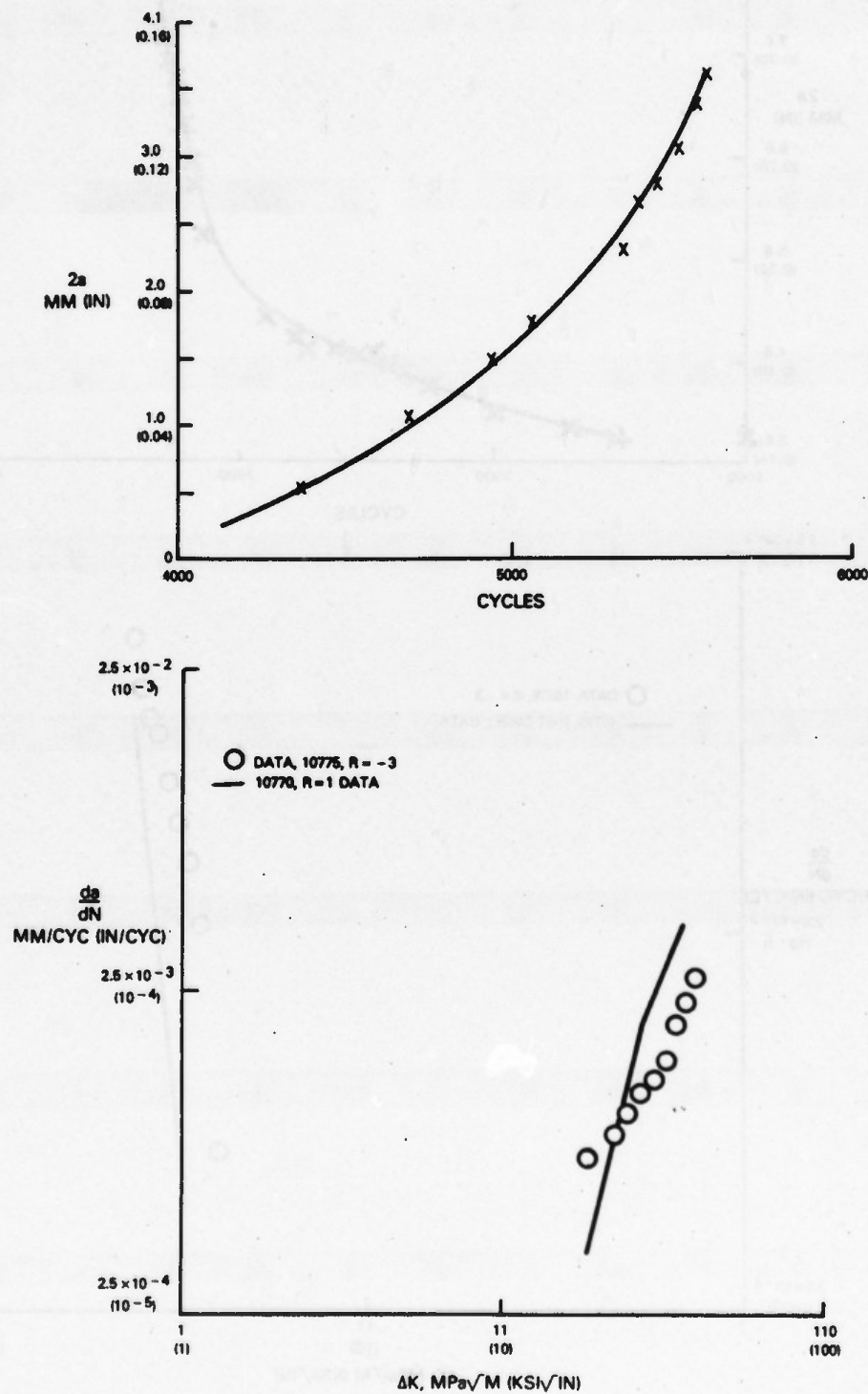


Figure 47

Crack Growth Data for Strain Controlled Specimen 10775, Tested at 736°C (1360°F) $R = -3$ Conditions, Rapid Cycle Results. a) Crack Length ($2a$) Versus Cycles (N); b) da/dN Versus Delta K

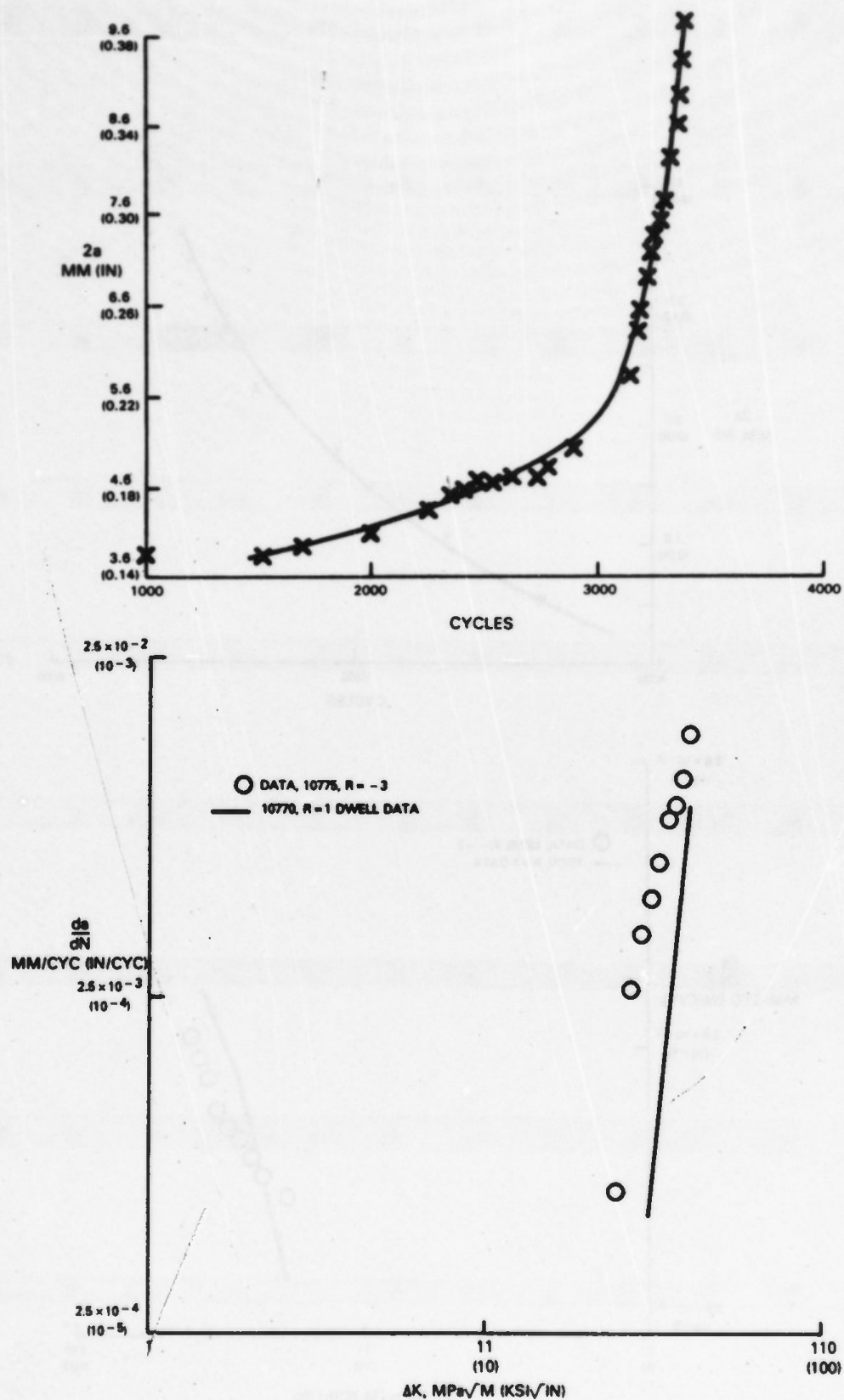
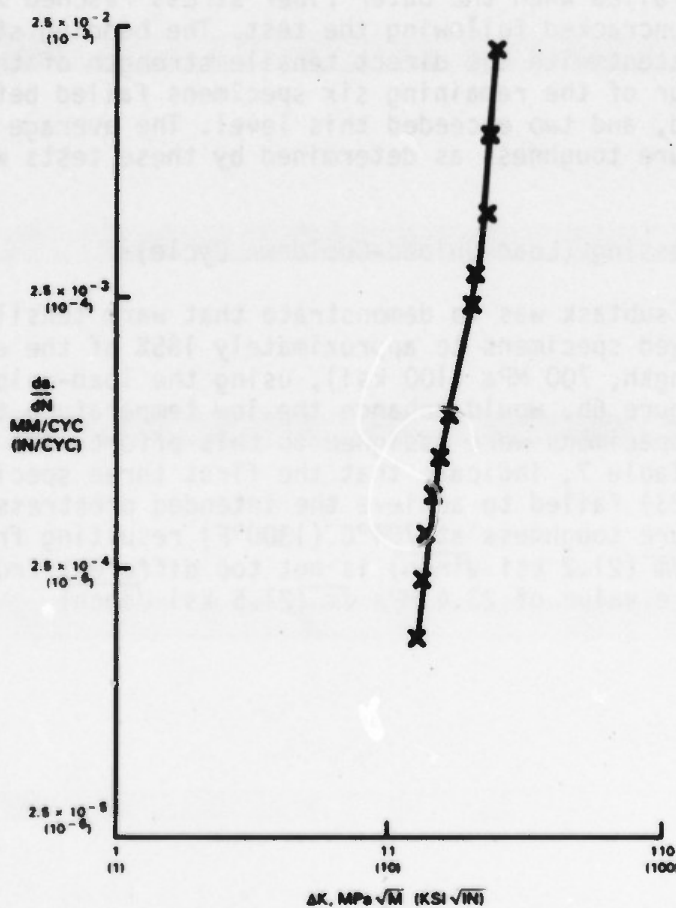
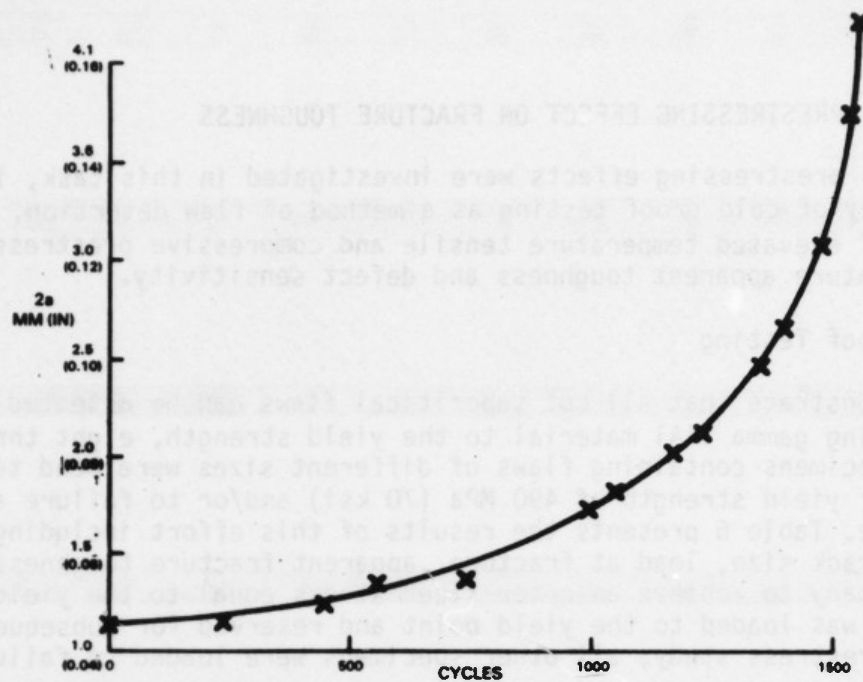


Figure 48

Crack Growth Data for Strain Controlled Specimen 10775, Tested at 736°C (1360°F), R = -3 Conditions With a One Minute Hold in Compression. a) Crack Length (2a) Versus Cycles (N); b) da/dN Versus Delta K



2. Task V PRESTRESSING EFFECT ON FRACTURE TOUGHNESS

Several prestressing effects were investigated in this task, including 1) the efficacy of cold proof testing as a method of flaw detection, and 2) the benefits of elevated temperature tensile and compressive prestressing on the low temperature apparent toughness and defect sensitivity.

a. Cold Proof Testing

To demonstrate that all but subcritical flaws can be detected by cold proof testing gamma TiAl material to the yield strength, eight three-point bending specimens containing flaws of different sizes were bend tested to the outer fiber yield strength of 490 MPa (70 ksi) and/or to failure at room temperature. Table 6 presents the results of this effort including the critical crack size, load at fracture, apparent fracture toughness and the load necessary to achieve an outer fiber stress equal to the yield strength. Specimen 7 was loaded to the yield point and reserved for subsequent use in the warm prestress study, all other specimens were loaded to failure.

Specimen 1, which failed when the outer fiber stress reached 714 MPa (102 ksi), was found to be uncracked following the test. The bending strength of this specimen is consistent with the direct tensile strength of the alloy reported elsewhere. Four of the remaining six specimens failed before the yield point was reached, and two exceeded this level. The average value of the apparent room temperature toughness as determined by these tests was 23.4 MPa \sqrt{m} (21.5 ksi \sqrt{inch}).

b. Tensile Warm Prestressing (Load-Unload-Cooldown Cycle)

The intent of this subtask was to demonstrate that warm tensile prestressing of preflawed specimens to approximately 185% of the elevated temperature yield strength, 700 MPa (100 ksi), using the load-unload-cooldown cycle diagrammed in Figure 6b, would enhance the low temperature toughness and flaw resistance. Five specimens were assigned to this effort. The test results, presented in Table 7, indicate that the first three specimens tested (number 12731, 17 and 23) failed to achieve the intended prestress level. The average apparent fracture toughness at 704°C (1300°F) resulting from these three tests, 23.1 MPa \sqrt{m} (21.2 ksi \sqrt{inch}) is not too different from the average room temperature value of 23.4 MPa \sqrt{m} (21.5 ksi \sqrt{inch}).

TABLE 6
COLD PROOF TEST RESULTS
OF THREE POINT BEND SPECIMENS

Specimen Number	Crack Shape/Size mm (in)	P _{yield} ⁽¹⁾ Newtons (lbf)	P _{critical} Newtons (lbf)	Apparent Toughness MPa \sqrt{m} (ksi \sqrt{in})	Disposition of Specimen
1	No crack	6390 (1436)	9324 (2095)	$f = 714 \text{ MPa}$ (102ksi)	Failed
22	0.7 (0.027)	5709 (1283)	6007 (1350)	23.9 (21.9)	Failed
2	0.9 (0.035)	6621 (1488)	5651 (1270)	22 (20.2)	Failed
19	0.5 (0.021)	5560 (1254)	5918 (1330)	20.7 (19.0)	Failed
12727	6.2 (0.243)	8508 (1912)	2581 (580)	26.4 (24.2)	Failed
12732	8.6 (0.338)	8174 (1837)	1023 (230)	23.9 (21.9)	Failed
7	0.8 (0.0305) 1.8 (0.0732)	6581 (1479)	D.N.F. @ 6581 (1479)	--	Reserved for Prestress Study
10	1.5 (0.0595)	6706 (1507)	4850 (1090)	24 (22)	Failed

(1) Load Level to Achieve 490 MPa (70 ksi) Outer Fiber Stress

TABLE 7
TENSILE WARM PRESTRESS RESULTS
(LOAD-UNLOAD-COOLDOWN CYCLES)

Specimen Number	Crack Shape/Size mm (in)	Prestress(1) MPa (ksi)	Disposition	Apparent Toughness or Fatigue Life
12731	 7.1 (0.280)→	—	Failure	24.9 MPa \sqrt{m} @ 704°C (22.9 ksi \sqrt{in} @ 1300°F)
17	 1.1 (0.043) 3.8 (0.148)	—	Failure	24.4 MPa \sqrt{m} @ 704°C (22.4 ksi \sqrt{in} @ 1300°F)
23	 0.6 (0.025) 2.2 (0.086)	—	Failure	19.9 MPa \sqrt{m} @ 704°C (18.3 ksi \sqrt{in} @ 1300°F)
16	 0.6 (0.025) 4.0 (0.165)	490 (70)	Tensile Fatigue -420MPa (-60 ksi)	700 cycles
21	 1.1 (0.042) 3.2 (0.127)	490 (70)	Tensile Bend Test	22.1 MPa \sqrt{m} @ RT (20.35 ksi \sqrt{in} @ RT)

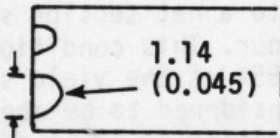
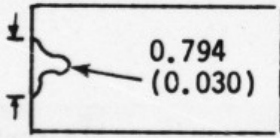
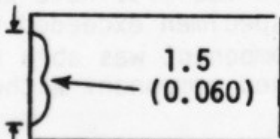
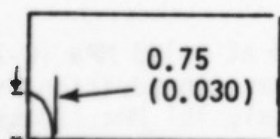
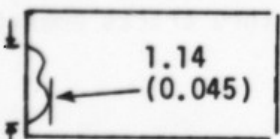
(1) Intended Level 700 MPa (100 ksi) Outer Fiber Stress

The two remaining specimens, 16 and 21, were successfully prestained to 130% of the yield strength at 704°C/490 MPa (1300°F/70 ksi). Specimen 21 was subsequently tested to failure at room temperature, failing at an outer fiber stress of 518 MPa (74 ksi). No change in the apparent fracture toughness was noted. Specimen 16 was fatigue cycled at an outer fiber stress of 0-420 MPa (0-60 ksi) and survived for 700 cycles.

c. Compressive Warm Prestressing (Load-Cooldown-Unload)

To demonstrate that compressive warm prestressing of components (warm peening, for example) can be beneficial to the low temperature flaw sensitivity, an additional five specimens were subjected to the load-cooldown-unload cycle illustrated in Figure 5c. A compressive stress of 490 MPa (70 ksi) and prestress temperature of 704°C (1300°F) were selected as prestress conditions. Results of this testing are presented in Table 8. Two specimens, numbers 7 and 14, were subsequently bend tested to failure at room temperature. No apparent increase in fracture toughness, as measured from the null load condition, was indicated. The remaining three specimens, numbers 13, 18 and 24, were fatigue cycled in bending at an outer fiber stress range of 420 MPa (60 ksi) and 280 MPa (-40 ksi) mean stress to simulate cycle conditions in a warm prestressed notch detail with a residual compressure stress of 70 ksi. All tests were suspended at 10,000 cycles.

TABLE 8
COMPRESSIVE WARM PRESTRESS RESULTS
(LOAD-COOLDOWN-UNLOAD CYCLE)

Specimen Number	Crack Size mm (in)	Prestress Level MPa (ksi)	Disposition	Apparent Toughness* or Fatigue Life
18	3.17 (0.125) 	-490(-70)	Fatigue**	10,000 cycles
13	1.58 (0.062) 	-490(-70)	Fatigue**	10,000 cycles
14	5 (0.198) 	-490(-70)	Failure at RT	18.2 MPa \sqrt{m} (16.7 ksi \sqrt{in})
7	1.9 (0.073) 	-490(-70)	Failure at RT	24.6 MPa \sqrt{m} (22.6 ksi \sqrt{in})
24	3.37 (0.133) 	-490(-70)	Fatigue**	10,000 cycles

* Measured From Null Load Condition

** Outer fiber stress -70 to -490 MPa (-10 to -70 ksi)

3. TASK VI- SUBCOMPONENT TESTING TO DEMONSTRATE BENEFITS OF PRESTRESSING

The purpose of this task was to verify that the cold proof test and warm prestress effect studied in Task V are valid for the case of a center notched, bolt hole type specimen which serves as a simulated component, and 1) to demonstrate that cold proof testing of preflawed components is or is not a potential method of flaw detection and 2) to establish to what degree warm overstressing of components effectively increases the tolerance to pre-existent defects.

Six center cracked panel specimens were cycled in tension until a fatigue crack somewhat longer than 6.3mm (0.125mm) was obtained in each specimen. Final ΔK levels varied from 76-94 MPa \sqrt{m} (10.8-13.5 ksi \sqrt{inch}). A hole was centered in each plate to remove all but 0.12-0.56mm (0.005-0.022 inch) of each crack. Specimens were heat tinted and replicated under load to establish, for each specimen, the flaw size and shape. It was not always possible to discern the length of the crack on the replica due to surface irregularities, nor was the heat tinting always effective in clearly delineating the shape of the flaw due to the tightness of the crack which inhibited oxidation. Table 9 presents the best estimate of the defect number, shape and size in each specimen. Clearly, irregularities of the precrack flaw shape resulted in significant variation of the final flaw physical characteristics.

Three specimens, 5, 6, and 7, were prestressed to a net section stress of 270 MPa (38.6 ksi) at 704°C (1300°F) for one-half hour. This condition, resulting in local elastic stresses approximately 185% of the yield strength and 170% of the anticipated operating stress, is considered to be about 20% above the maximum overstress achievable without resulting in gross distortion of the TiAl component or carrier disk. Following prestressing, specimens were allocated for cold tensile and fatigue testing.

a. Tensile Testing

Virgin Specimen 3 and proof strained Specimen 7, were tensile tested to failure at room temperature. Results are presented in Table 9. Note that the local notch failure stress for the non-prestressed specimen exceeded the yield strength ($K_T \approx 2.6$) and that the warm prestrained component was able to sustain a load in excess of that for a non-prestrained component without failing.

b. Fatigue Testing

The remaining four specimens were fatigue tested at 0-196 MPa (0-28 ksi) net section stress at room temperature. Specimen 4 was, in addition, subjected to approximately 34,000 cycles at a lower stress level, 161 MPa (23 ksi). The results indicate that the residual life is inversely proportional to the initial flaw size. Also note that warm prestressing has little if any retardation effect on 0.25-0.30mm (0.10-0.012 inch) thru cracks emanating from the notch (Specimen 5).

TABLE 9
SUBCOMPONENT TEST RESULTS

Specimen Number	K Level Precracking MPa \sqrt{m} (ksi \sqrt{in})	(1) Crack Size and Shape	Warm Prestrain @704°C, 270MPa @1300°F, 38.5ksi	Hot Section Critical Stress MPa (ksi)	Critical Crack Size mm (in)	K _{app} (2) MPa \sqrt{m} (ksi \sqrt{in})	Net Section Cyclic Stress MPa (ksi)	Cycles to Failure
3	12.3 (11.25)		No	237 (33.84)	.5 (.020) Corner	22.6 (20.7)	Tensile	Test
4	11.8 (10.86)		No	—	Grip Failure	No Growth	19.55 (23.0) 23.8 (28.0)	33650 9955 Grip Failure
5	13.8 (12.68)		Yes	196 (28.0)	Unknown	Unknown	28.0	176
6	13.9 (12.75)		Yes	196 (28.0)	Unknown	Unknown	28.0	8644
7	14.9 (13.49)		Yes	295 (42.2)	.79 (.031) Thru Crack	34.4 (31.6)	Tensile	Test
8	13.8 (12.65)		No	196 (28.0)	10.5 (.412) Thru Crack	21.1 (19.4)	28.0	1297

(1) Best estimate from heat tint and/or replica

(2) Estimated K critical based on largest flow present in the vicinity of notch

4. TASK VII - ATHERMAL CRACK GROWTH (TMF) TESTING

The objectives of this task were to establish crack growth behavior for the Ti-48Al-1V alloy when subjected to component relevant TMF cycles and relate the observed TMF crack growth behavior to estimates obtained from simple cycle data.

The cycles selected for study do not involve reversible temperature strain variation; therefore, a convenient procedure for defining the magnitude of TMF effects is to traverse the cycles in both clockwise and counterclockwise direction and compare the results, this was done to some extent in this program.

a. Specimen 11291, Cycle I TMF, 315-736°C (600-1500°F), Clockwise

The control computer was programmed to produce the strain temperature response illustrated in Figure 50. The cycling was initiated at a strain amplitude of +0.07% but no growth was noted at the starter slot. The strain amplitude was increased to +0.20% in three increments, at which point crack initiation was observed. The crack advanced to a total length of 2.3mm (0.089 inch) at which point the test was suspended. Minimal cyclic plasticity and no cyclic hardening or softening were noted during the testing at the 0.4% strain amplitude. 2a versus N data were recorded, these data and the corresponding plot of da/dN versus ΔK are shown in Figures 51 and 52.

The strain amplitude was subsequently decreased to +0.1% and then incremented to +0.125% to obtain additional data. Cycling at the +0.125% level successfully reinitiated crack growth. The material response to this amplitude was entirely elastic. 2a versus N relationships and the corresponding plot of da/dN versus ΔK are shown in Figures 52 and 53.

b. Specimen 11292, Cycle II TMF, 315-736°C (600-1360°F), Clockwise

The control computer was programmed to produce the strain-temperature response illustrated in Figure 54. TMF cycling was initiated at a strain amplitude of 0 to 0.2% but no growth was noted at the starter slot. The strain amplitude was increased to 0.25%, 0.275% and finally 0.300%; unfortunately, no evidence of crack initiation was noted. Precracking difficulty can be partially explained by the rapid relaxation of mean stress during the early cycling at each strain amplitude. To expedite testing, the specimen was precracked at 650°C (1200°F), $R = -1$ conditions to a total length of 0.66mm (0.026 inch). TMF testing was then resumed at a strain amplitude of 0.3%, but no further growth was noted. The strain amplitude was then increased to 0 to 0.325% and crack growth data were taken until the crack reached a length of 10.7mm (0.412 inch).

Nominal cyclic plasticity and no hardening or softening were noted during the testing. The mean stress, however, was noted to decrease from 23 ksi at the beginning of the test to 12 ksi at its termination. 2a versus N and the corresponding da/dN versus ΔK curve are shown in Figure 55.

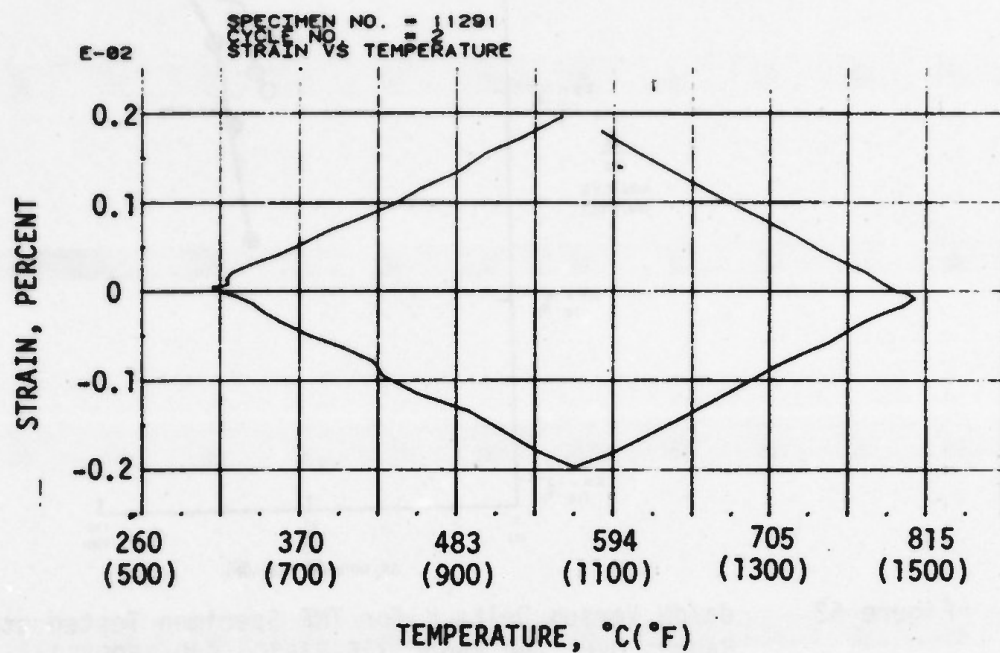


Figure 50 Thermocycle Selected for Initial Evaluation of TMF Specimen 11291

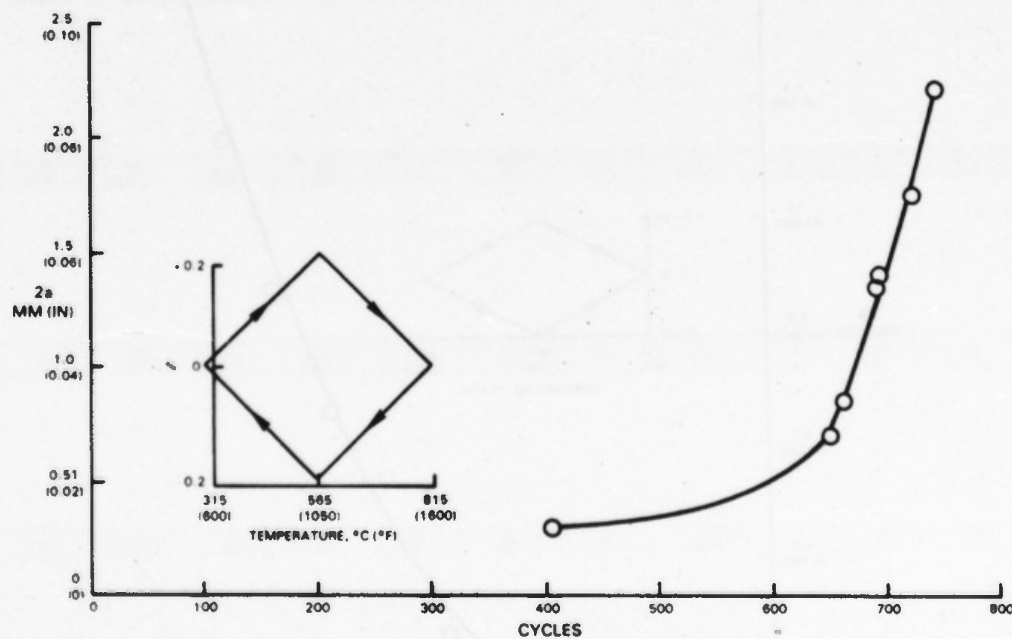


Figure 51 Crack Length (2a) Versus Cycles (N) for TMF Specimen 11291 Cycled as Shown

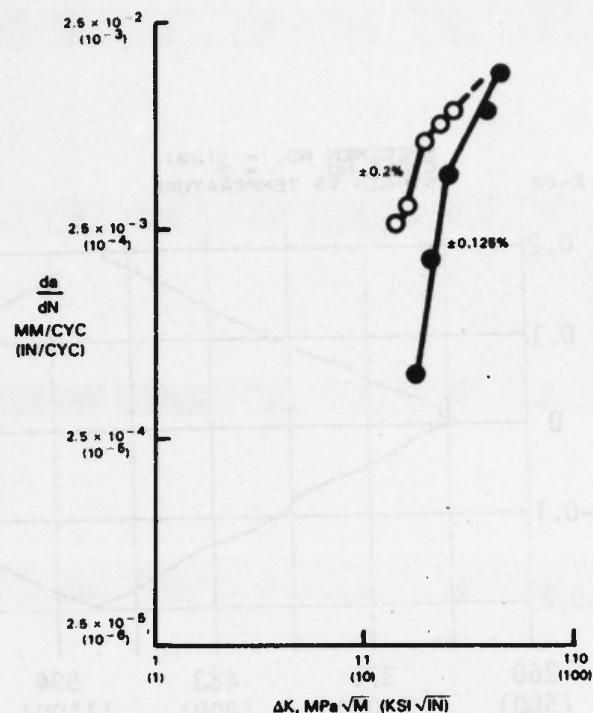


Figure 52 da/dN Versus Delta K for TMF Specimen Tested at Two Strain Ranges Over the Range 315-815°C (600-1500°F)

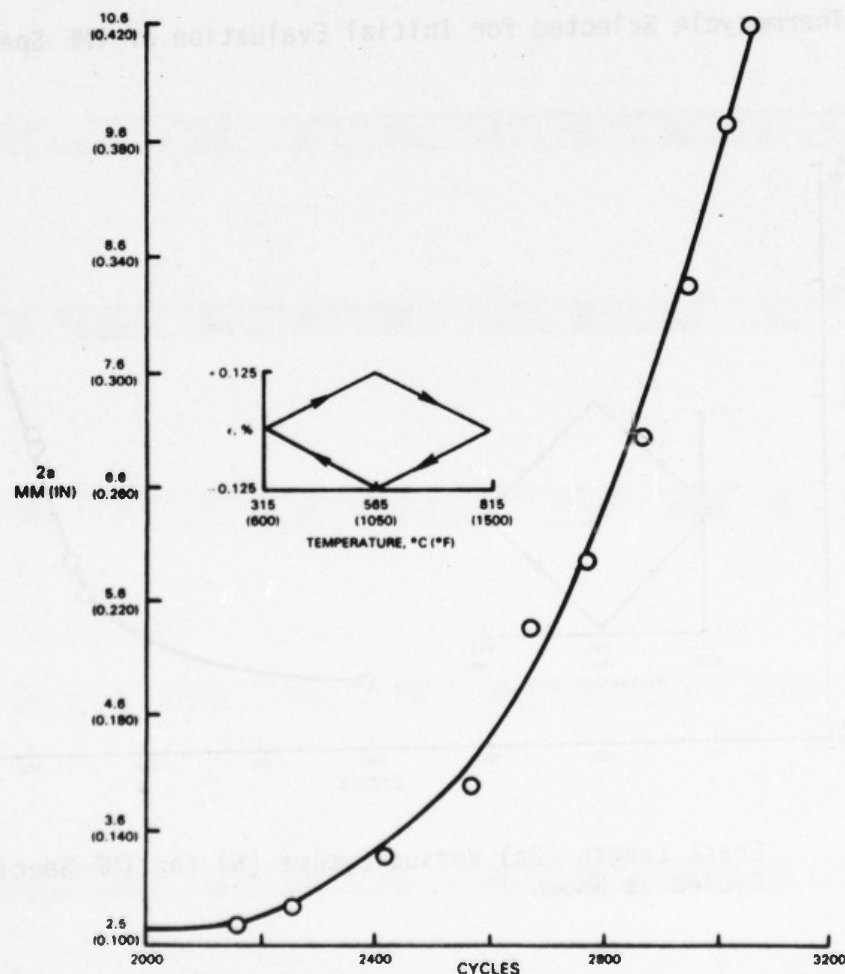


Figure 53 Crack Length ($2a$) Versus Cycles (N) for TMF Specimen 11291, Cycled as Shown

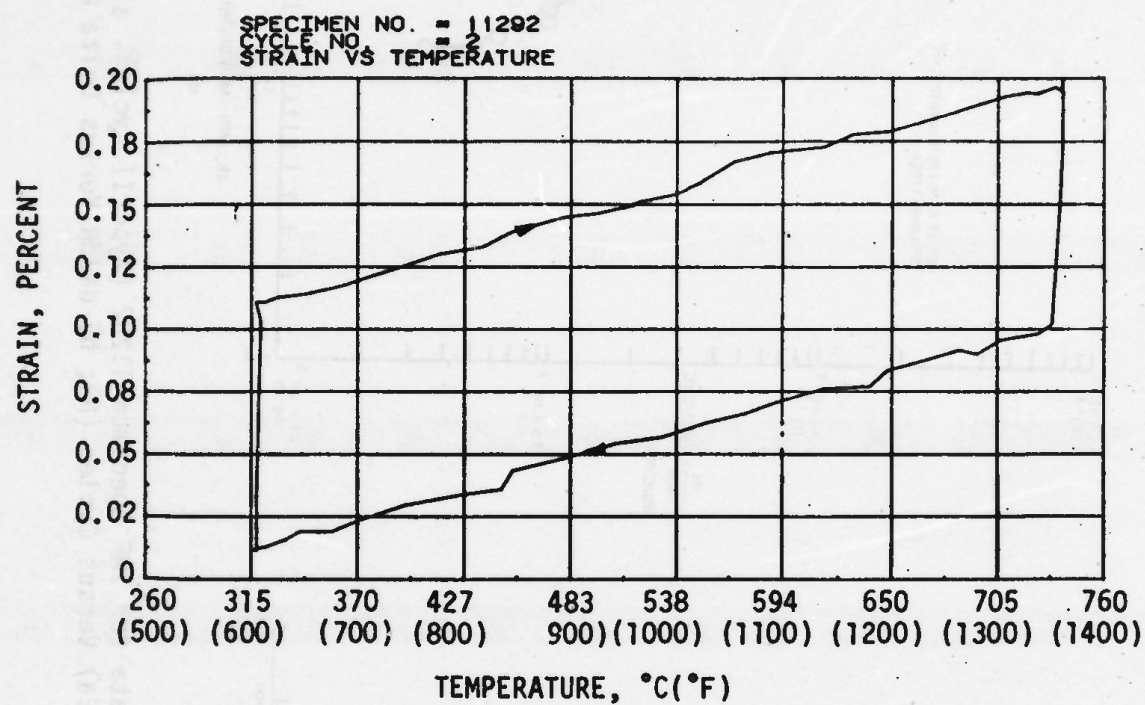


Figure 54 Strain Versus Temperature Curve for TMF Specimen 11292 Run in a Type II Cycle Between 315-736°C (600-1360°F) at $R = 0$

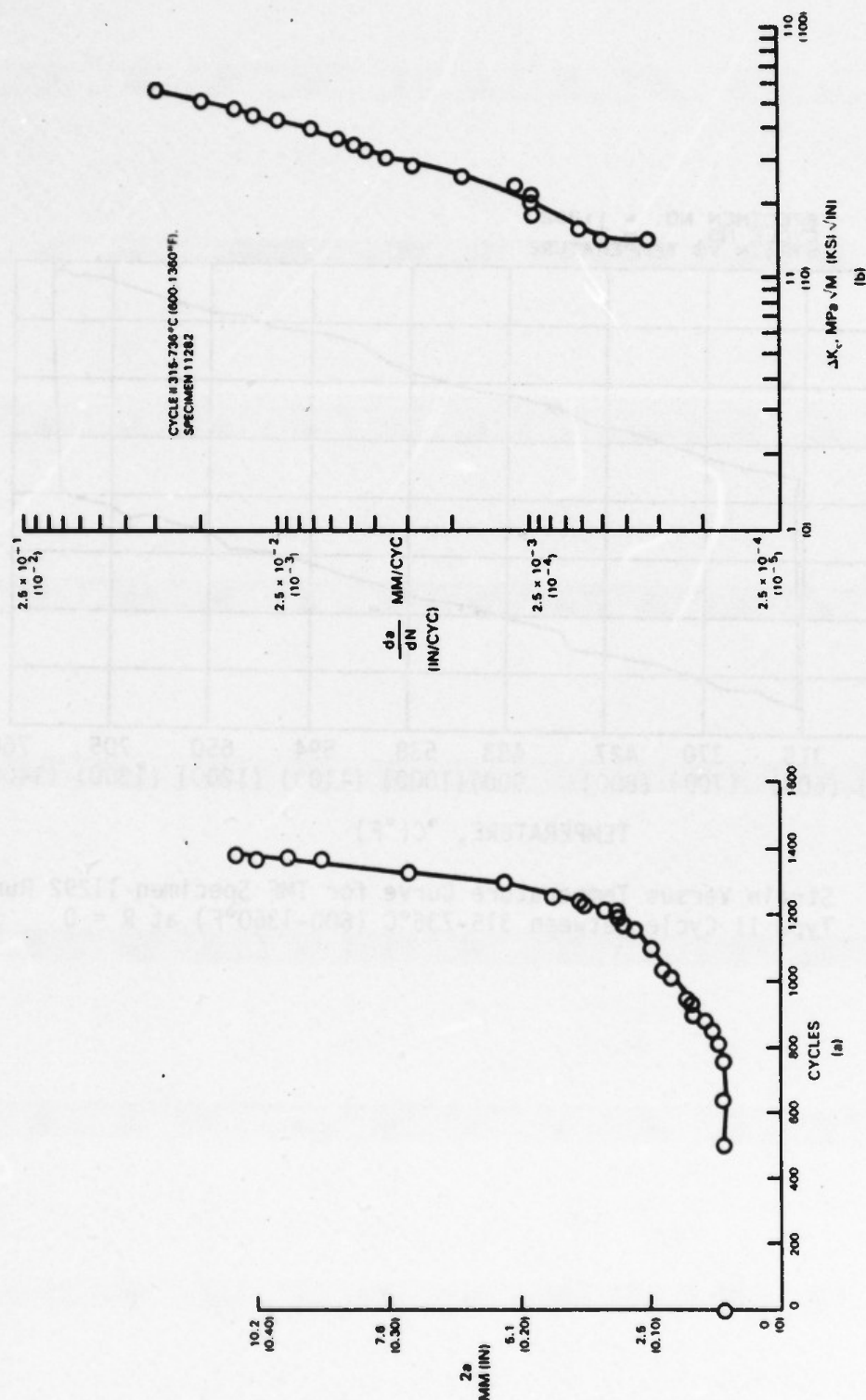


Figure 55 Crack Growth Data for TMF Specimen 11292 (Type II Cycle). a) Crack Length (2a) Versus Cycles (N); b) da/dN Versus Delta K

c. Specimen 11293, Cycle III TMF, 315-650° (600-1200°F), Clockwise

Load controlled TMF cycling was initiated with the stress-temperature waveform illustrated in Figure 56. Flaw growth initiated after approximately 3000 cycles elapsed. Data were obtained until the total flaw length reached 5.4mm (0.214 inch) at which point the specimen fractured. The 2a versus N and corresponding da/dN versus ΔK curves are presented in Figure 57. The R = 0, 650°C (1200°F) isothermal crack growth curve is included for reference.

d. Specimen 11294, Cycle III TMF, 315-650°C (600-1200°F), Counterclockwise

An additional Cycle III TMF test was initiated with the identical stress-temperature waveform illustrated in Figure 56, but traversed in the counterclockwise direction. The stress amplitude required to initiate and sustain crack growth was slightly larger than in the previous test, 356 MPa (48 ksi). At this test condition, initiation occurred after approximately 750 cycles. Data were obtained until the specimen fractured at a crack length of 4.5mm (0.176 inch). The 2a versus N and corresponding da/dN versus ΔK curves are presented in Figure 58. The 650°C (1200°F), R = 0 isothermal test data and the results of the previous test are shown for comparison.

e. Specimen 11295, Cycle I TMF, 315-815°C (600-1500°F), Counterclockwise

An additional Cycle I TMF test was initiated with the identical strain temperature waveform illustrated in Figure 50, but traversed in a counterclockwise direction. Cycling was initiated at a strain amplitude of +0.15%, and crack growth was observed to initiate at the starter slot after 2500 cycles had elapsed. Data were obtained until the crack reached a total length of 8.1mm (0.318 inch). The 2a versus N and corresponding da/dN versus ΔK curves are presented in Figure 59. The results of the Specimen 11291 test are presented for reference. Note that the direction of strain temperature cycling does not appear to affect the rate of crack growth except at low ΔK levels.

f. Specimen 11296, Cycle II TMF, 315-736°C (600-1360°F), Clockwise with One Minute Dwell at Maximum Strain

Two tests were performed to determine the influence of a one minute constant strain hold on the resultant crack growth rate for both Type I and Type II TMF cycling.

Clockwise cycling 315-737°C (600-1360°F) of Specimen 11276 was initiated at a 0-0.325% strain amplitude. A one minute constant strain hold was inserted at maximum strain conditions in each cycle. No growth was noted in 4355 cycles. The strain amplitude was increased to 0-0.35% but, again, no growth was observed. At this point the specimen was subjected to a precrack cycle of +245 MPa (+35 ksi) at 650°C (1200°F) to obtain 0.94mm (0.037 inch) of growth from the starter notch. TMF cycling was resumed at 0-0.325% and crack growth continued although at a progressively decreasing rate until it ceased entirely at a length of 2.0mm (0.080 inch). During this portion of the test, the maximum stress in the cycle decreased from 316MPa (45.1 ksi) to 216MPa (30.9 ksi). The minimum load in the cycle was initialized to zero and TMF cycling resumed.

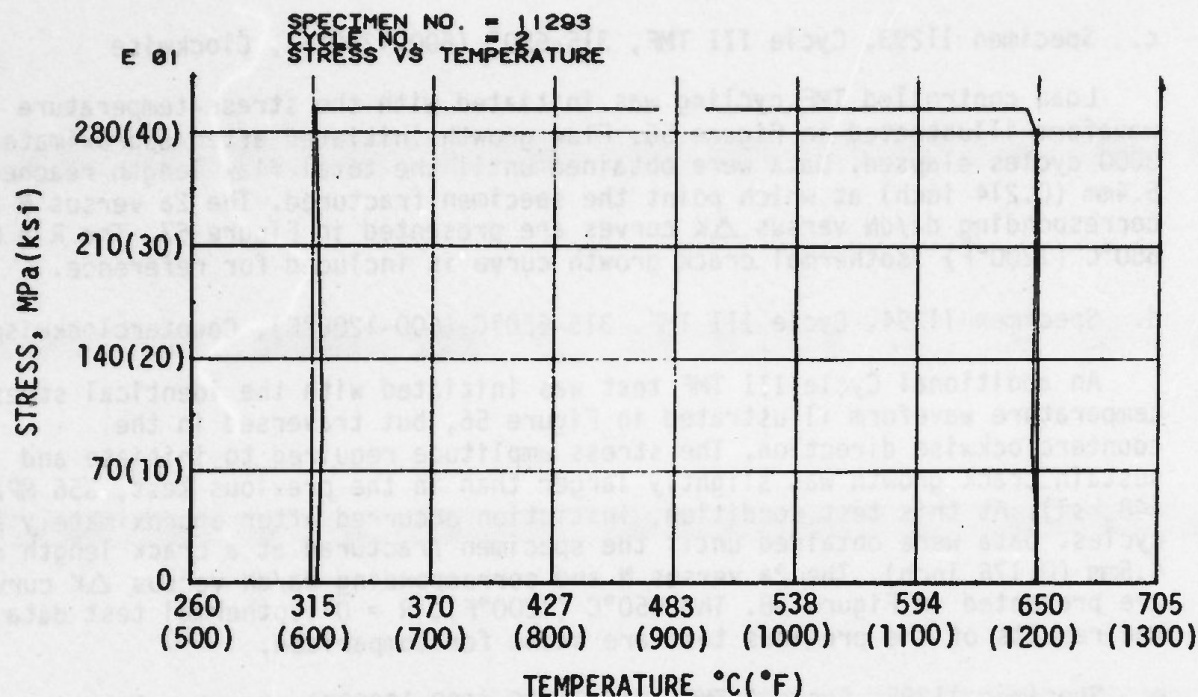


Figure 56 Stress Versus Temperature Curves for TMF Specimen 11293 Run in a Type III Cycle From 315-650°C (600-1200°F) in a Clockwise Manner

Crack growth reinitiated and progressed at an increasing rate until the test was discontinued at a length of 9.2mm (0.364 inch). 2a versus N data and the corresponding da/dN versus ΔK data are presented in Figure 60. Rapid cycle Type II TMF data are also presented for reference, showing the dramatic influence of the one minute constant strain hold at 736°C (1360°F) on the resultant crack growth behavior.

- g. Specimen 11297, Cycle I TMF with a one minute hold at maximum temperature, 315-815°C (600°F-1500°F) counterclockwise.

The third and final cycle I test was conducted at the same strain/temperature conditions used for Specimen 11295 with the exception that a one minute hold at maximum temperature was included in the cycle. Cycling was initiated at a strain amplitude of +0.15% and crack growth was observed to initiate after approximately 700 cycles. Data were obtained until the apparent crack length reached 8.7mm (0.341 inch). The 2a versus N and corresponding da/dN versus ΔK curves are shown in figure 61. The results of the Specimen 11295 and 11291 tests are presented for reference. Note that the one minute hold at zero strain and maximum temperature did not appear to affect the rate of crack growth.

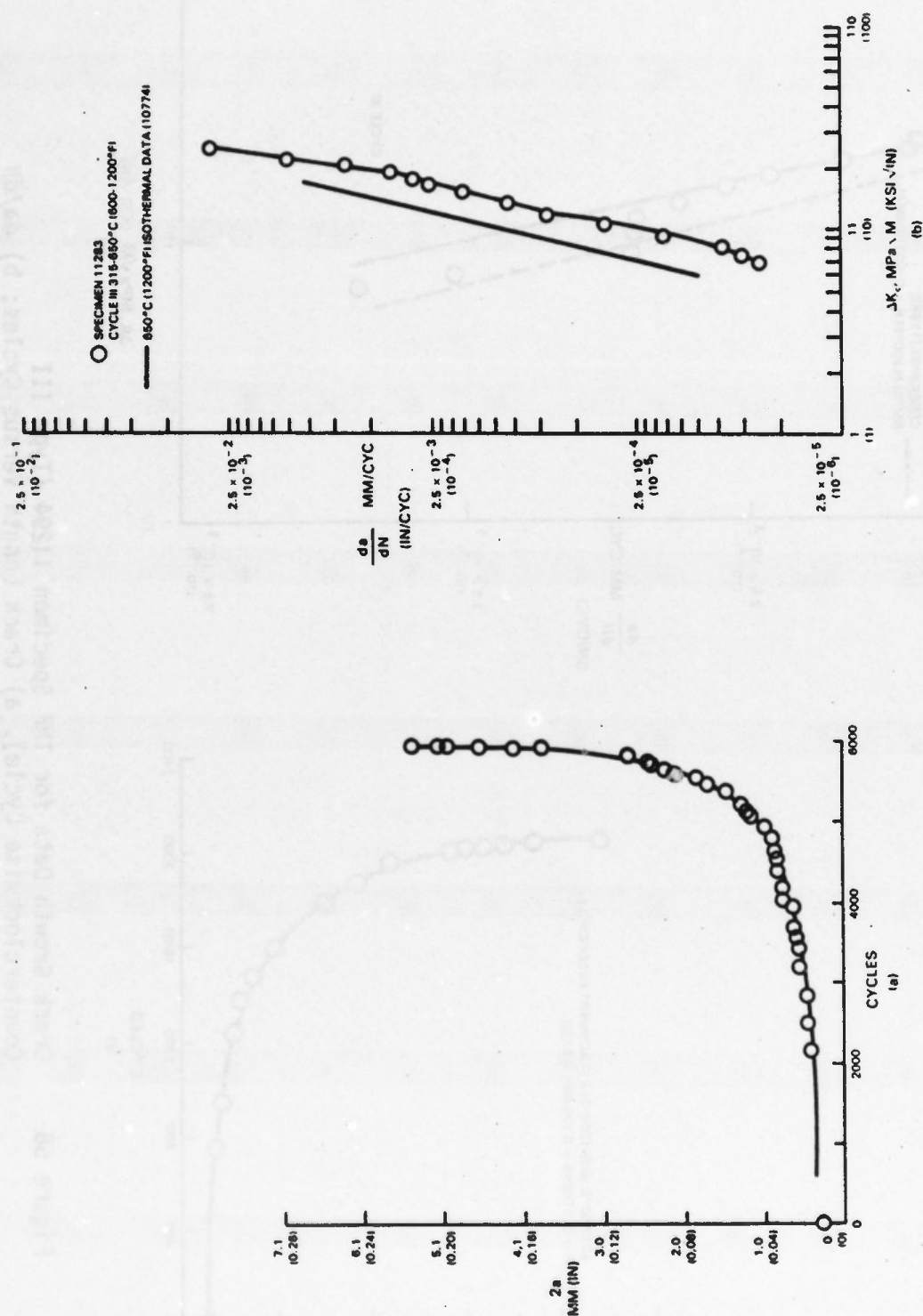


Figure 57 Crack Growth Data for TMF Specimen 11297 (Type III Clockwise Cycle). a) Crack Length (2a) Versus Cycles (N); b) da/dN Versus Delta K

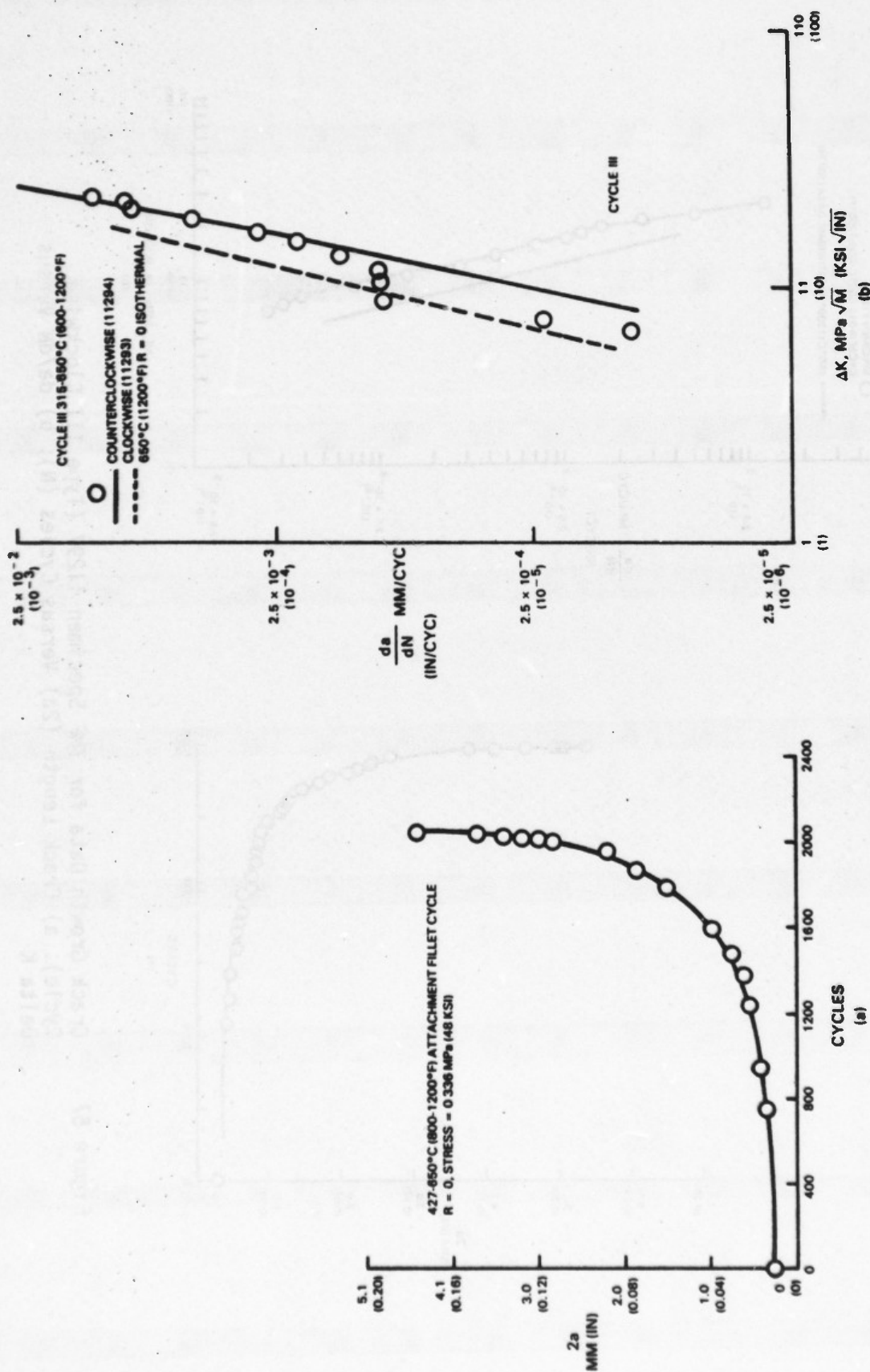


Figure 58 Crack Growth Data for TMF Specimen 11294 (Type III Counterclockwise Cycle). a) Crack Length Versus Cycles; b) da/dN Versus Delta K

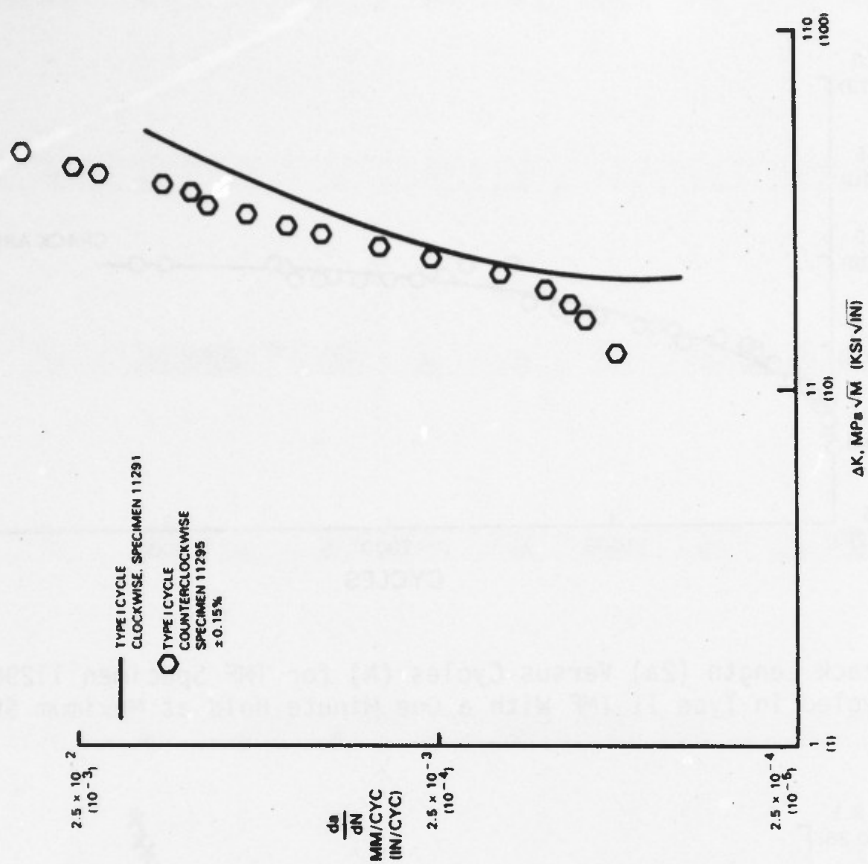
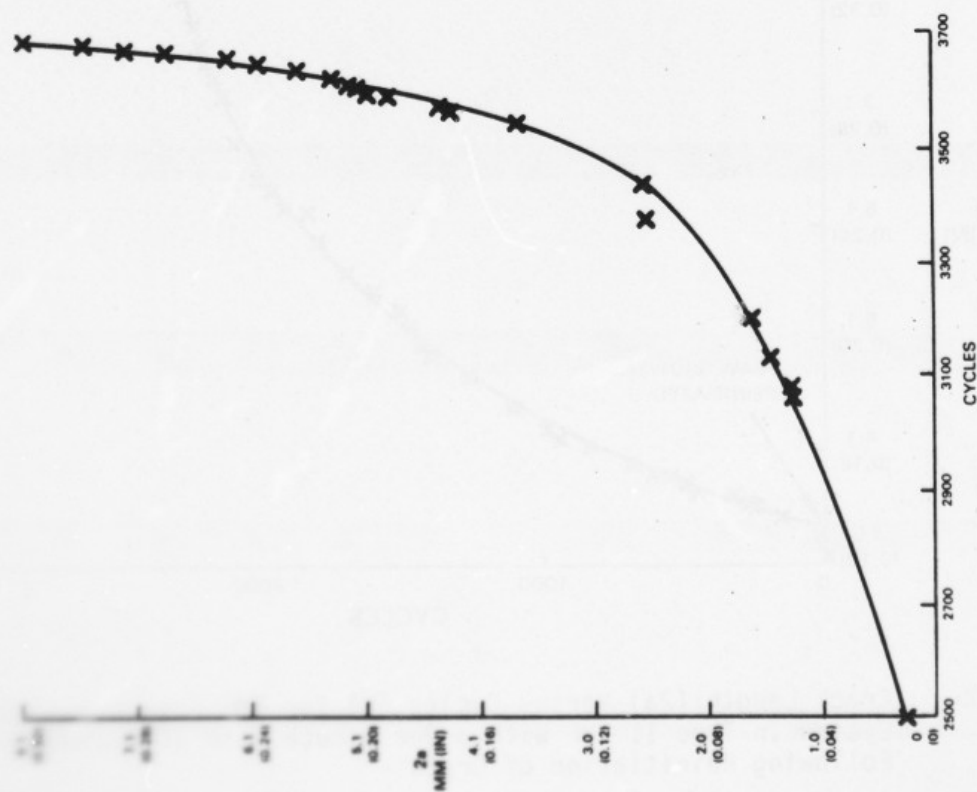


Figure 59a Crack Growth Data for TMF Specimen 11295 (Type I Cycle Counterclockwise). a) Crack Length (2a) versus Cycles (N); b) da/dN versus Delta K

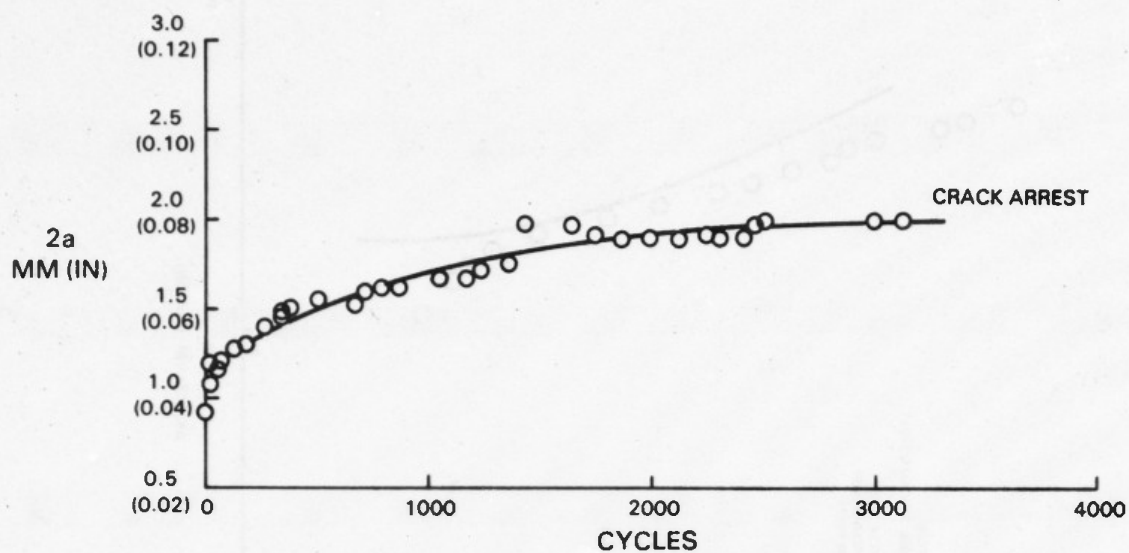


Figure 60a Crack Length (2a) Versus Cycles (N) for TMF Specimen 11296 Cycled In Type II TMF With a One Minute Hold at Maximum Strain

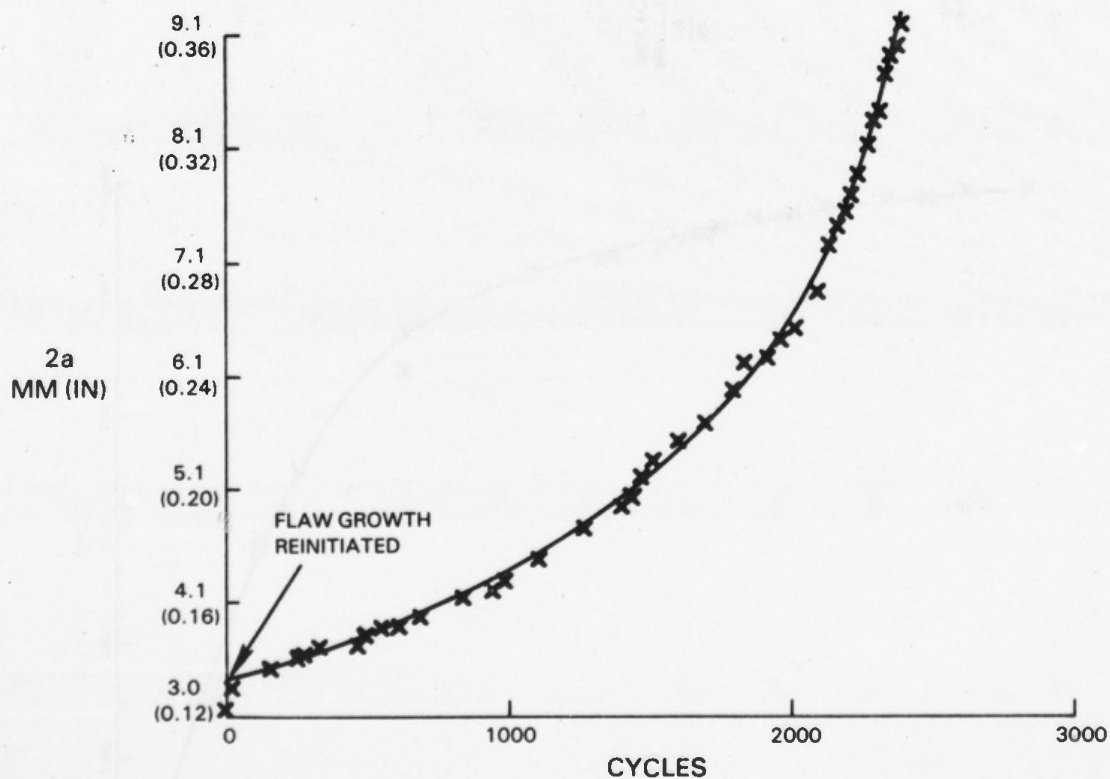


Figure 60b Crack Length (2a) Versus Cycles (N) for TMF Specimen 11296 Cycled In Type II TMF With a One Minute Hold at Maximum Strain Following Reinitiation of Crack

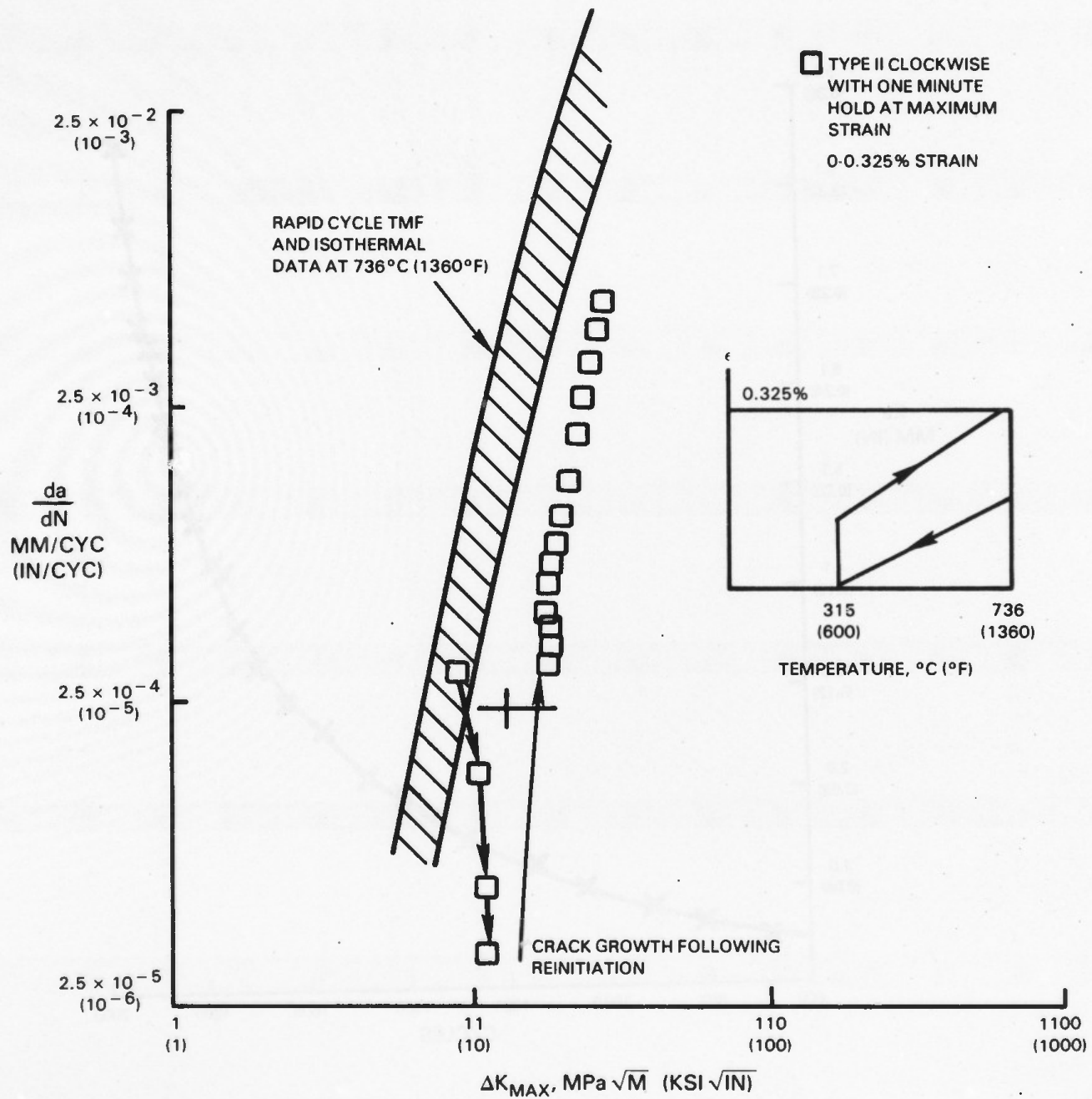


Figure 60c da/dN Delta Kmax for Specimen 11296, Type II TMF Cycling With a One Minute Hold at Maximum Strain

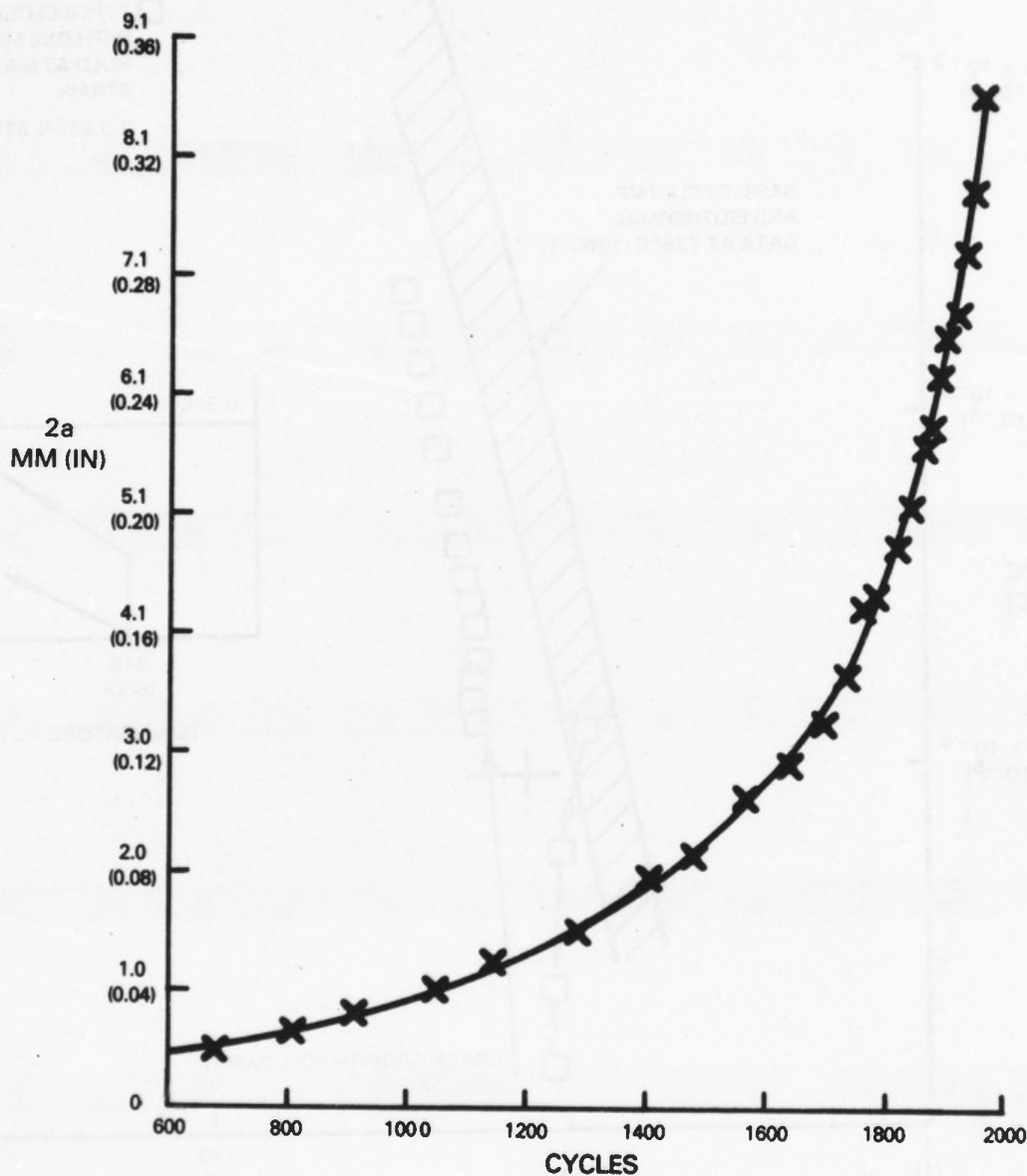


Figure 61a Crack Growth Data for TMF Specimen 11297 Counterclockwise Cycling With a One Minute Hold at Maximum Temperature. Crack Length (2a) Versus Cycles (N); b) da/dN Versus ΔK

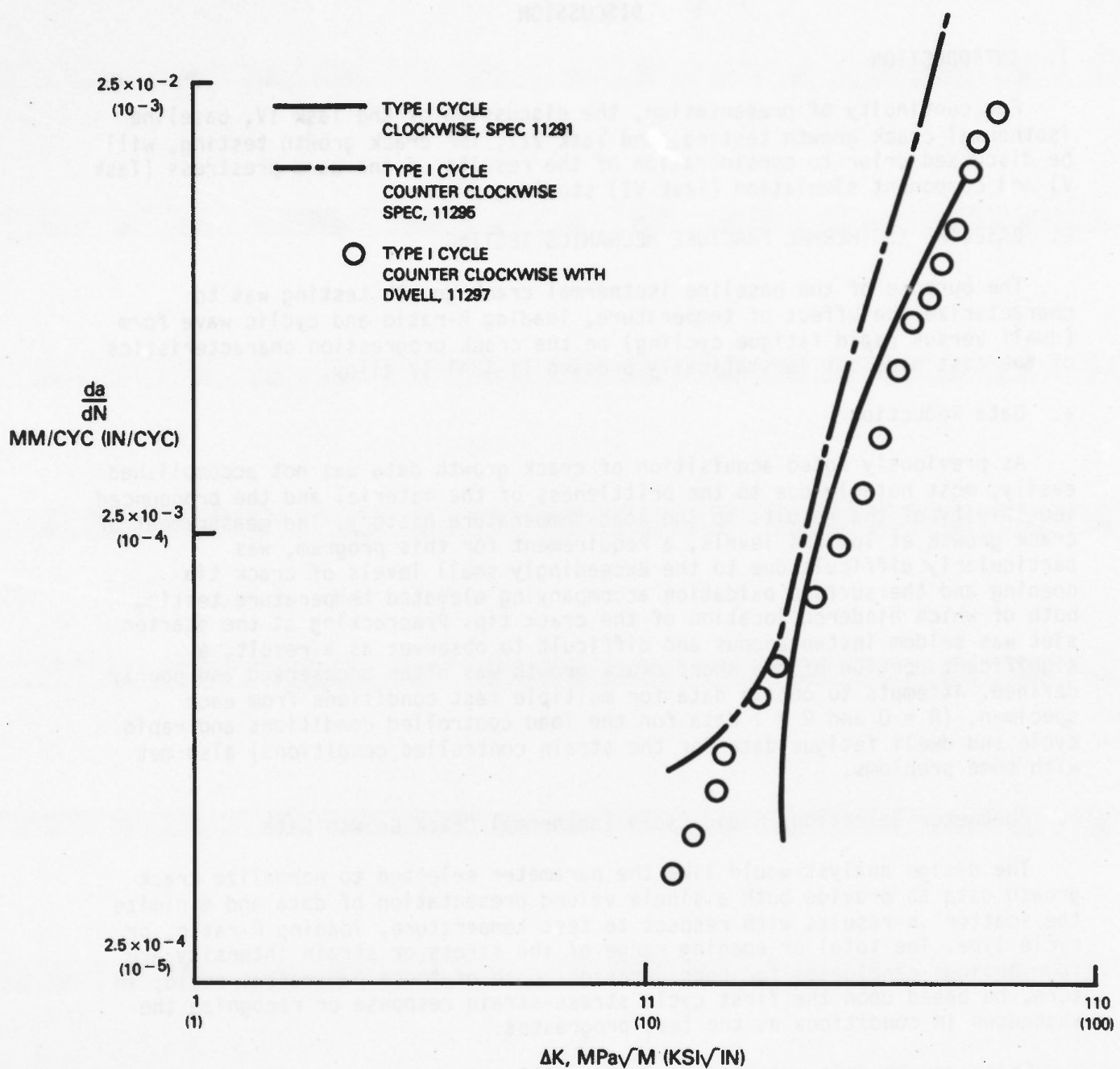


Figure 61

Crack Growth Data for TMF Specimen 11297 Counterclockwise Cycling With a One Minute Hold at Maximum Temperature. Crack Length (2a) Versus Cycles (N); b) da/dN Versus Delta K

SECTION IV

DISCUSSION

1. INTRODUCTION

For continuity of presentation, the discussion of the Task IV, baseline isothermal crack growth testing, and Task VII, TMF crack growth testing, will be discussed prior to consideration of the results of the warm prestress (Task V) and component simulation (Task VI) studies.

2. BASELINE ISOTHERMAL FRACTURE MECHANICS TESTING

The purpose of the baseline isothermal crack growth testing was to characterize the effect of temperature, loading R-ratio and cyclic wave form (dwell versus rapid fatigue cycling) on the crack progression characteristics of the cast plus hot isostatically pressed Ti-48Al-1V alloy.

a. Data Reduction

As previously noted acquisition of crack growth data was not accomplished easily, most notably due to the brittleness of the material and the pronounced sensitivity of the results to the load-temperature history. The measurement of crack growth at low ΔK levels, a requirement for this program, was particularly difficult due to the exceedingly small levels of crack tip opening and the surface oxidation accompanying elevated temperature testing both of which hindered location of the crack tip. Precracking at the starter slot was seldom instantaneous and difficult to observe; as a result, a significant portion of the short crack growth was often unobserved and poorly defined. Attempts to obtain data for multiple test conditions from each specimen, ($R = 0$ and $R = 1$ data for the load controlled conditions and rapid cycle and dwell fatigue data for the strain controlled conditions) also met with some problems.

b. Parameter Selection, Rapid Cycle Isothermal Crack Growth Data

The design analyst would like the parameter selected to normalize crack growth data to provide both a single valued presentation of data and minimize the scatter in results with respect to test temperature, loading R-ratio, or cycle type. The total or opening range of the stress or strain intensity are four obvious candidates for consideration. Each of these parameters could, in turn, be based upon the first cycle stress-strain response or recognize the shakedown in conditions as the test progresses.

Crack growth data reported in Section III have been presented using the peak to peak range of stress intensity as the normalizing parameter. A summary review of the data indicates that this parameter does not properly order results with respect to loading R-ratio, temperature, or cycle type.

The next logical parameter to consider is opening value of stress intensity.

Figures 62 through 64 summarize the rapid cycle isothermal crack growth results for the $R = 0$, -1 and -3 conditions; respectively. For this presentation, the maximum stress intensity in the cycle has been selected as the normalizing parameter. During asymmetric strain controlled testing at 736°C (1360°F) and above a relaxation in the mean stress occurs during the course of each test. The shakedown in stress is recognized in the determination of the maximum stress intensity factor. Representation of the data using the maximum stress intensity based upon the initial stress in each test as the normalizing parameter did not result in as consistent an ordering of the data with respect to test temperature or R -ratio. A review of the data presented in Figures 62 to 64 indicates that, at a given K_{\max} value, the rate of crack growth generally increases with increasing test temperature. No transition in crack growth behavior is noted as the ductile-brittle transition $704\text{--}760^{\circ}\text{C}$ ($1300\text{--}1400^{\circ}\text{F}$) is traversed. Representation of the data against K_{\max} also results in a fair intermixing of the $R = 0$, -1 , and -3 data; suggesting that crack tip closure occurs when the remotely applied load becomes compressive.

In spite of the apparent differences in slope of the fully reversed and one way tension crack growth data resulting from the load controlled testing (attributable to load sequence effects), the $R = 0$, $R = -1$, and $R = -3$ data intermixes fairly well and generally indicate an increasing crack growth rate with test temperature. These results suggest that the variation in crack tip opening displacement might yet be a superior correlating parameter, functionally:

$$\frac{da}{dn} = f(\Delta C_{\text{TOD}}) = f(\delta_{\max} - \delta_{\text{opening}})$$

where δ_{opening} is the equivalent elastic crack tip displacement required to overcome the combined effect of plastic wake, residual stresses, and crack face wedging due to surface irregularity and fatigue debris. δ_{opening} should be a function of test temperature. As the test temperature increases,

the plane of propagation becomes less branched and irregular. $\delta_{\text{opening}}^{(T)}$ should, therefore, decrease with increasing temperature.

Assuming small scale yielding we may expect

$$\frac{da}{dn} = f\left(\frac{K_{\max}^2}{\sigma_o(T)E(T)} - \delta_{\text{opening}}^{(T)}\right)$$

The variation of E and yield strength with temperature are presented in Figure 65a and b. It was assumed that δ_{opening} varied with test temperature in the manner shown in Figure 65c.

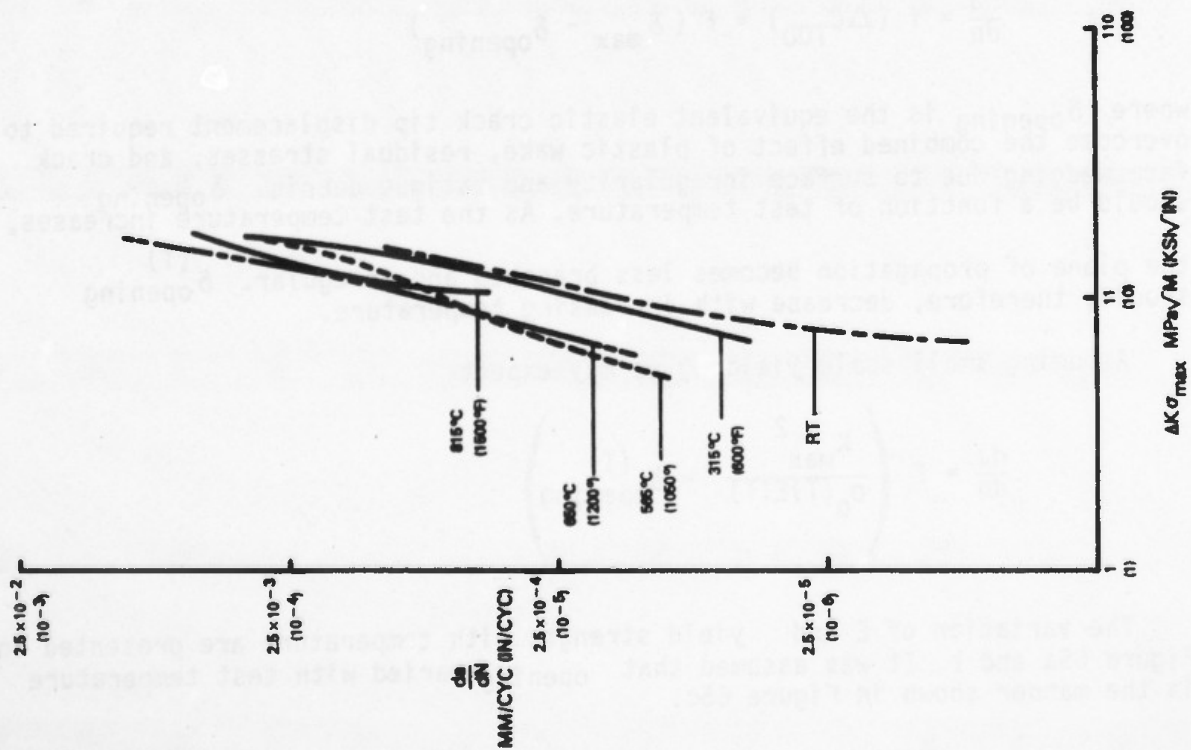


Figure 62 Composite Plot, Rapid Cycle da/dN Versus K_{max} $p = 0$

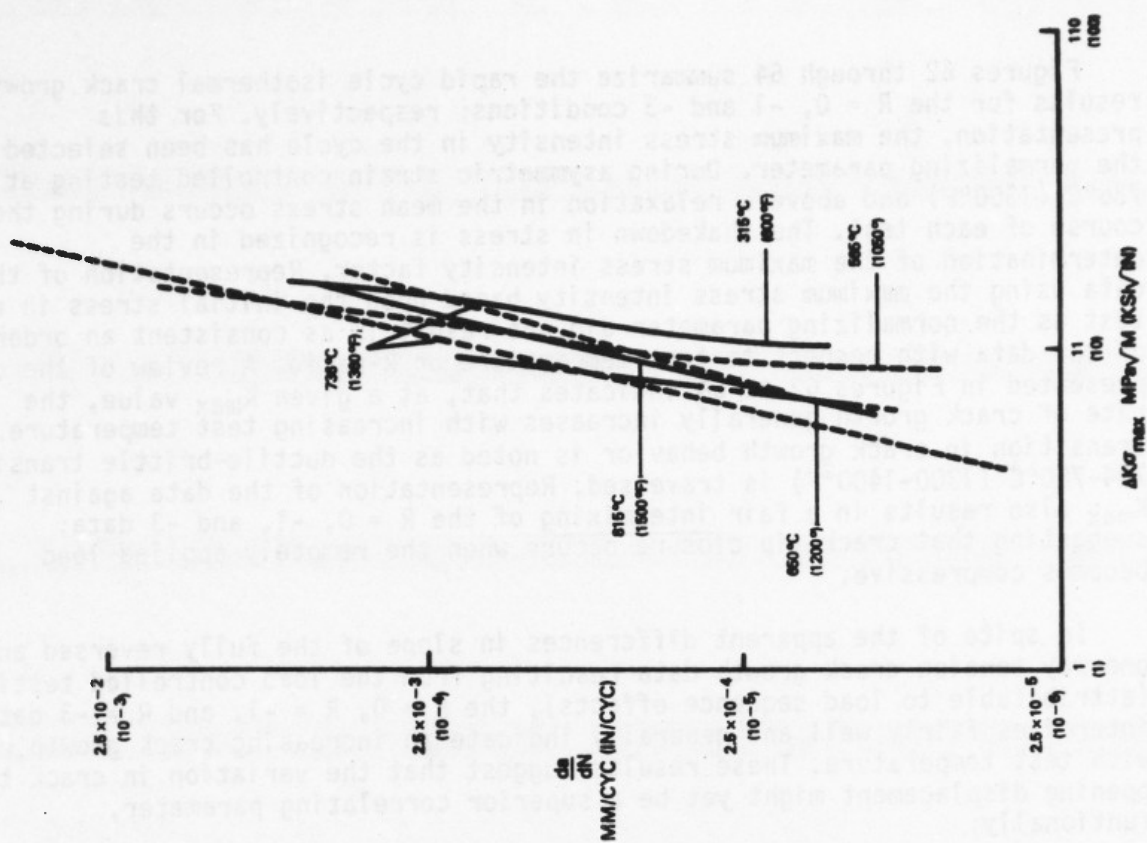


Figure 63 Composite Plot, Rapid Cycle da/dN Versus K_{max} $R = -1$

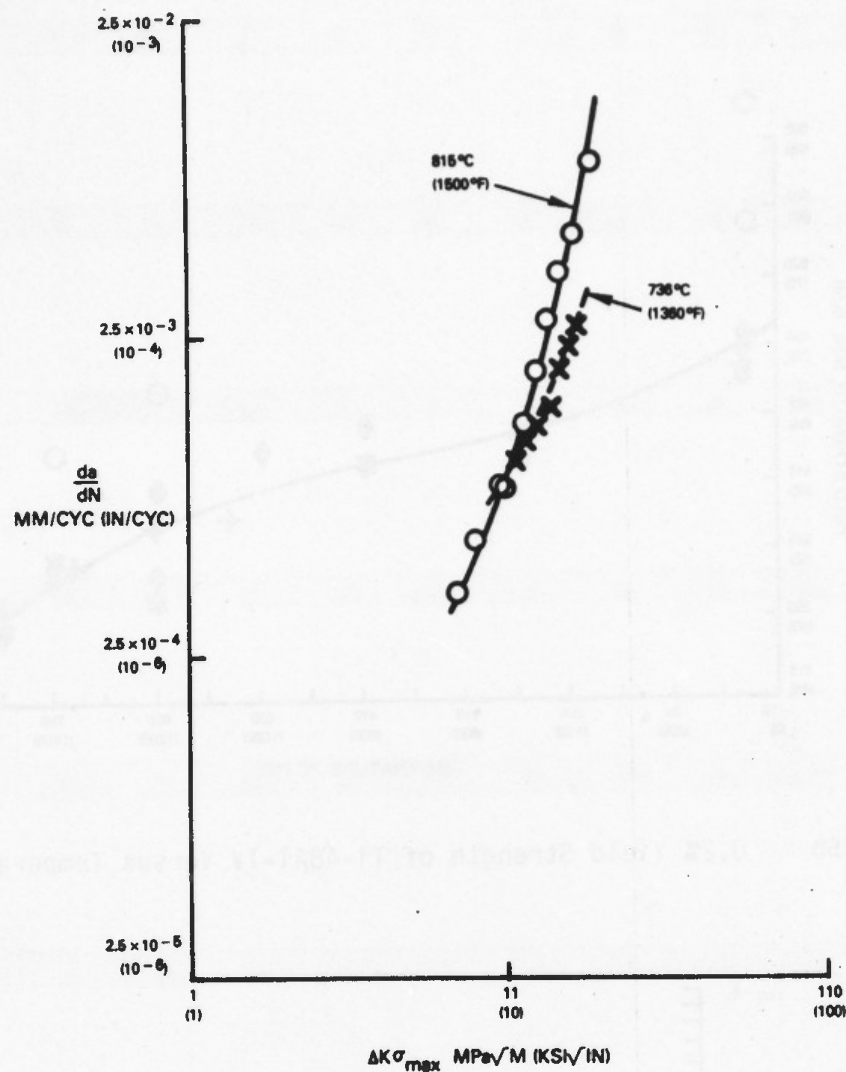


Figure 64 Composite Plot, Rapid Cycle $\frac{da}{dN}$ Versus K_{max} $R = -3$

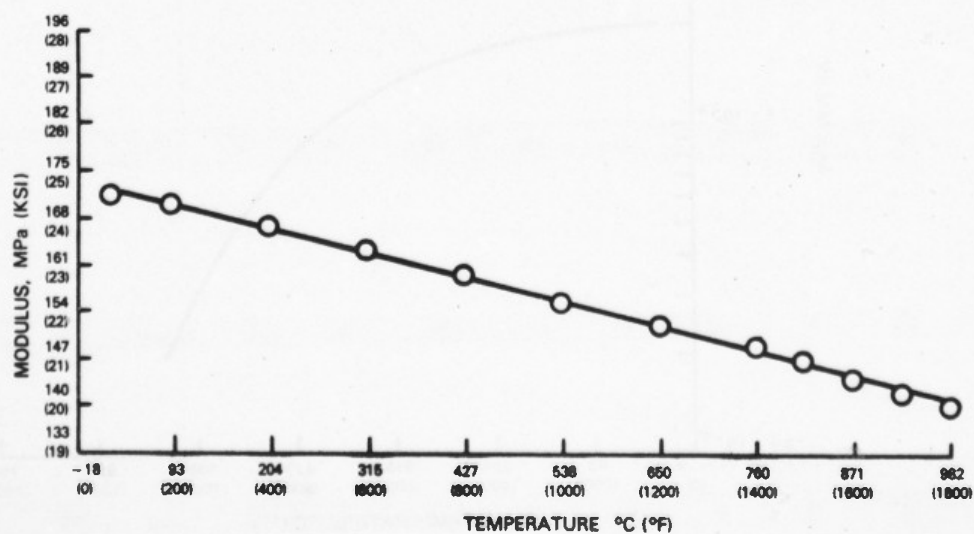


Figure 65a Dynamic Modulus of Ti-48Al-1V Versus Temperature

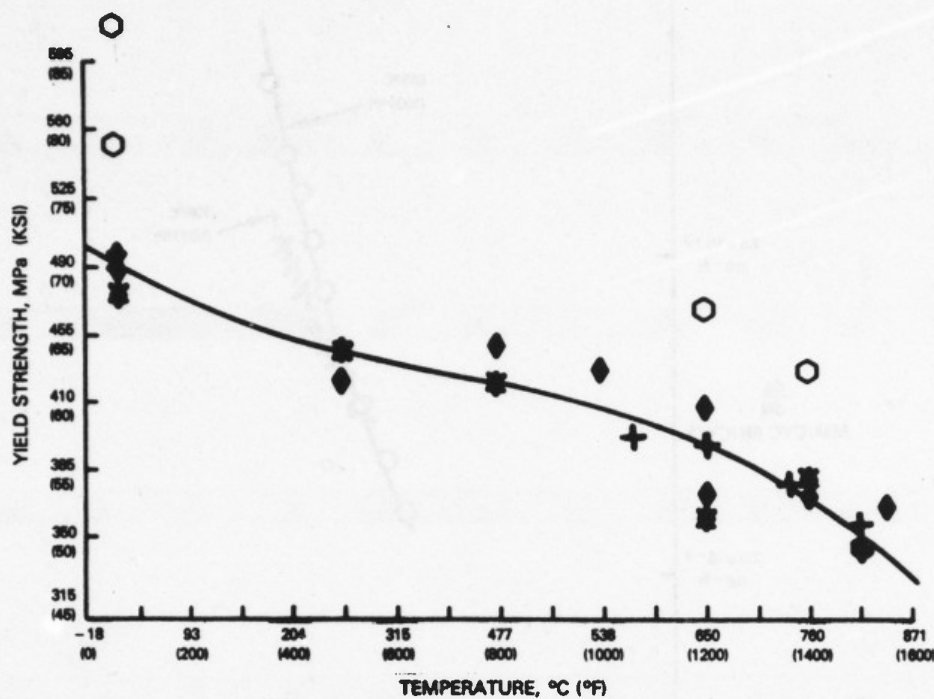


Figure 65b 0.2% Yield Strength of Ti-48Al-1V Versus Temperature

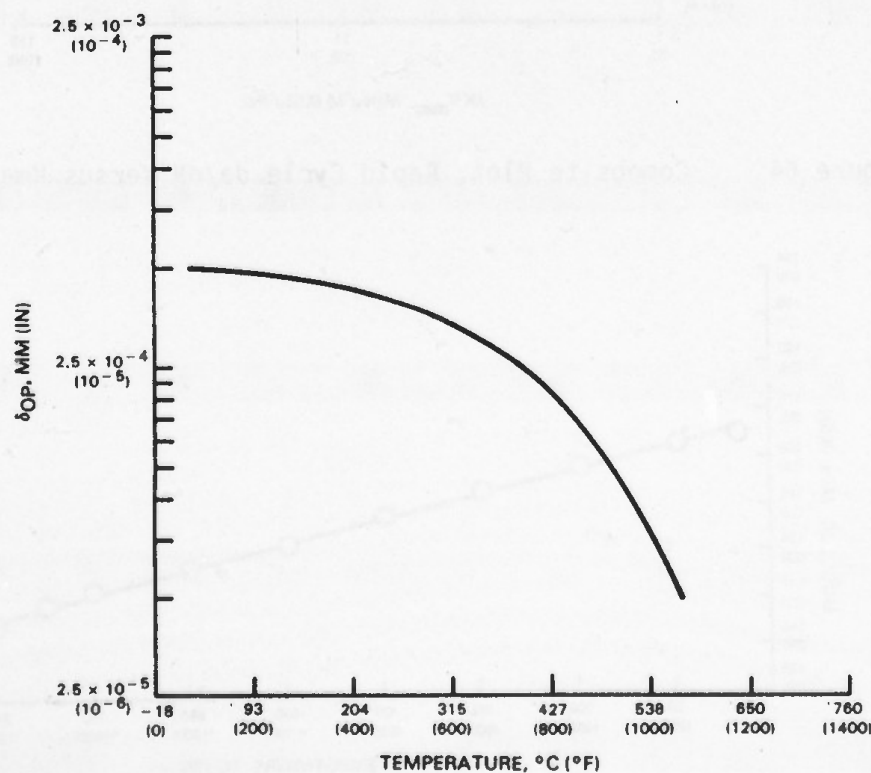


Figure 65c Opening Crack Tip Stretch Versus Temperature

Rapid cycle crack growth data for one way tensile and fully reversed load controlled conditions are plotted against $\Delta CTOD$ in Figure 66. A good mix of results occurs with respect to temperature and R-ratio. The median crack growth curve for R-ratios of 0 to -1 can be expressed as:

$$\frac{da}{dn} = 24 \left(\frac{K_{max}^2}{E(T)\sigma_o(T)} - \delta_{opening}^{(T)} \right)^{1.46}$$

Rapid cycle crack growth data for Ti-48Al-1V for R = 0, -1 and -3 strain controlled conditions are plotted against $\Delta CTOD$ in Figure 67; note that the data generally fall within the scatter band defined by the lower temperature load controlled testing.

c. Normalizing Parameter Selection, Isothermal Dwell Fatigue Test Data

The effect of a one minute elevated temperature hold at the tensile (R = 0 and -1) and compressive (R = -1 and -3) strain limits is shown in Figure 68. For crack growth rates exceeding 5×10^{-4} mm/cycle (2×10^{-4} in/cycle), the imposed dwell hold results in little or no change in the crack growth rate relative to the rapid cycle data. For rates of growth slower than 5×10^{-4} mm/cycle (2×10^{-4} in/cycle), a moderating effect of the tensile dwell period on the rate of crack growth is noted with the bimodal slope suggesting an apparent increase in the threshold opening level due to the dwell period. A dwell in compression has little additional effect on the rate of growth beyond that attributable to the ratcheting upward in the mean stress in the cycle. Figure 69 presents the dwell-fatigue data for a load controlled R = 0 test at 650°C (1200°F). The results suggest that a one minute tensile hold has an effect but to a lesser degree than that observed at 736°C (1360°F) and 815°C (1500°F).

At elevated temperature, a severe oxide buildup is noted on the fatigue surfaces. This suggests that the bimodal appearance of the growth curve may be related to crack tip wedging due to the oxide formation. Functionally one may hypothesize:

$$\frac{da}{dn}_{Dwell} = 24 \left(\delta_{max} - \delta_{opening}^{(T)} - \delta_{oxide} \right)^{1.46}$$

where δ_{oxide} represents the increase in the effective opening crack tip stretch due to the presence of the oxide film. A simple model for predicting the magnitude of δ_{oxide} assumes that at any point on the crack face the thickness of the oxide layer is related by the parabolic oxidation law to the elapsed time since the crack surface was formed, and that the crack tip stress intensity factor due to the wedging action of the oxide can be obtained by using Barenblatt's solution (Reference 12) for the splitting of a body by a semi-infinite wedge of height dh.

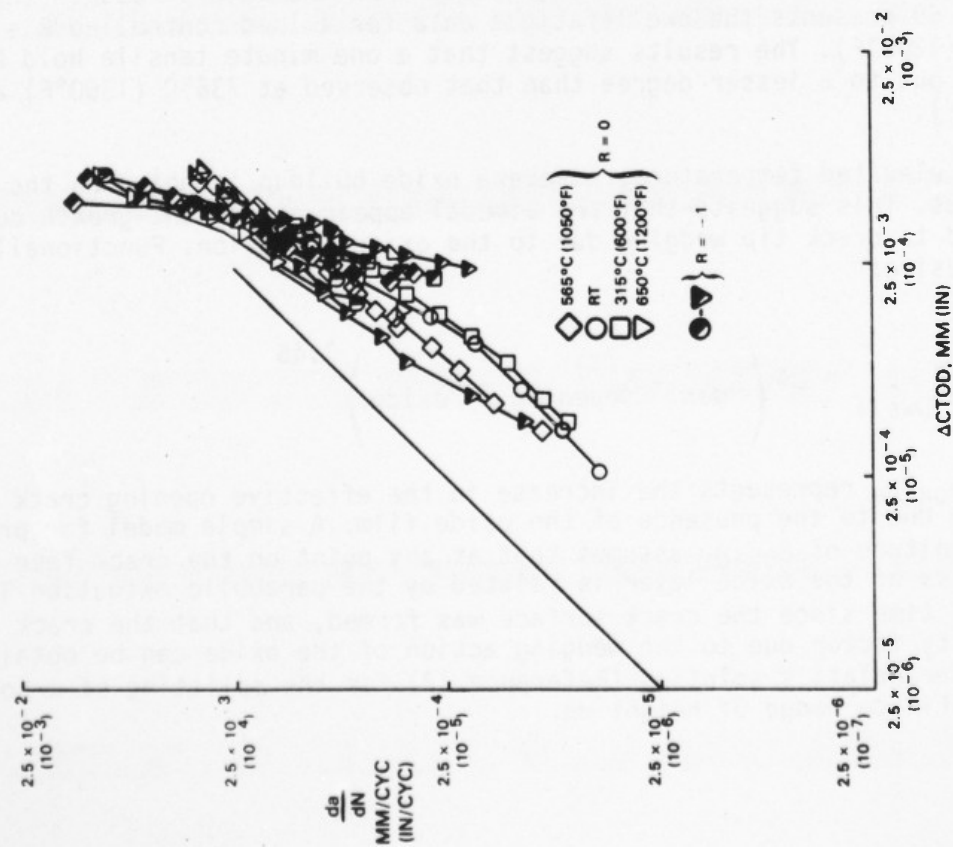


Figure 66 da/dN Versus Crack Tip Opening, Rapid Cycle Load Controlled Test Results

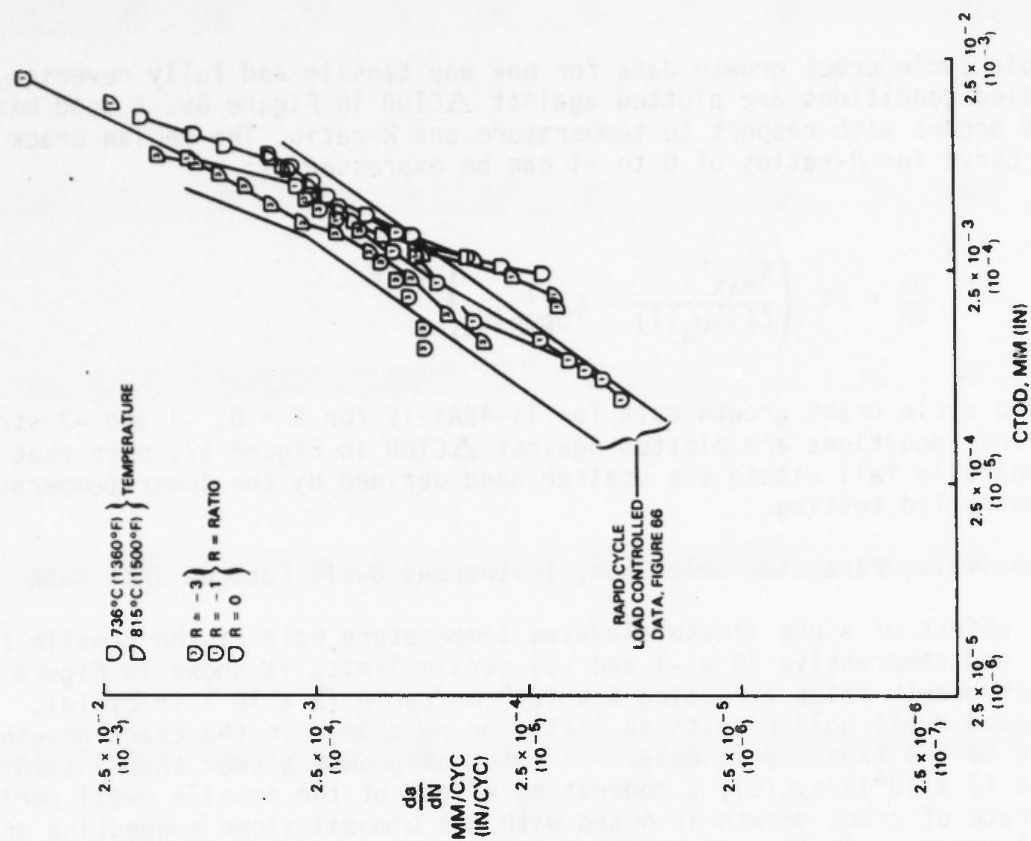


Figure 67 da/dN Versus Crack Tip Opening, Rapid Cycle Strain Controlled Test Results

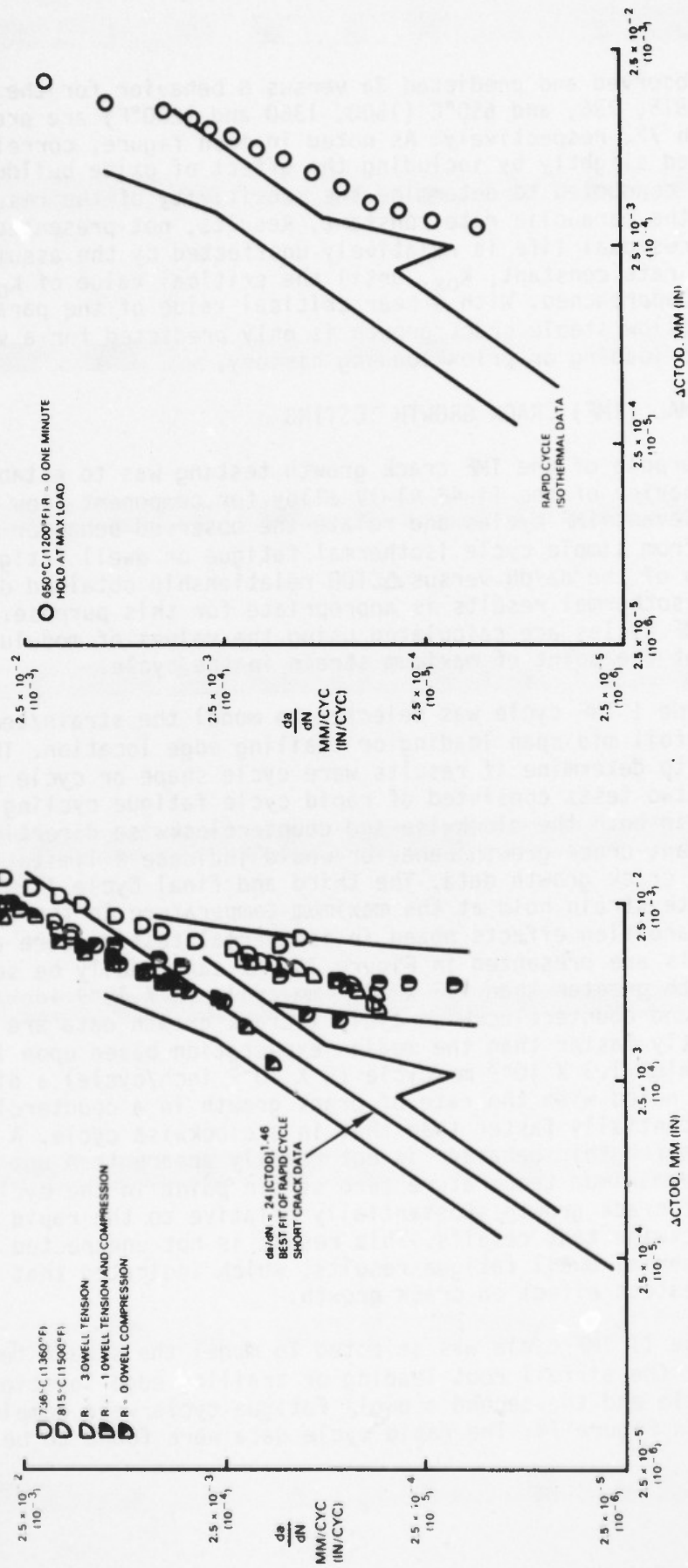


Figure 68 Strain Controlled da/dN Versus Crack Tip Opening, Dwell Data

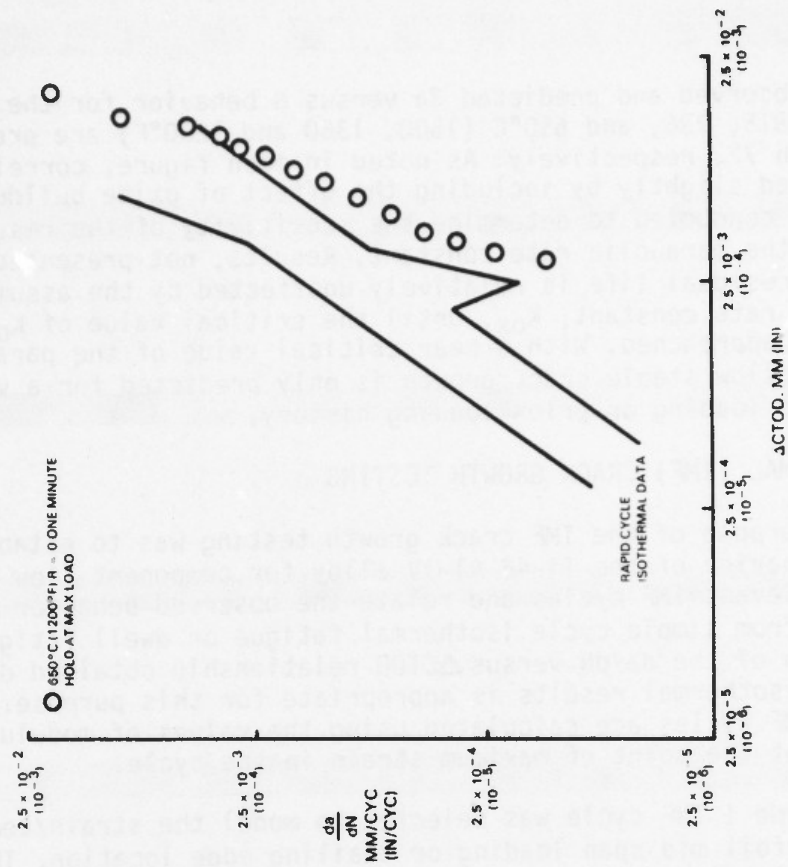


Figure 69 Load Controlled da/dN Versus Crack Tip Opening, Dwell Data

The observed and predicted 2a versus N behavior for the dwell fatigue tests at 815, 736, and 650°C (1500, 1360 and 1200°F) are presented in Figures 70 through 72, respectively. As noted in each figure, correlation of the data is improved slightly by including the effect of oxide buildup. A parametric study was conducted to determine the sensitivity of the results to the assumed value of the parabolic rate constant. Results, not presented here, indicate that the residual life is relatively unaffected by the assumed value of the parabolic rate constant, K_{ox} , until the critical value of K_{ox} for crack arrest is approached. With a near critical value of the parabolic rate constant, slow stable crack growth is only predicted for a very limited range of imposed loading or prior loading history.

3. ATHERMAL (TMF) CRACK GROWTH TESTING

The purpose of the TMF crack growth testing was to establish the crack growth behavior of the Ti-48 Al-1V alloy for component (low pressure turbine blade) relevant TMF cycles and relate the observed behavior to estimates obtained from simple cycle isothermal fatigue or dwell fatigue test data. A comparison of the da/dN versus $\Delta CTOD$ relationship obtained during TMF cycling with the isothermal results is appropriate for this purpose. $\Delta CTOD$ estimates for the TMF cycles are calculated using the values of modulus and yield strength at the point of maximum strain in the cycle.

The type I TMF cycle was selected to model the strain/temperature response at the airfoil mid span leading or trailing edge location. These tests were performed to determine if results were cycle shape or cycle rate dependent. The first two tests consisted of rapid cycle fatigue cycling with the T- ϵ variation in both the clockwise and counterclockwise direction. Differences in the resultant crack growth behavior would indicate a limitation in using isothermal crack growth data. The third and final Cycle I TMF test introduced a one minute strain hold at the maximum temperature in the cycle to determine if the retardation effects noted in isothermal testing were also present in TMF. Results are presented in Figure 73. As can readily be seen, at rates of crack growth greater than 1.3×10^{-3} mm/cycle (5×10^{-5} inch/cycle) the clockwise and counterclockwise cycle I crack growth data are comparable and only slightly faster than the median expectation based upon isothermal test results. Below 1.3×10^{-3} mm/cycle (5×10^{-5} inch/cycle) a divergence in results is noted with the rate of crack growth in a counterclockwise cycle being substantially faster than that in a clockwise cycle. A physical explanation for this behavior is not readily apparent. A one minute strain hold at the maximum temperature zero strain point in the cycle did not alter the rate of crack growth substantially relative to the rapid cycle counterclockwise test results. This result is not unexpected based upon the prior isothermal dwell fatigue results, which indicated that dwell in tension has the greatest effect on crack growth.

The type II TMF cycle was selected to model the strain temperature response at the airfoil root leading or trailing edge location. Two tests, one a rapid cycle and the second a dwell fatigue cycle were completed. Results are presented in Figure 74. The rapid cycle data were found to be in general

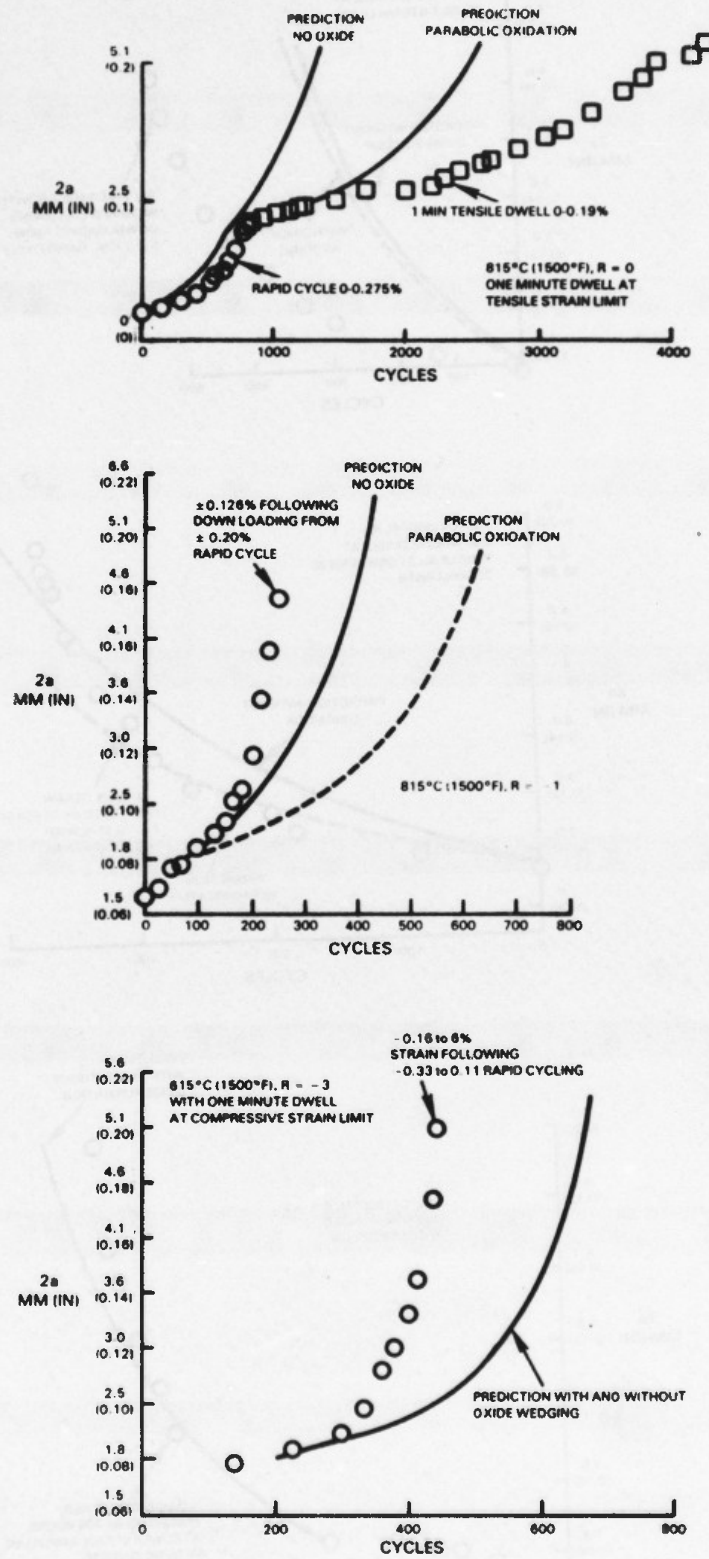


Figure 70 Dwell Fatigue Test data at 815°C (1500°F), Oxide Wedging Model Improves Correlation

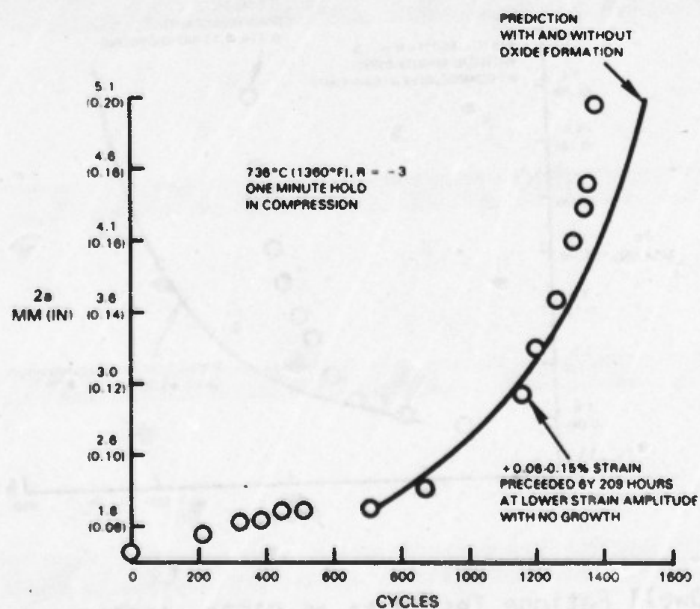
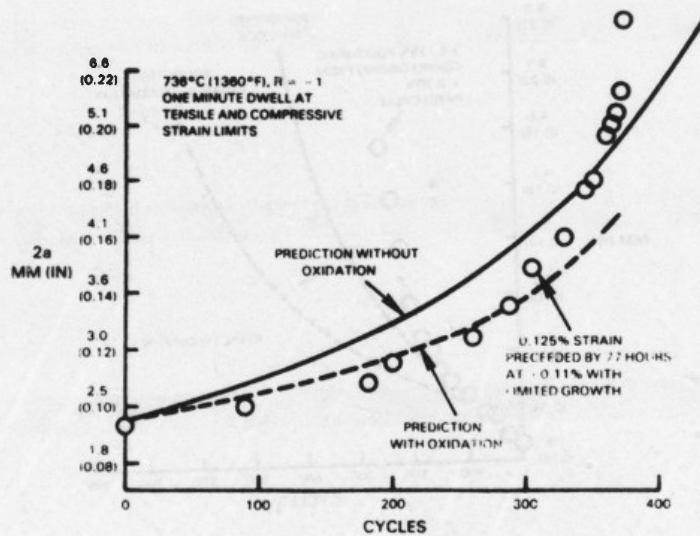
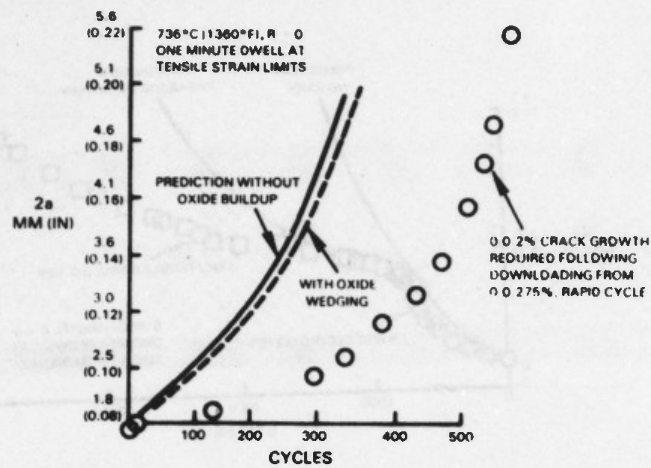


Figure 71 Dwell Fatigue Test Data at 736°C (1360°F), Oxide Wedging Model Improves Correlation

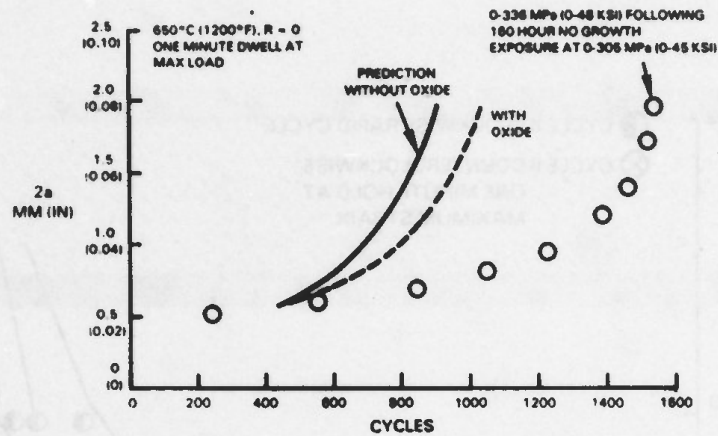


Figure 72 Dwell Fatigue Tests at 650° (1200°F)

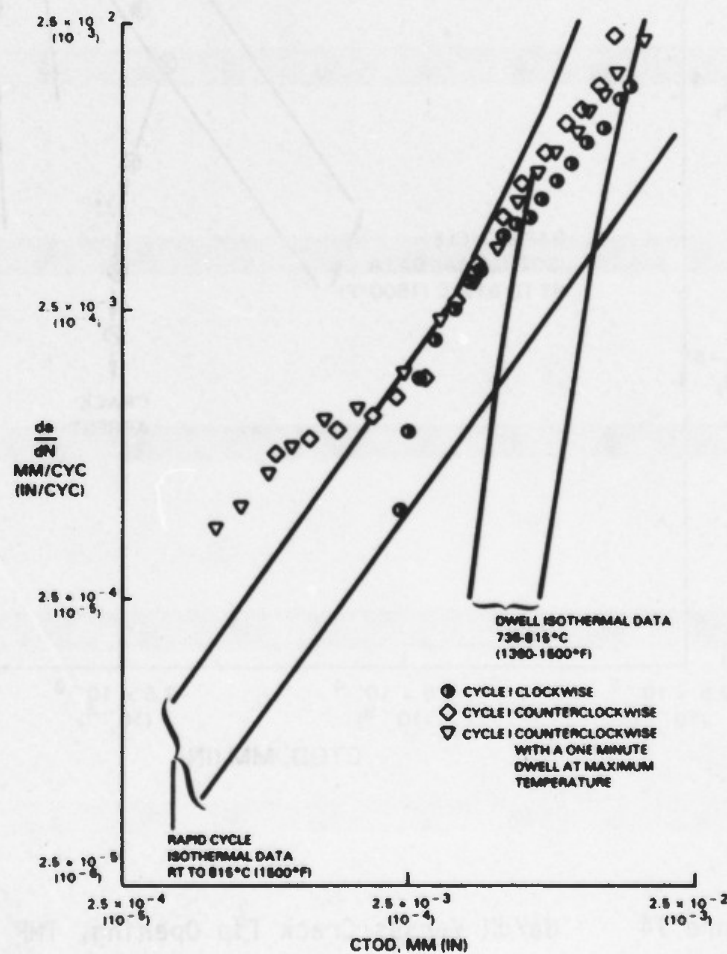


Figure 73 da/dN Versus Cracking Tip Opening, TMF Cycle I

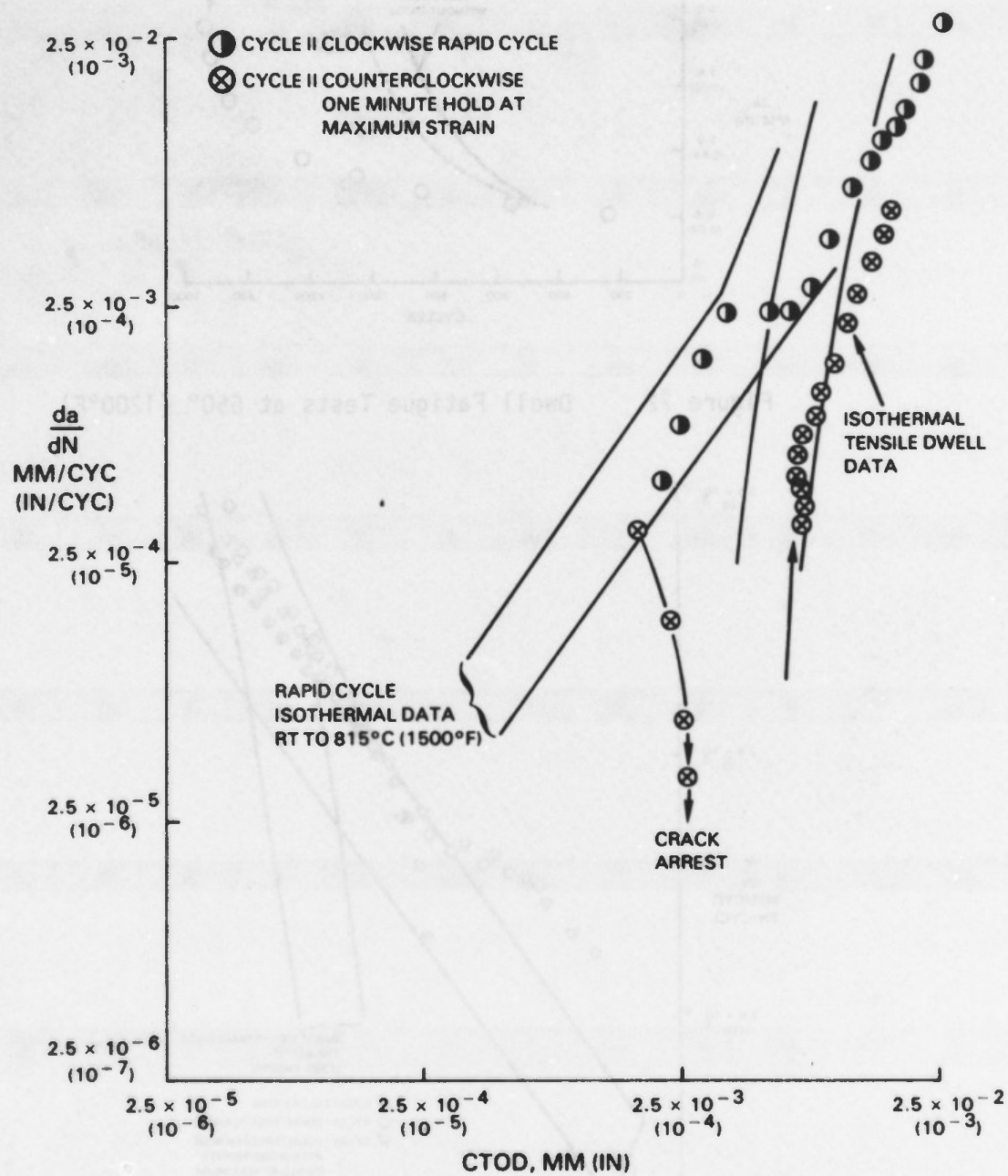


Figure 74 da/dN Versus Crack Tip Opening, TMF Cycle II

agreement with expectations based upon the rapid cycle isothermal results. The effect of a one minute hold at maximum strain was most dramatic. It might be argued that if the rate of crack growth immediately following imposition of a dwell period is not sufficient to remove the crack tip from the region of oxide buildup or blunting, the rate of crack growth will decrease until crack arrest occurs. Reinitiation of crack growth at a rate greater than the threshold level (approximately 4.1×10^{-4} mm/cycle (1.5×10^{-5} in/cycle)), results in continued growth to failure. This is in general agreement with the isothermal dwell-fatigue results.

The type III TMF cycle was selected to model the stress-temperature response at the attachment fillet location. Two tests were performed to determine if crack growth rates were sensitive to the direction of cycle. Results shown in Figure 75 are in general agreement with expectation based upon the isothermal rapid cycle results, particular at the higher crack growth rates.

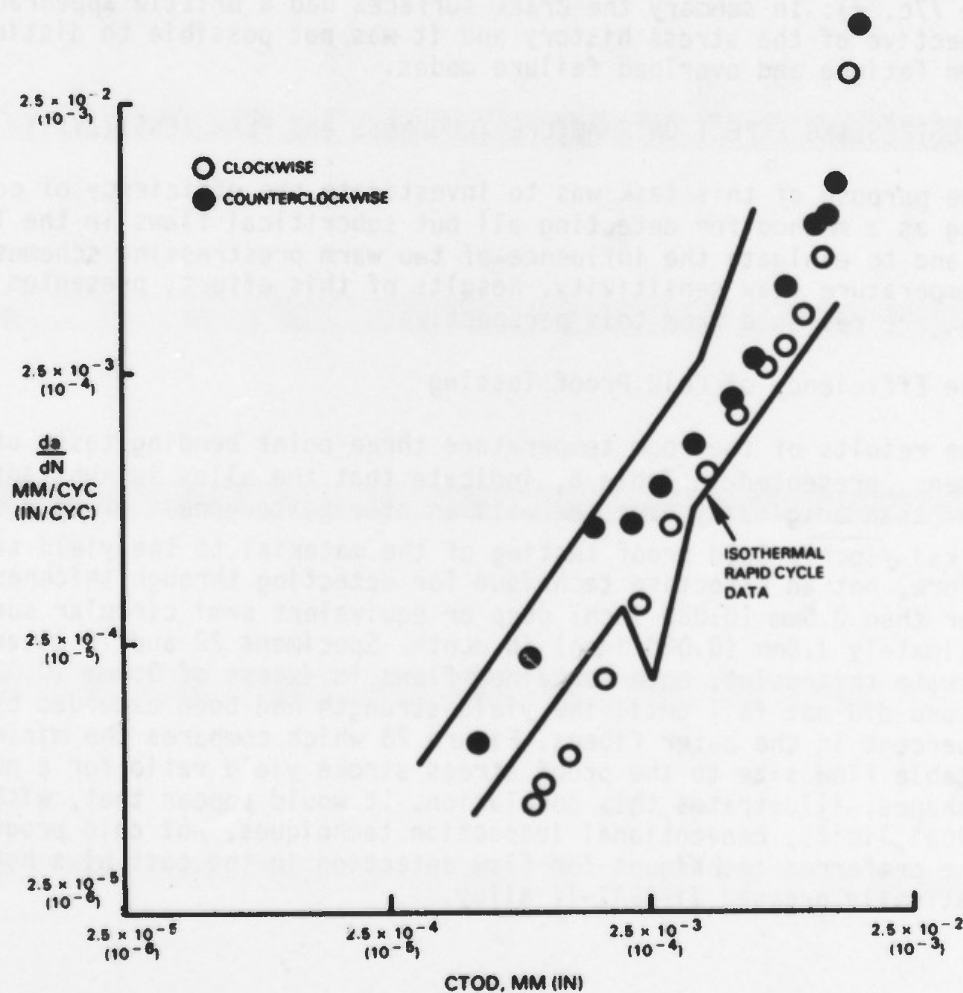


Figure 75 da/dN Versus Crack Tip Opening, TMF Cycle III

Fractography

A limited amount of fractographic analysis of selected specimens was conducted in an attempt to evaluate the details of the cracking behavior. Specimen 10766 was selected as being illustrative of most of the features observed. The fracture surface near the starter slot was heavily oxidized to the extent that surface features were obscured and crack initiation and propagation modes could not be determined (Figure 76b). As the crack front progressed, the heavy yellowish-brown oxide became a lighter blue color and finally a clean surface where the tensile overload occurred. These areas exhibited a brittle cleavage appearance with little evidence of ductile striations or tensile dimples (Figure 76c, d). Cross section metallographic examination confirmed the presence of a heavy, uniform oxide layer near the starter slot which appeared to taper off as the crack progressed (Figure 77a, b). Crack propagation appeared to be a combination of inter and transgranular fracture. Cross platelet shear was also apparent. A specimen tested at 736°C (1360°F) also showed an oxide layer, but none was detected at 630°C (1200°F) (Figure 77c, d). In summary the crack surfaces had a brittle appearance irrespective of the stress history and it was not possible to distinguish between fatigue and overload failure modes.

4. PRESTRESSING EFFECT ON FRACTURE TOUGHNESS AND FLAW SENSITIVITY

The purpose of this task was to investigate the efficiency of cold proof testing as a method for detecting all but subcritical flaws in the Ti-48Al-1V alloy and to evaluate the influence of two warm prestressing schemes on the low temperature flaw sensitivity. Results of this effort, presented in Tables 4 to 6, are reviewed from this perspective.

a. The Efficiency of Cold Proof Testing

The results of the room temperature three point bending tests of preflawed specimens, presented in Table 6, indicate that the alloy is substantially tougher than originally expected with an average toughness of $24.3 \text{ MPa} \sqrt{\text{m}}$ ($21.5 \text{ ksi} \sqrt{\text{inch}}$). Cold proof testing of the material to the yield strength is, therefore, not an effective technique for detecting through thickness cracks smaller than 0.5mm (0.020 inch) deep or equivalent semi circular surface flaws approximately 1.5mm (0.060 inch) in depth. Specimens 22 and 19 clearly illustrate this point, both contained flaws in excess of 0.5mm (0.020 inch) in depth and did not fail until the yield strength had been exceeded by at least five percent in the outer fibers. Figure 78 which compares the minimum detectable flaw size to the proof stress stroke yield ratio for a number of flaw shapes, illustrates this conclusion. It would appear that, within practical limits, conventional inspection techniques, not cold proof testing, are the preferred techniques for flaw detection in the cast plus hot isostatically pressed Ti-48Al-1V alloy.

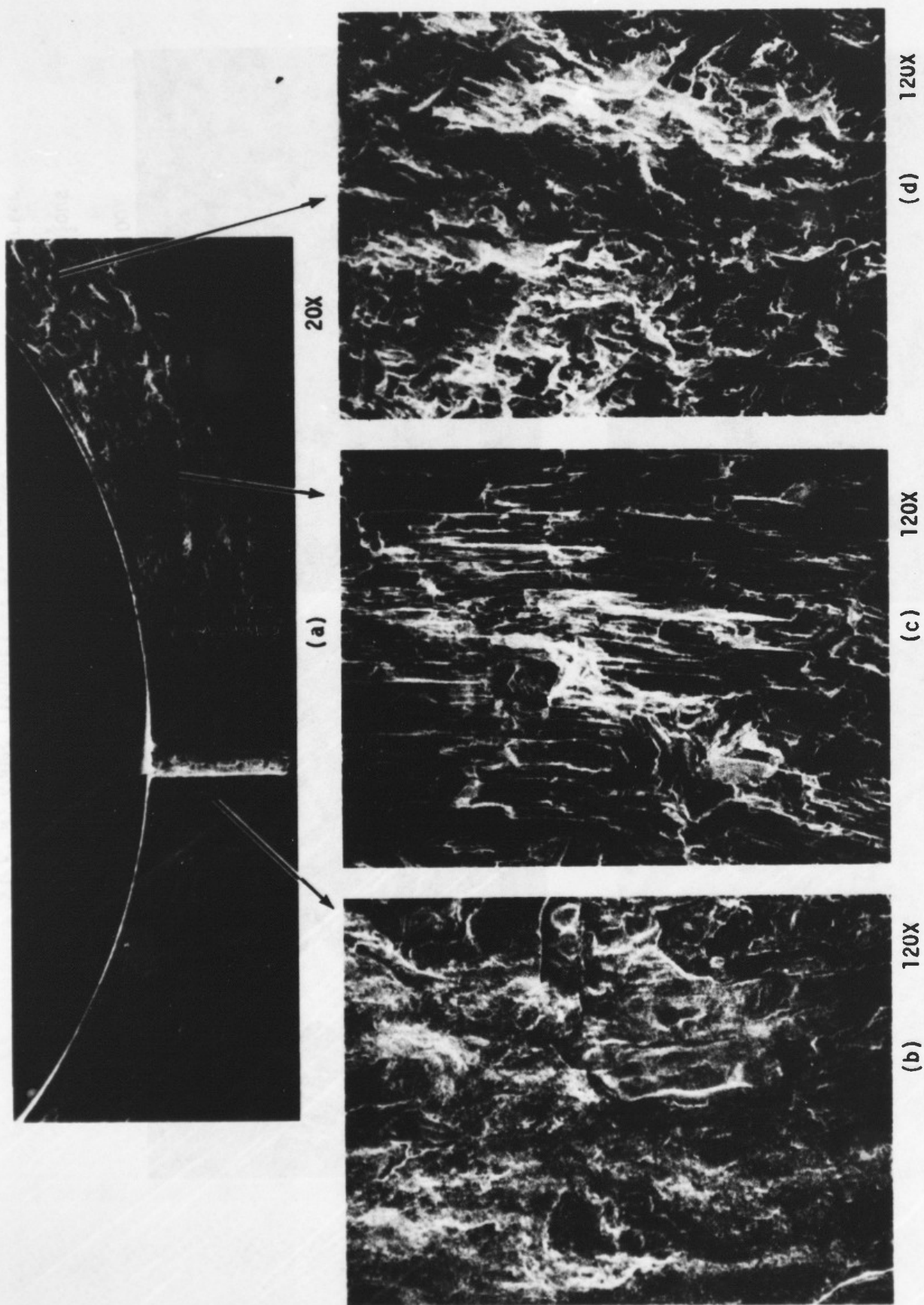
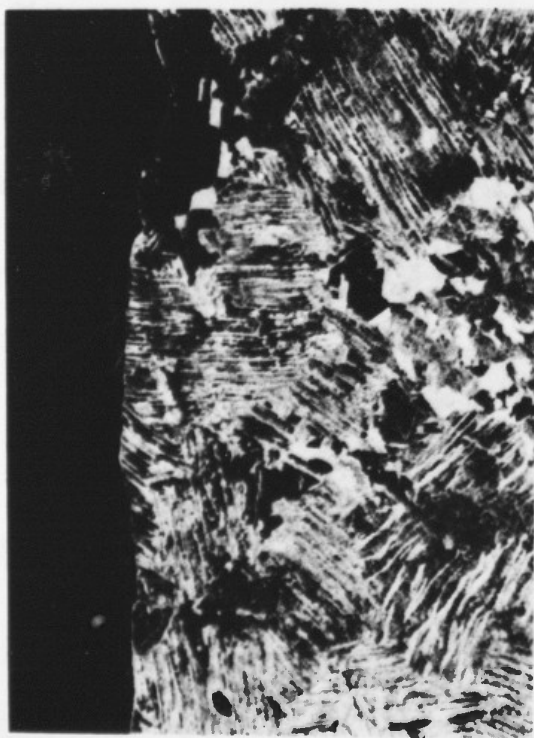
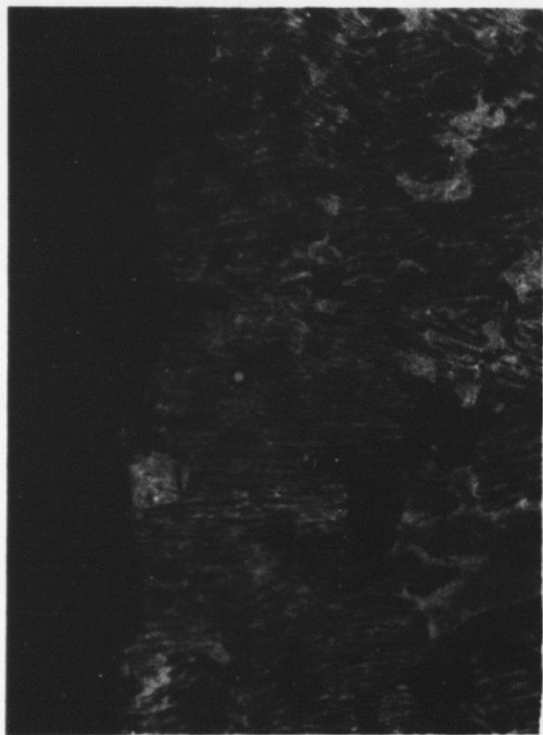


Figure 76 Fracture Surface of da/dN Specimen 10766 after Misc. 815°C (1500°F) dwell test. Note heavy oxide in (b) and cleavage fracture in (c) and (d).



a



b



c



d

100X

Figure 77 Cross Section of Isothermal da/dN Specimens Tested at Various Temperatures. a) 815°C (1500°F) at Starter Slot b) 815°C (1500°F) away from Starter Slot c) 736°C (1360°F) at Starter Slot d) 650°C (1200°F) at Starter Slot

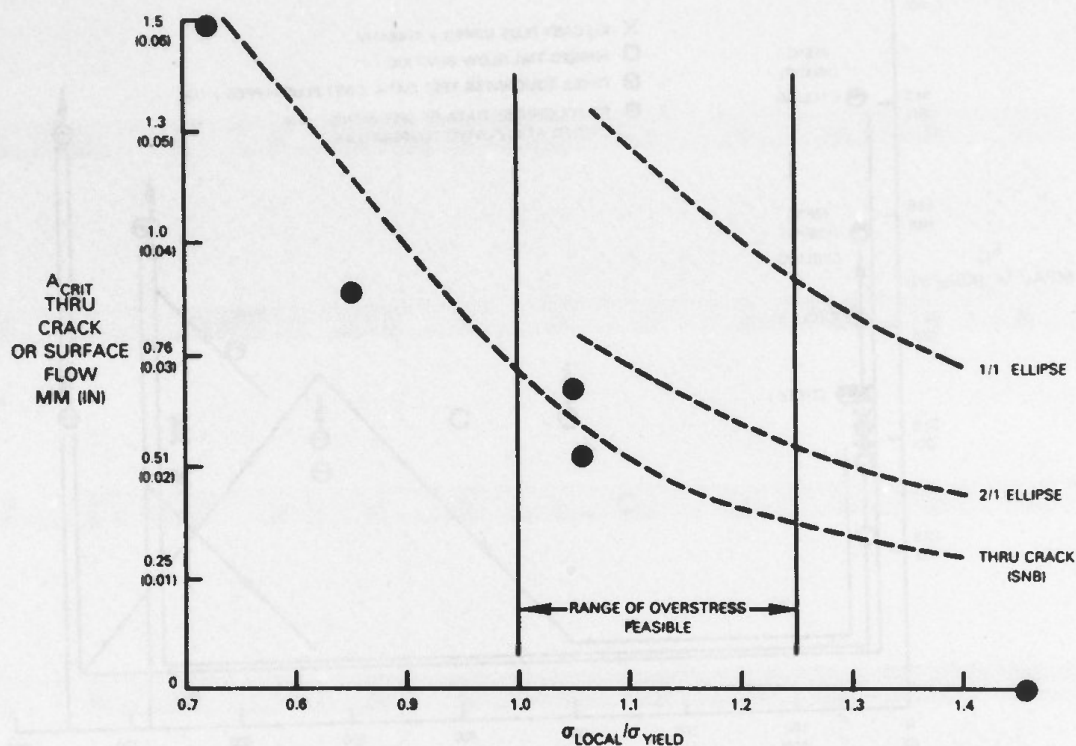


Figure 78 Cold Proof Test, Results and Analysis

b. The Effect of Temperature on the Apparent Fracture Toughness of the Cast Plus Hot Isostatic Pressed Ti-48Al-1V Alloy

The unexpectedly high room temperature apparent fracture toughness was also accompanied by an unexpectedly low apparent fracture toughness at 704°C (1300°F), as seen in Table 7. These data are compared in Figure 79 with previous slow bend K_{IC} data for the forged Ti-48Al-1V alloy and information obtained in the course of the current cyclic crack growth program, described previously. The data indicate that the cast plus hot isostatically pressed material is tougher than the forged product form up to approximately 427°C (800°F), and that the ductile-brittle transition temperature is between 704°C (1300°F) and 760°C (1400°F) in the cast plus hot isotropic pressed material. Cycling may increase the apparent fracture toughness value at any elevated temperature. The effect of prior elevated temperature cyclic exposure on the subsequent room temperature apparent fracture toughness is clearly evident. Specimens cycled isothermally at 736°C (1300°F) and 815°C (1500°F) and one cycle II TMF specimen, when cooled to room temperature, were able to be loaded nearly to the stress intensity level at which they had been cycling before failing. This finding led to a more systematic consideration of warm prestress benefits at design relevant conditions, described below.

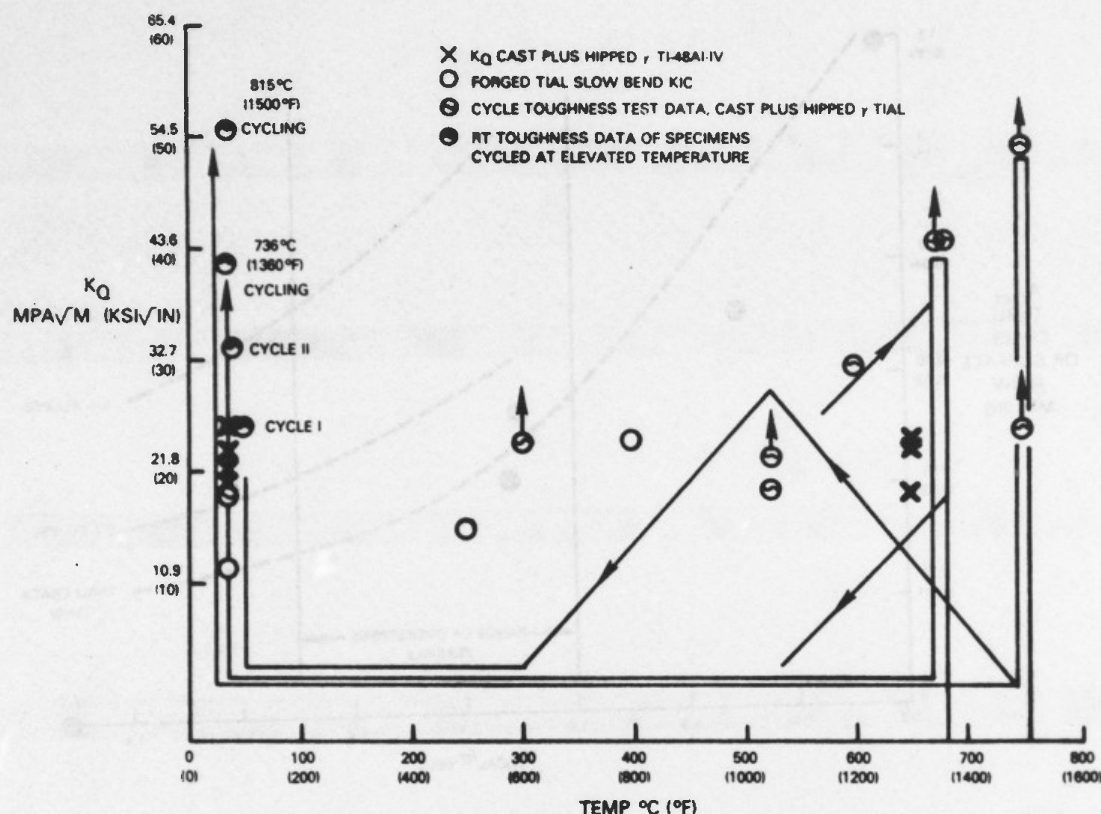


Figure 79 The Effect of Test Temperature and Sequence on the Apparent Fracture Toughness

c. Benefits of Warm Tensile Prestressing (Load-Unload-Cooldown Cycle)

Two three point bending Specimens 16 and 21 were successfully prestressed to 130% of the 704°C (1300°F) yield strength without failing, as noted in Table 7. Subsequent tensile testing of Specimen 21 suggested no change in the room temperature apparent fracture toughness. Specimen 16 was fatigue cycled at design relevant stress levels 0-420 MPa (0-60 ksi) and survived for 700 cycles. Taken together with the warm prestress data presented in Figure 77, the results for Specimen 21 suggest that the effect of a sustained load exposure at elevated temperature is to increase the apparent room temperature fracture toughness to the level of stress intensity achieved at temperature. A second benefit is to retard the growth of the crack immediately following the prestress operation. The residual life of Specimen 16 was predicted to be less than 100 cycles without credit taken for the overload cycle.

Tensile warm prestressing is of limited benefit as a technique for altering the room temperature fracture toughness or increasing the residual life due to 1) the practical constraints on the overstress temperature 704°C (1300°F) and magnitude of the overstress (150%) and 2) minimal variation of toughness with test temperature to 704°C (1300°F.)

d. Benefits of Warm Compressive Prestressing (Load-Cooldown-Unload Cycle)

A warm compression prestress cycle does not have any material effect on the room temperature apparent fracture toughness (specimen tests 14 and 7, Table 8) when measured from the null load point. The average toughness value, $21.4 \text{ MPa}\sqrt{\text{m}}$ ($19.6 \text{ ksi}\sqrt{\text{inch}}$) is slightly below the average value for non-prestressed specimens. If, however, the warm compression operation results in a compressive residual stress of sufficient depth to encompass the crack (as might result from a warm prestress operation, for instance), an ostensible increase in the apparent fracture toughness might result. Compression fatigue testing of specimens 18, 13 and 24 following the warm compression prestress exposure clearly points to the benefit of mean stress on durability. Each of these specimens achieved 10,000 cycles without failure.

5. SUBCOMPONENT TESTING TO DEMONSTRATE THE BENEFITS OF PRESTRESSING AND COLD PROOF TESTING

The purpose of this task was to verify that the cold proof test and warm prestress effects studied in Task V apply to a center notched, bolt hole type, specimen (serving as a simulated component). The results, presented in Table 9, are reviewed from this perspective.

a. The Efficacy of Cold Proof Testing

Slow bend testing, reviewed above, indicated that the apparent room temperature fracture toughness was too large for the cold proof test concept to be applied to screen critical defects from service. This finding was confirmed as the result of the Ti-48Al-1V subcomponent testing. Specimen 3, Table 9, was loaded to failure at room temperature. The local elastic notch stress at failure was about 128% of the yield strength. If proof testing were limited to the yield strength, the critical flaw size would clearly exceed the $0.51 \times 1.0 \text{ mm}$ ($0.020 \times 0.039 \text{ inch}$) flaw present in Specimen 3. Fatigue testing at engine relevant stress levels (Specimens 6 and 8) indicates a flaw of this size would precipitate failure in less than the design life of the component (ten thousand cycles). Incidentally, the apparent toughness values from the failure of Specimens 3 and 8, 22.6 and $21.2 \text{ MPa}\sqrt{\text{m}}$ (20.7 and $19.4 \text{ ksi}\sqrt{\text{inch}}$), respectively, are consistent with the three-point bending data at room temperature.

b. The Effect of Warm Tensile Prestressing on Room Temperature Toughness

Specimens 5, 6, and 7, Table 3, were stressed at 270 MPa (38.5 ksi) net section stress for one-half hour at 704°C (1300°F). This condition resulted in local elastic stresses approximately twice the yield strength at elevated temperature. Survival of the specimens suggests that the toughness of the plate material at 704°C (1300°F) may be greater than that for the bar stock tested previously; $31.4 \text{ MPa}\sqrt{\text{m}}$ ($28.8 \text{ ksi}\sqrt{\text{inch}}$) in the plate versus an average of $23.1 \text{ MPa}\sqrt{\text{m}}$ ($21.2 \text{ ksi}\sqrt{\text{inch}}$) in the bar stock.

Specimen 7 was tensile tested at room temperature and an encouraging 50% increase in the apparent fracture toughness was noted. The prestress condition was, however, about twenty percent above that readily achievable in a bladed disk.

c. Fatigue Results

Four of the six specimens, Table 9, were fatigue tested at room temperature, Specimens 4 and 8 in the as-precracked condition, and Specimens 5 and 6 in the precracked and warm prestressed condition.

The size and shape of the starting flaw in Specimens 4 and 8 were very similar, 0.23 x 0.51mm and 0.23 x 0.83mm (0.009 x 0.830 inch and 0.009 x 0.033 inch). The resultant fatigue lives were, however, significantly different; a result not unexpected with a material with a very high Paris law exponent. Specimen 4 did not fail in 9955 cycles at 0-196 MPa (0-28 ksi) compared to only 1297 cycles attained with Specimen 8 at the same load level. These results, taken together, suggest that the critical flaw size for a non-prestressed component is no bigger than about a 0.25 x 0.5mm (0.010 x 0.020 inch) surface crack. Cracks this small cannot be detected by cold proof testing nor by conventional inspection techniques. The predicted lives of Specimen 4, 0.23 x 0.51mm (0.009 x 0.020 inch) edge crack, and Specimen 8, 0.23 x 0.83mm (0.009 x 0.033 inch) edge crack, are 2400 and 1650 cycles, respectively.

Fatigue testing of Specimen 6, which was prestrained at 704°C (1300°F), indicates a benefit was obtained as a result of the process. The starting flaw size was substantially larger than that in Specimen 8 yet the residual life increased substantially, 8644 cycles versus 1297 cycles. Specimen 5 was more severely cracked and did not benefit substantially from the prestress operation. These two tests suggest that the critical flaw size in a prestrained component is no bigger than about the 0.41 x 1.1mm (0.016 x 0.045 inch) surface flaw in Specimen 6. Cracks this small are only marginally more detectable than the 0.25 x 0.51mm (0.010 x 0.020 inch) critical defects in the non-prestrained geometry. The predicted residual life, with due consideration given to the prestrain operation, is 1500 cycles for Specimen 6. No growth is predicted for Specimen 5.

6. Overall Implications

The purpose of this program was to obtain additional crack growth and fracture toughness information for an γ TiAl alloy and to determine if various strategies (cold and warm proofstressing, for example) could be established for reducing the sensitivity of the material to pre-existent defects. The overall objective is to directly substitute γ TiAl for a conventional nickel base material in a dynamic (rotating) engine component thereby realizing a significant reduction in hot section weight.

Estimates of the threshold stress intensity from the testing are lower than those for the conventional nickel base material with the implication that γ TiAl components will be more sensitive to defects in the presence of high

frequency vibratory loading (which do not scale by density). Density normalized crack growth rate data for the γ TiAl material is also faster than that for nickel materials; the rate of low cycle fatigue crack growth will therefore also be greater in the TiAl components. Test and analysis indicates that the room temperature toughness is too great for cold prestressing to be a viable technique for screening defective parts from the population. The material appears to remain brittle up to 1300°F. Warm tensile prestressing has some benefit on damage tolerance but the acceptable flaw size in a notched detail subjected to a load level consistent with the inherent tensile, creep and fatigue strength of the material is only 0.41 x 1.1 mm (0.016 x 0.045 inch). A flaw of this size is only marginally detectable using current (in progress) NDI methods (fluorescent penetrant inspection). Damage tolerance considerations, therefore, require rigorous quality requirements and use of advanced quality inspection methods to utilize γ TiAl on a direct substitution basis. Alternately, the operating stress levels may be reached below those levels deemed acceptable from conventional design calculations to attain damage tolerance but not without a sacrifice in weight savings.

SECTION V

SUMMARY AND RECOMMENDATIONS

1. TEST SUMMARY

a. The rate of isothermal, simple cycle fatigue crack growth when expressed as a function of the maximum stress intensity in the cycle is not a strong function of R-ratio ($R \neq 0$) but increases with increasing test temperature. No abrupt differences were noted in the rate of crack growth at a given value of K_{\max} as the tensile ductile-brittle transition temperature was traversed.

b. Temperature and R-ratio effects on the rate of isothermal fatigue crack growth are more accurately described if the crack tip opening displacement,

$K_{\max}^2 / E\sigma$, is used as the normalizing parameter.

c. A tensile strain or stress hold in the isothermal fatigue test cycle at temperatures exceeding 736°C (1360°F) generally retards the rate of crack growth when test conditions would result in rapid cycle crack growth rates less than 6×10^{-3} mm/cycle (2×10^{-4} inch/cycle). The retardation effect is tentatively ascribed to the wedging action of the oxide buildup on the crack surface that reduces the opening crack tip displacement.

d. Thermomechanical fatigue crack growth tests were performed to simulate loading-temperature cycles at critical locations in a turbine airfoil. Resultant crack growth data were in general agreement with expectations based upon isothermal testing.

e. The effect of a constant strain hold on TMF crack growth was similar to that observed in the isothermal tests.

f. Slow bend specimen testing indicated that the room temperature apparent fracture toughness of the Ti-48Al-1V is too high for cold proof testing to be an effective device for defect detection. Conventional inspection techniques are the preferred detection methods for flaws in this alloy.

g. Slow bend fracture testing indicated no change in the apparent fracture toughness between room temperature and 704°C (1300°F). Tensile warm prestressing is, therefore, of limited benefit as a technique for enhancing the room temperature apparent fracture toughness or increasing the residual life.

h. Compressive warm prestressing of slow bend fracture specimens was not found to affect the low temperature tensile properties (residual life or apparent fracture toughness). The residual compressive stress induced by warm working the detail or warm tensile prestraining would, however, appear to be beneficial.

i. Cold proof and fatigue testing of preflawed bolt hole specimens, some of which were subjected to a warm tensile prestress operation, were found to yield results in general agreement with the results cited above for the slow bending specimens. Surface flaws no longer than 0.25 x 0.5mm (0.010 x 0.020 inch) are acceptable in a non prestrained notched ($K_t = 2.6$) detail cycling at component relevant stress levels. Tensile warm prestraining increases the acceptable flaw size to something less than 0.41 x 1.1mm (0.016 x 0.045 inch).

2. Assessment

j. The damage tolerance of the Ti-48Al-1V alloy is marginal considering the reliability and sensitivity of current in process NDI methods. Operating stress levels must, therefore, be limited to assure defect tolerance and not be based upon fatigue crack initiation capability.

k. Application of the Cast + HIP'ed Ti-48Al-1V alloy should be limited to components where risk of impact damage is slight and/or where failure would have no effect on immediate flight safety.

l. Direct substitution of γ TiAl for a nickel base material in a stress limited dynamic hot section component is not possible. Redesign to satisfy the damage tolerance criteria will reduce the weight advantage of the material.

3. RECOMMENDATIONS

m. Alloy modification studies to increase impact resistance and toughness at intermediate temperatures should be considered.

REFERENCES

1. Blackburn M.J., Ruckle D.L. and Bevan C.E., "Research to Conduct an Exploratory and Analytical Investigation of Alloys," AMFL-TR-78-18, March 1978.
2. Blackburn M.J. and Smith M.P., "The Understanding and Exploitation of Alloys Based on the Compound TiAl (Gamma Phase)." AFML TR-78-78, June 1978.
3. Blackburn M.J. and Smith M.P., "The Understanding and Exploitation of Alloys Based on the Compound TiAl ()," AFML TR-79-4056, May 1979.
4. O'Connell T.E., "Study of Intermetallic Compounds," AFML TR-79-4177, December 1979.
5. Blackburn M.J. and Smith M.P., "Research to Conduct an Exploratory Experimental and Analytical Investigation of Alloys," AFWAL TR-80-4175, November 1980.
6. Blackburn M.J. and Smith M.P., "Research to Conduct an Exploratory Experimental and Analytical Investigation of Alloys," AFWAL-TR-81-4046., June 1981.
7. Blackburn M.J. and Smith M.P., "Research on Composition and Processing of Titanium Aluminide Alloys for Turbine Engines," AFWAL-TR-82-4086, June 1982.
8. Blackburn M.J., Hill J.T. and Smith M.P., "R & D on Composition and Processing of Titanium Aluminide Alloys for Gas Turbine Engines," Interim Report FR-17353, 29 July 1983.
9. PWA Unpublished Data.
10. Erdogan, F., and Ratwani, M. "Fatigue and Fracture of Cylindrical Shells," I. Jour. of Frac. Mech., Vol. 6, 1970, pp 379-392.
11. Erdogan, F., and Delale, "Transverse Shear Effects in a Circumferentially Cracked Cylindrical Shell," Q. of Appl. Math., Oct. 1979, pp 239-258.
12. Barenblatt, G.I. "Mathematical Theory of Equilibrium Cracks in Brittle Fracture," Adv. in Appl. Math., Vol VII, p. 55, Academic Press.